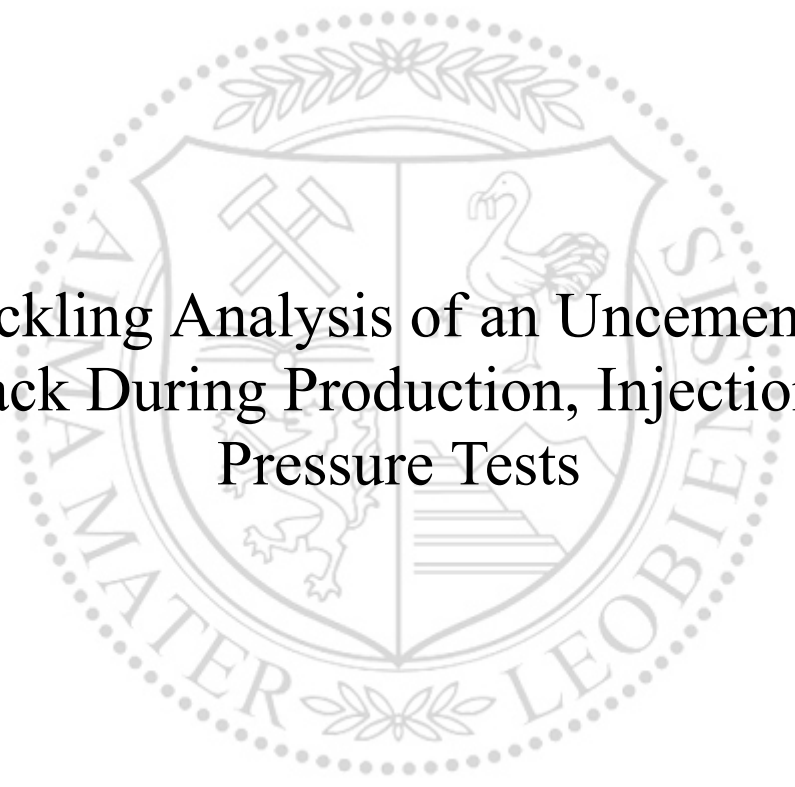Chair of Petroleum and Geothermal Energy Recovery
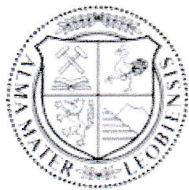
Master's Thesis

Buckling Analysis of an Uncemented Tieback During Production, Injection and Pressure Tests

Benjamin Ulrich, BSc

February 2021

EIDESSTATTLICHE ERKLÄRUNG

Ich erkläre an Eides statt, dass ich diese Arbeit selbständig verfasst, andere als die angegebenen Quellen und Hilfsmittel nicht benutzt, und mich auch sonst keiner unerlaubten Hilfsmittel bedient habe.

Ich erkläre, dass ich die Richtlinien des Senats der Montanuniversität Leoben zu "Gute wissenschaftliche Praxis" gelesen, verstanden und befolgt habe.

Weiters erkläre ich, dass die elektronische und gedruckte Version der eingereichten wissenschaftlichen Abschlussarbeit formal und inhaltlich identisch sind.

Datum 25.02.2021

Unterschrift Verfasser/in
Benjamin Ulrich

MONTANUNIVERSITÄT LEOBEN
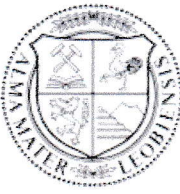
AFFIDAVIT

I declare on oath that I wrote this thesis independently, did not use other than the specified sources and aids, and did not otherwise use any unauthorized aids.

I declare that I have read, understood, and complied with the guidelines of the senate of the Montanuniversität Leoben for "Good Scientific Practice".

Furthermore, I declare that the electronic and printed version of the submitted thesis are identical, both, formally and with regard to content.

Date 25.02.2021

Signature Author
Benjamin Ulrich

Kurzfassung

Ein MATLAB-Modell wird vorgestellt, das auf einer detaillierten Untersuchung der Berechnungen und des Verhaltens einer nicht zementierten Liner Rückverlängerung (Tieback) in einem vertikalen Bohrloch eines Enhanced Geothermal System (EGS) basiert. Es verwendet die Eingabeparameter und ein gegebenes Komplettierungsdesigns als Grundlage für die Berechnungen. Ein nicht zementierter Tieback unterliegt Last- und Buckling-Untersuchungen unter verschiedenen Betriebsarten. Die Ergebnisse werden in einer benutzerfreundlichen Umgebung präsentiert.

Das Modell berücksichtigt alle auftretenden Axialkräfte, Biegespannungen, Temperaturen sowie Innen- und Außendrücke. Konstruktionsfaktoren müssen in einem bi-axialen Konstruktionsansatz gegen axiale, Berst- und Kollapsversagensbeständigkeit verifiziert werden. Beeinflussbare Temperaturverteilungen für die Betriebsarten und temperaturabhängige Druckberechnungen des Wassers im Tieback simulieren realistische Bedingungen. Es wird bewertet, ob unter den bereitgestellten Benutzerinformationen ein sinusförmiges oder helikales Buckling auftritt oder nicht. Eine Visualisierung der numerischen und grafischen Ergebnisse während der Produktions-, Injektion- und Druckprüfungsaktivitäten wird implementiert. Die Lastfälle werden gegen einen Basisfall ohne Betriebslasten analysiert.

Eine EGS- Komplettierung kann mit einem starren Design ohne Bewegungsfreiheit oder einem vertikal frei beweglichen Design realisiert werden. Während die Wahrscheinlichkeit des Bucklings von der Summe aller auftretenden Kräfte abhängt, gehören induzierte Belastungen aufgrund von Temperaturänderungen und Änderungen des wirkenden Innendrucks zu den einflussreichsten. Eine hohe Kompression kann zum Einsetzen des Bucklings führen, entweder sinusförmig oder spiralförmig. Die Bestimmung des Beginns von Buckling ist aufgrund der verschiedenen in der Literatur vorgestellten Modelle keine exakte Wissenschaft. Das Buckling kann zusätzliche lokale Biegespannungen und Kontraktionen des Stahls verursachen. Zug- und Druckbelastungen wirken sich gleichzeitig mildernd, aber auch verschlechternd auf die verschiedenen Berechnungen der Ausfallkriterien aus. Die Ergebnisse legen nahe, dass einfache Methoden zur Minderung des Bucklings wie Expansionsvorrichtungen ein ausreichendes Mittel gegen umfangreiche Druckbelastungen darstellen könnten. Bei Komplettierungen, die das Ausgleichen von Lasten mit einer Längenänderung ermöglichen, können negative axiale Lasten eine Kontraktion verursachen, während positive axiale Lasten zu einer Dehnung führen. Somit zeigt eine frei bewegliche Komplettierungsdesign Vorteile gegenüber einem starren Design in Bezug auf Buckling.

Das einfach zu installierende und benutzerfreundliche Modell bietet einen guten ersten Überblick über ein vorhandenes Komplettierungsdesign unter verschiedenen Lastfällen, ohne dass teure kommerzielle Softwarepakete erforderlich sind.

Abstract

A MATLAB model is presented based on a detailed investigation of an uncemented tieback's behaviour and calculations in a vertical borehole of an Enhanced Geothermal System (EGS). It uses the input parameters and a given completion design as its basis for the calculations. An uncemented tieback is subject to load and buckling investigations under various operational modes. Results are presented in a user-friendly environment.

The model considers all occurring axial loads, bending stresses, temperatures, internal and external pressures. Design factors need to be verified against axial, burst and collapse failure resistance in a biaxial design approach. Influenceable temperature distributions for the operational modes and temperature-dependent pressure calculations of the water inside the tieback simulate realistic conditions. An assessment is conducted on whether or not sinusoidal or helical buckling occurs under the provided user information. A visualisation of the numerical and graphical findings during production, injection and pressure test activities is implemented. The load cases are analysed against a base case without any operational loads.

An EGS completion can be realised with a rigid design without freedom of movement or a vertically freely movable design. While the chance of buckling depends on the summation of all occurring forces, induced loads due to temperature changes and changes of the acting inside pressure are amongst the most influential ones. High compression can lead to the onset of buckling, either sinusoidal or helical. The buckling onset's determination is no exact science because of the various models presented in pieces of literature. Buckling can cause additional local bending stresses and contractions of the steel. Tensile and compressive loads have at the same time a mitigating but also deteriorating influence on the different failure criteria calculations. The findings suggest that simple buckling mitigation methods such as expansion devices could provide a sufficient remedy to extensive compressive loads. For completions that allow compensating loads with a change in length, negative axial loads can cause contraction while positive axial loads will lead to elongation. Thus, a freely moveable completion design shows benefits over a rigid design in regards to buckling.

The easy to install and user-friendly model can provide a good first overview of an existing completion design under varying load cases without the necessity of expensive commercial software packages.

Table of Content

Page

1   Introduction

The company Erdwerk uses a freely moveable uncemented tieback in one of their projects. Erdwerk uses the software Landmark Solutions to plan their completions and this software gives them indications if a completion string is subject to buckling. However, it does not specify exactly which type of buckling occurs (sinusoidal or helical). Landmark is a commercial software, and the background knowledge of the calculations is limited. Also, the parameters are flexible only to a certain extent. There is no easy way to modify a system quickly by adding custom modifications to the load and buckling calculations and getting a first impression of how these modifications may influence buckling's onset or severity.

Erdwerk provided a sample completion of the uncemented tieback, which is the basis and reference for the investigation. Additionally, details about the occurring pressures during injection (up to 590 [bar] at the wellhead), the expected reservoir temperature (around 155 [°C]) and the borehole geometry have been provided. The sample tieback features a tapered design with a 9 5/8 [inch] outside diameter (OD) from 0 to 700 meters measured depth (MD) and 7 [inch] OD from 700 to 3886 meters MD. The entire tieback is made of L80 steel with Buttress Thread Coupling (BTC) connections.

The completion may be completed as a freely moveable variation or in a rigid design without movement. Both cases are typical completions and subject to investigation. The completion can be used for more than one operational mode. It could be possible that the completion is designed to produce hot water from great depth. At some point in the well's lifecycle, a change in the mode of operation to the injection of cold water under high pressure could be necessary. The ideal outcome would be to anticipate these operational changes and plan a completion fit for usage even under changed conditions to avoid costly workovers later on.

During the different operational scenarios, many loads can influence the overall performance of a complete design. One of the most influential loads is the temperature-induced force which may be tensile or compressive depending on the acting temperatures. Another strong influence is the ballooning effect due to relative pressure changes during high-pressure injection or pressure tests. If the tieback is allowed to move freely in a vertical direction, loads cause length changes. These length changes are generally contractions for negative axial loads and elongations for positive loads. Local bending stresses may be present due to initial dogleg severities (DLS) from the drilling process or induced due to buckling.

If the acting compression reaches a threshold, buckling of the tieback occurs. This buckling can then create additional bending stresses and contractions. In less severe cases, buckling can lead to non-compliance of the company's design factors, but structural failure could be the outcome in extreme cases.

This thesis desired outcome is developing a realistic and accurate model that is easily adjustable for different load scenarios while considering all influencing factors in the results. Unlike commercial software, an assessment is conducted on whether or not sinusoidal or helical buckling occurs under the provided user input.

2 EGS Project Considerations

Numerous factors influence the planning and execution of a geothermal EGS project. While all of these influences are worth discussing, this thesis scope allows only to briefly touch certain essential financial aspects and reservoir-related issues. Some of the aspects discussed throughout the following chapters influence the development of the MATLAB model or its results. Other aspects are purely theoretically and not directly connected to the MATLAB application.

2.1 Geothermal Principles

The earth's heat may be used in different ways, such as power generation, direct use or geothermal heat pumps (application close to the surface). The outcome of a geothermal project is decided, besides the desired purpose of course, with key factors like reservoir temperature (geothermal temperature gradient), reservoir pressure, reservoir depth, geological properties (permeability, porosity, thermodynamic properties, rock types), reservoir fluid (may contain corrosive agents), geographical availability to install surface facilities, government restrictions and project financing, amongst others. Usually, the reservoir pressure and temperature increase with increasing depth, but proportionally also the difficulty to develop the project, its risks and costs are increased.

The generation of electrical power requires the highest temperatures typically at around 100°C and more. To achieve such temperatures a geological region with a sufficiently high enough geothermal gradient is necessary. The direct use of geothermal energy requires lower but still elevated temperatures at around 50°C up to and above 100°C. Sometimes the generation of electrical power is coupled with the direct use of the geothermal heat to achieve the project's maximum efficiency. There are many proven ways and systems (Flash, Binary, Organic Rankine Cycle power plants to just name a view) to maximise the outcome of electricity generation and/or direct use of geothermal energy. These mechanisms are not subjects of this thesis and are therefore not further covered in detail. The least heat is required for geothermal heat pumps. Those heat pumps are typically installed with a type of shallow geothermal system (for example borehole heat exchanger or horizontal ground loop) that serves domestic purposes. Figure 1 shows a rough overview of the depth and temperature relationship of some geothermal applications. (Boden 2016, 9–14)
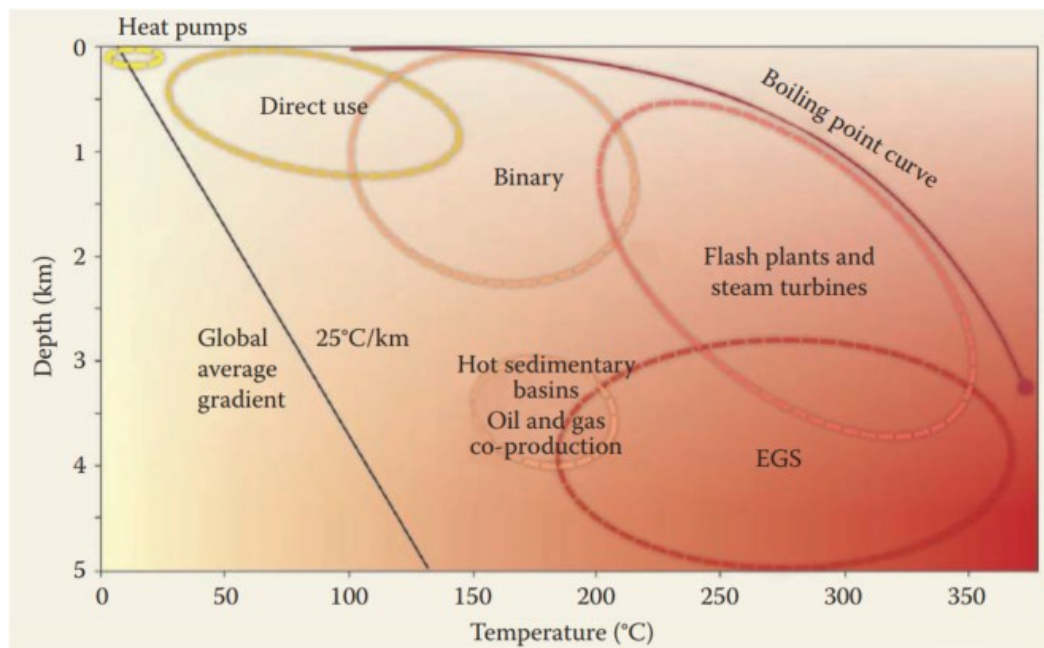
Figure 1: Temperature & depth correlation for geothermal applications (Boden 2016, 10)

EGS are a comparatively new technology that focuses on even deeper and hotter regions of the earth's crust as being shown in the previous Figure 1. An EGS is typically developed in hot, but relatively dry rocks with low permeability. These conditions are also called Hot Dry Rock (HDR), if no formation fluid is present at all and Hot Wet Rock (HWR) if the reservoir contains fluid, but the permeability is very low. There is little to no natural circulation of fluid inside the reservoir in these systems in contrast to conventional geothermal systems. Thus, any kind of circulation needs to be artificially enhanced or created. It is typically achieved by pumping cold water under high pressure into the area that needs stimulation, leading to an expansion of existing fractures and creating additional fractures caused by thermal contraction. Due to the hydraulic fracturing enhancement, the circulation of fluids within the reservoir can achieve economic levels. The cold injection water flows towards the production well(s) by travelling through the new and enhanced fractures. While moving from the injection well to the production well(s) the water heats up and then flows to the surface through the production well where it is used in a power plant to generate electricity. Finally, the produced water can be treated at the surface if necessary, to avoid complications while injecting the water once more to the reservoir. Figure 2 shows a concept EGS with the described close water loop. Many investigations have been undertaken to optimise the fracture process and determine a perfect hydraulic fracture job for geothermal reservoir enhancements such as the orientation of existing fractures, injection pressures needed, the spacing of injection and production wells and many more. For this thesis with another focus, a rough overview of the used mechanics is sufficient, and therefore those investigations are not further covered in more detail.

(Grant and Bixley 2011, 9-28 & 269–281; Stober and Bucher 2013, 165-181; Boden 2016, 323–364; Onay 2020, 1–4)
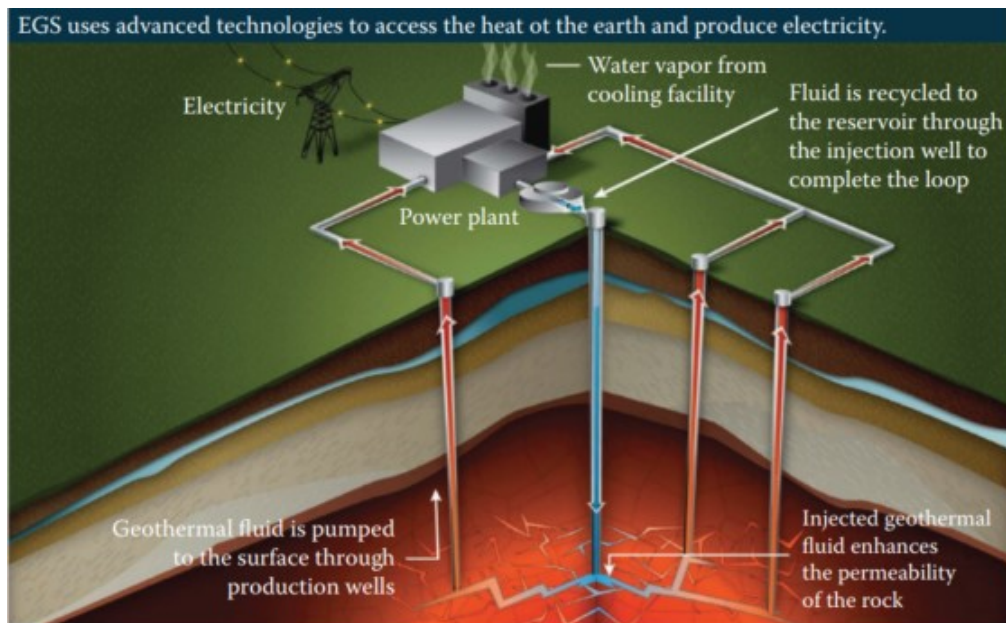
Figure 2: Concept of an enhanced geothermal system (Boden 2016, 324)

2.2 Essential Financial Aspects

The single most crucial factor to economic success of a geothermal project is the produced energy output over the project's expected lifetime, whether it is measured through the generation of power, the amount of direct heat used or a combination of both. While EGS projects come with many risks, they have been proven to be economical projects while providing green energy. Figure 3 shows a good overview of the occurring risks and actions needed to be undertaken in each EGS project phase.

(DiPippo 2016) suggests that for projects focused on the generation of electricity a geothermal temperature gradient of 35-40 [°C] and higher per kilometre, sufficient fluid circulation and an absolute reservoir temperature of 150 [°C] and above together with drilling depths between 5 and 7 kilometres or even lower are reasonable indications for an efficient project.

Further, it is suggested that for direct heat projects reasonable indications are an absolute reservoir temperature of 80 [°C] and above coupled with drilling depths of 3-5 kilometres in the vicinity of the location where the heat is being distributed and used (up to 1-2 kilometres).

The most of an EGS project's budget has to be invested before a guaranteed economic outcome can be assured. The core investments include:

- The exploration of the reservoir.
- Drilling and completion of the production and injection wells (includes material costs). This may also include exploratory wells. Such costs increase proportionally with well depth.
- Reservoir engineering measurements, such as the hydraulic stimulation of the reservoir for example.

- Construction of surface facilities, such as plants for power and/or heat generation. May include installing the geothermal fluid loop system, fluid treatment procedures (scaling, hazardous media such as hydrogen sulphide), and other surface facilities.

Additional costs like project planning, risk insurances, administrative costs, material replacements, taxes, and others need to be considered as well.

Finally, variable costs come to play during the operation phase once the EGS project is in place and fully developed. Variable costs include:

- Salaries for personnel
- Supply material
- Maintenance of subsurface equipment and surface facilities
- Auxiliary power (Applicable for direct heat plants without power generation).

(Huenges 2010, 373-421; DiPippo 2016, 499–533)

Phase	Risk characteristics	Information or action needed for next step
Needs determination	Low	Response to call for capacity Interpret demand based on unit retirement, change in technology or environmental standards Forecast cost-benefit assessment
Predrilling resource assessment	Moderate risk, moderate uncertainty, use of equity interest contributions	Develop geoscientific data Interpret and extrapolate oil and gas assessments
Resource assessment and permitting Phase 1	High risk, high uncertainty, use of venture capital	Test well assessment following exploratory or initial production wells Obtaining all regulatory approvals Securing any affected stakeholders' support, the emerging issue of the "social license"
Resource assessment and permitting Phase 2	High risk, high uncertainty	Drilling test injection and production wells and interpreting results, analyzing potential seismic risk (for EGS) Comprehensive cost-benefit analysis
Production and development of well complex, installation of generation facilities, interconnection permitted and built	Moderate risk, moderate uncertainty	Completion of the well complex, after interconnection and testing are complete
Operation	Low risk, low uncertainty	Grid payments and competition from conventional thermal resources such as coal or nuclear
Decommission of facility	Moderate risk, uncertainty over timing and the requirements at time of decommissioning	Agreement with permitting agency on applicable standards and fees

Figure 3: Phase and risk characteristics of an EGS project. (DiPippo 2016, 514)

2.3 Thermal Rock Properties

Importance has to be given to the geological aspects of the present stratigraphy in an area of interest while designing and developing a geothermal project. Thermal rock properties influence shallow geothermal installations as much as deep geothermal EGS, whether for direct heat usage or the generation of power purposes. Physical rock properties can be directly linked to the occurring temperatures (geothermal temperature gradient) in the reservoir and the rock layers above them. They can also give indications to the present pressure regimes.

A short introduction to rock properties related to the storage and transport of heat and fluids in the subsurface is presented in this chapter. Those properties include thermal conductivity, specific heat capacity, heat production, and hydraulic related properties such as porosity and permeability. All rocks possess a certain number of voids presented as pores and fractures, possibly filled with fluids (water or gas). The governing factor for the amount and degree of pores is the porosity. Permeability indicates the ability of these fluids to pass through the porous rocks. While the permeability and porosity play a role in developing a geothermal reservoir, those aspects are too vast to cover more in detail.

Two primary mechanisms can transport geothermal heat. These mechanisms are heat transfer by conduction through rocks and by a moving fluid passing through rocks, a mechanism referred to as advection. The internal energy supply of a geothermal reservoir is mostly caused by heat conduction across the impenetrable rock layers beneath it.

A rocks' thermal conductivity describes the ability to transport heat and varies for different types of rocks (see Figure 4). Crystalline rocks such as granites and gneisses conduct heat 2-3 times better than unconsolidated materials, for example, sand and gravel. The thermal conductivity of rocks is generally anisotropic. It depends on the rock's composition, different degrees of compaction, cementation, alteration, and the rocks' layering and structuring.

The temperature distribution in the rock formations is not uniform. If significant deviations are present, the anomalies are named positive or negative. Geological causes for positive anomalies can include active volcanism, upwelling hot deep water of hydrothermal systems, and large rock volumes with high thermal conductivity such as rock salt deposits. Salt diapirs conduct more heat to the surface than other surrounding layers of sedimentary rocks, which means high heat flow channels in the salt diapirs. Thick insulating layers such as shales with low thermal conductivity are often strongly anisotropic. They may decelerate the heat transfer to the surface. Unusually high heat production originating from rocks due to natural radioactivity can also be a reason of heat anomalies. Positive anomalies are prime target areas for geothermal projects' location because their exploration and development require smaller drilling depth compared to areas where no anomalies are present.

(Stober and Bucher 2013, 1–13; Bauer et al. 2014, 1–17; Tóth and Bobok 2016, 77–92)

Rocks/fluids	Thermal conductivity λ [J s^{-1} m^{-1} K^{-1}]	Specific heat capacity [kJ kg^{-1} K^{-1}]
Gravel, sand dry	0.3–0.8	0.50–0.59
Gravel, sand wet	1.7–5.0	0.85–1.90
Clay, loam moist	0.9–2.3	0.80–2.30
Limestone	2.5–4.0	0.80–1.00
Dolomite	1.6–5.5	0.92–1.06
Marble	1.6–4.0	0.86–0.92
Sandstone	1.3–5.1	0.82–1.00
Shale	0.6–4.0	0.82–1.18
Granite	2.1–4.1	0.75–1.22
Gneiss	1.9–4.0	0.75–0.90
Basalt	1.3–2.3	0.72–1.00
Quartzite	3.6–6.6	0.78–0.92
Rocksalt	5.4	0.84
Air	0.02	1.0054
Water	0.59	4.12

Figure 4: Thermal Properties of different Rock Types (Stober and Bucher 2013, 9)

2.4 Geothermal Fluid

Geothermal fluid is a general term which may refer to the brine in a regular geothermal reservoir or the working fluid in an EGS.

Geothermal brine in a regular geothermal reservoir can be classified into four categories based on their main ion content:

- Alkali-chloride water with pH ranges between 4 and 11 are least common in young rocks. These are mostly sodium and potassium chloride waters, although in brines the calcium concentration is often significant. Alkali-chloride water is found, for example, in some mature geothermal waters in Iceland.
- Acid sulphate water is water that results from the oxidation of hydrogen sulphide to sulphate near the surface, and most of its components are dissolved from the surface rock. These waters are generally not a good indication for subsurface properties.
- Acid sulphate-chloride water may be a mixture of alkali chloride water and acid sulphate water. It can also result from the oxidation of hydrogen sulphide to sulphate in alkali-chloride water or dissolution of sulphur from rock followed by oxidation. This type of water may reflect an equilibrium subsurface and can be used for prediction of geological properties.
- Bicarbonate water may result from carbon dioxide-rich water. This type is relatively common in old geothermal waters. They are frequently at equilibrium and may be used to predict subsurface properties.

Changes in the operating temperature or pressure or the ion concentration in the geothermal water may lead to precipitations, so-called scales. These scales can lower the geothermal well's productivity since they represent an additional obstacle in the flow path. Scaling leads, on the one hand, to higher pressure losses in the tubular, on the other hand, it can lead to corrosion as a consequence.

(Gunnlaugsson et al.; Stober and Bucher 2013, 255-277; Boden 2016, 232–234; DiPippo 2016, 443–452; Wood Group Intetech Ltd 2017, 96)

As working fluids for EGS with a purely artificially created reservoir, one often refers to simple water, but carbon dioxide is acknowledged as a decent alternative. Both approaches have their pros and cons and also depend on the prevailing conditions. The specific heat capacity of water is higher than the carbon dioxide's, which leads to the fact that water can extract more heat from the earth if the same flow rate is applied. Water consumes more pressure inside the reservoir, and its pressure decrease is more significant with increasing flow rates. Thus, carbon dioxide requires lower injection pressures for high flow rates compared to water. The density of water mainly depends on the temperature, and only a smaller contribution falls to the effects of pressure changes. Carbon dioxide is also temperature-dependent, but more critically, its density varies significantly with higher pressures applied. (Liu et al. 2019)

For this investigation, only water is considered as a working fluid.

2.4.1   Properties of Water

Water is one of the most diverse chemical compounds known to humankind. While water features many properties for all sorts of applications, not all can be discussed here. Only a few properties, namely the density, the specific heat capacity (amount of energy that can be extracted from a geothermal reservoir and stored in water) and the dynamic viscosity (resistance of water to flow) are of interest.

As mentioned before, water density depends mainly on the temperature and to a lesser extent on the pressure. The specific heat capacity and dynamic viscosity exhibit similar behaviours, with the main influencing factor being temperature.

To gain detailed information about water properties at different temperature and pressure points, literature containing detailed tables such as (Kretzschmar and Wagner 2019) or (Pang 2014, 89-202) may be helpful.

Nowadays, this kind of information is also available online, making it more accessible to everyone, for example, on www.engineeringtoolbox.com or www.peacesoftware.de. Values from the internet are always to be used cautiously and must be cross-referenced to be validated.

(Tóth and Bobok 2016, 94) take into account the temperature dependency of the water density with a linear temperature gradient and the depth (Equation 1). This equation is used to estimate the density of water at different temperatures and depths. The temperature effects on the

dynamic viscosity and the specific heat capacity are not automatically accounted for and are subject to user supervision. Once the values for the dynamic viscosity and specific heat capacity are verified through the user, these values are assumed to be constant for the whole completion length.

$$\rho_{Water,Temp,Dn} = \rho_{Water,Surface} * \left(1 - A_T * \left(\frac{dT}{dD}\right)_{Formation} * D_{n,TVD} - B_T * \left(\frac{dT}{dD}\right)_{Formation}^2 * D_{n,TVD}^2\right)$$

Equation 1

Where $\rho_{Water,Temp,Dn}$ is the temperature-accounted water density at depth n [kg/m³], $\rho_{Water,Surface}$ is the density of water under surface conditions [kg/m³], $\left(\frac{dT}{dD}\right)_{Formation}$ is the linear geothermal temperature gradient of the formation [°C/m], $D_{n,TVD}$ is the TVD at depth n [m], A_T is a constant and equals $1{,}712 * 10^{-4}$ [1/°C], B_T is a constant and equals $3{,}232 * 10^{-6}$ [1/°C²].

2.5 Temperature and Pressure Evaluation

To differentiate between a regular and a purely artificially created geothermal reservoir, they are labelled as regular geothermal reservoirs and EGS. The term geothermal reservoir refers to both regular and EGS.

Tapping in a geothermal reservoir, means that heat and mass in the form of the reservoir's water are being withdrawn. Some fraction of this reservoir fluid (for regular reservoirs this usually is some sort of brine) or working fluid (water and carbon dioxide are commonly used in EGS) may be reinjected to the reservoir after possible treatment processes. Additionally, hot or cold recharge fluid may flow naturally into a regular geothermal reservoir. Thus, temperature and pressure are no static values over a geothermal reservoir's lifetime while undergoing production and/or injection cycles.

A simple concept of the geothermal fluid flow regime in a geothermal reservoir is the correlation of liquid water flow in a confined aquifer. If the current temperature in a reservoir is reasonably uniform, the flow can be understood as isothermal. Temperature distribution within the geothermal reservoir with a present reinjection of cold fluids can be modelled and computed with a motion of thermal changes along streamlines. Figure 5 shows such a typical liquid flow in a liquid only regular geothermal reservoir, including pressure and temperature responses on injection and production wells. Analogies can also be made to EGS. While an initial pressure increase can be seen at the injection well, it quickly flattens to an almost steady horizontal line until a pressure drop occurs at the production well. In reality, the water's pressure response in the reservoir also depends on producer and injector flow rates besides many other factors. The cold water of the injection well has an almost steady cooling effect on the formation for a certain distance until a jump indicates a transition, and the almost steady heating of the waterfront towards the production well. (Grant and Bixley 2011, 9–28)
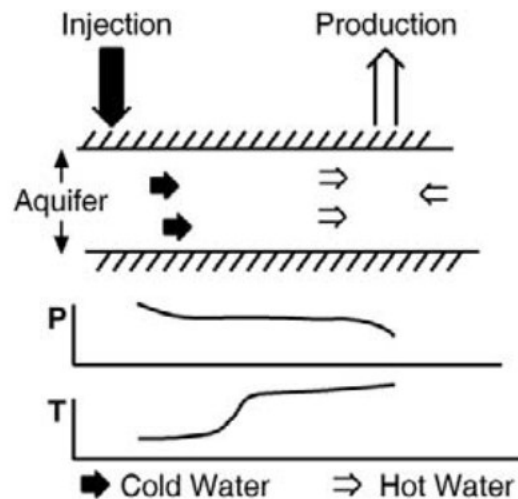
Figure 5: Liquid flow in an exploited liquid reservoir (Grant and Bixley 2011, 24)

Many scientific proposals for models governing geothermal fields (more than one injection and/or production wells in the same reservoir) and reservoirs with a mixture of liquid water and water vapour have been published up until now. In the presence of water vapour, reservoirs can further be classified as liquid or vapour dominated.

While these considerations are justified, they do not play an essential role in the buckling analysis and would somewhat complicate the application's development and the underneath lying models.

Thus, for the sake of simplification, a liquid-only geothermal reservoir with a single-phase water flow is considered in this thesis. The production water rising up to the surface and the injection water being pumped to the bottom of the well is both times single-phase liquid water.

For the buckling investigation at hand, also a steady-state flow of fluids is considered. Steady-state flow refers to no change in reservoir-related properties such as pressure, temperature, and velocity of the fluid concerning time or position (in this case, the production or injection well). In Figure 5, this would refer to the start and endpoints of the pressure and temperature graphs. There is no accumulation or loss of mass implied for a steady-state condition for geothermal reservoirs with an injective and productive mass flow rate.

Steady-state flow is more applicable to laboratory displacement experiments than to real-life scenarios. Nevertheless, it can be seen in reservoirs undergoing pressure maintenance either by water or gas injection or when a regular geothermal reservoir is completely recharging and supported by a substantial aquifer. Such a scenario is applicable for this simple liquid only EGS reservoir with one production and one injection well. Maintaining the pressure balance means that, the water's injected mass must be the same as the withdrawn mass. A pressure balance also implies a nearly perfect flow path from the injector to the producer, which allows all injected water to reach the producer without losses to the formation. Temperature maintenance can be assumed if the well spacing between injector and producer is adequate,

and the injected working fluid is allowed to reheat while flowing to the production well. At the same time, reservoir cool down effects over time are neglected. (Okotie and Ikporo 2019, 19-56)

Surface conditions such as the temperature $T_{Surface}$ and the pressure $P_{Surface}$ are to be defined as 20 [°C] and 1,01325 [bar] (1 [atm] or 1,01325*10^5 [Pa]). The water density under surface conditions $\rho_{Water,Surface}$ is 1000 [kg/m³]. The specific heat capacity and dynamic viscosity of water under surface conditions are 4150 [J/kg°C] and 1,0005 [cP] respectively.

For the following equations, it is essential to note that the reference point for the depth (0 meters) is the surface. Any depth below the surface is denoted with a positive sign. For example, the reservoir depth is considered positive, even if the reservoir is subsurface.

The equations are accounted for a possible change in direction with the appropriate sign. Thus, values for depth can always be used as positive values per convention.

2.5.1 Reservoir Temperature

Typically, geothermal temperature gradients are used to calculate the reservoir's temperature (Equation 2). An overall representable gradient for the whole depth can also be a good approximation if no individual gradient data is available.

$$T_{Reservoir} = T_{Surface} + \sum_{i=1} \left(\frac{dT}{dD}\right)_{Formation,i} * D_{i,TVD} \qquad \text{Equation 2}$$

Where $T_{Reservoir}$ is the reservoir temperature [°C], $T_{Surface}$ is the surface temperature [°C], $\left(\frac{dT}{dD}\right)_{Formation,i}$ is the geothermal temperature gradient of the formation section i [°C/m], $D_{i,TVD}$ is the TVD of section i [m].

2.5.2 Heat Transfer & Temperature Distribution inside the Tieback

The German guide for casing, tubing & liner calculations (*Leitfaden Futterrohrberechnung* 2006. Wirtschaftsverband Erdöl- und Erdgasgewinnung e.V.) suggests a simple approach to calculate the temperature distribution for production tubular or liners. A linear geothermal temperature gradient (Equation 3) or derived from the absolute reservoir temperature (Equation 4) can be used to determine the completion temperature at a certain depth of interest. Suppose no linear geothermal temperature gradient from the surface to reservoir TVD is provided. In that case, a good approximation can be achieved by simply dividing the absolute reservoir temperature (surface temperature subtracted) through the TVD of the reservoir.

While being simple, the approach gives a good indication of the temperature distribution with respect to the well's depth. Still, it requires the expected wellhead temperatures during production or while shut-in, with the well to be considered steady-state behaviour concerning the temperature.

$$T_{Dn} = T_{Wh,P/S} + \frac{\left(\frac{dT}{dD}\right)_{Formation} * D_{Res,TVD} + T_{Surface} - T_{Wh,P/S}}{D_{Res,TVD}} * D_{n,TVD} \qquad \text{Equation 3}$$

Where T_{Dn} is the temperature at a depth n [°C], $T_{Wh,P/S}$ is the expected wellhead temperature during production or while shut-in [°C], $\left(\frac{dT}{dD}\right)_{Formation}$ is the linear geothermal temperature gradient of the formation [°C/m], $D_{Res,TVD}$ is the reservoir TVD [m], $T_{Surface}$ is the surface temperature [°C], $D_{n,TVD}$ is the TVD at depth n [m].

$$T_{Dn} = T_{Wh,P/S} + \frac{T_{Reservoir} + T_{Surface} - T_{Wh,P/S}}{D_{Res,TVD}} * D_{n,TVD} \qquad \text{Equation 4}$$

Where T_{Dn} is the temperature at a depth n [°C], $T_{Wh,P/S}$ is the expected wellhead temperature during production or while shut-in [°C], $T_{Reservoir}$ is the reservoir temperature [°C], $T_{Surface}$ is the surface temperature [°C], $D_{Res,TVD}$ is the reservoir TVD [m], $D_{n,TVD}$ is the TVD at depth n [m].

(*Leitfaden Futterrohrberechnung* 2006. Wirtschaftsverband Erdöl- und Erdgasgewinnung e.V., 58)

Other authors suggest a more complex approach for calculating the temperature distribution of a single-phase fluid column inside the tieback. The temperature of the produced geothermal fluid can considerably decrease from the reservoir to the wellhead. Conversely, the injection water undergoes an increase in temperature from the wellhead to the reservoir. The upflowing fluid temperature is higher during production than the surrounding formation around the well. During injection, the downflowing fluid features a lower temperature than the surrounding formation. This temperature difference induces a radial heat flow from the well outward to the surrounding formation while producing and from the formation inward to the well while injecting water. As the temperature difference between the fluid and the rock decreases the radial heat flow is also reduced. The temperature of the surrounding formation increases or decreases in a prolonged transient process. The time dependency is caused by the large rock volume surrounding the well. Therefore, the reservoir water's temperature at the wellhead continuously increases during production until a steady-state is achieved. Conversely, the injection water's temperature at reservoir depth continuously decreases with time. Literature suggests that a steady-state can be achieved after around 30 days. Governing rock properties are here the thermal conductivity and thermal diffusivity of the formation.

The heat transfer of the flowing fluid inside the tieback is considered to be forced convection. The heat transfer through the tieback (and perhaps coating) and any present casing and cement sections are considered conductive. The annulus fluid usually is not in movement and features a free convective heat transfer. Finally, the surrounding formation is dominated by a conductive heat transfer. Figure 6 shows a temperature distribution considering the just mentioned thermal resistances.
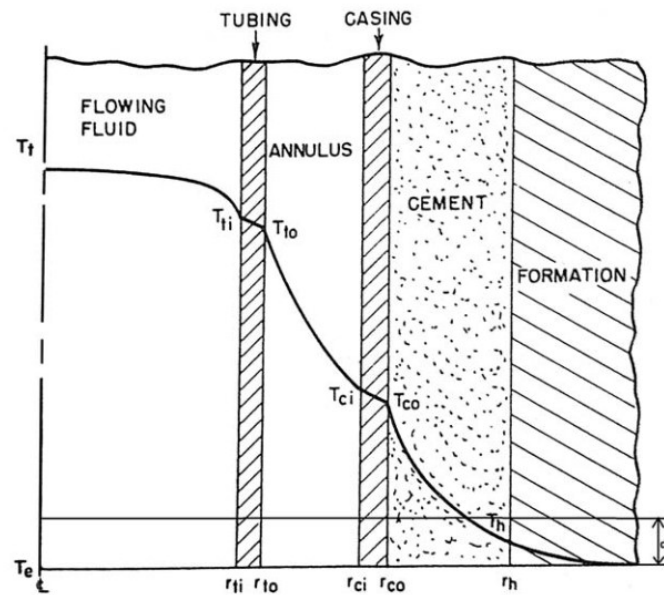
Figure 6: Heat transfer through completion and formation (Tóth and Bobok 2016, 183)

For a detailed calculation, all thermal resistances around the water inside the tieback need to be considered serially. These may include the tieback and any present completion elements such as coatings or insulations, annulus fluid(s), and casing and cement section(s), depending on completion type and depth. The thermal resistance from the surrounding formation usually is the most significant element.

Thus, thermal resistances of completion elements are considered to affect temperature distribution calculations far less than the thermal resistance of the formation. The effect of intermediate elements subject to heat transfer between the water inside the tieback and the formation is even more diminished after more extended periods when said elements equilibrate with the water temperature.

The temperature distribution with respect to the well's depth is also a transient function of the elapsed time and the mass flow rate of either the reservoir water during production or the injection water. Elapsed time refers to the time since the well has been switched from its previous state to its current operation mode (namely production or injection).

Influencing physical and thermal properties like the heat transfer coefficient and the heat conduction change with different completion stages and temperatures and thus the depth. Nevertheless, they need to be assumed constant with respect to the completion depth for calculations purposes. This assumption is generally acknowledged for steady-state flow conditions. Convective heat transfer coefficients for forced convection strongly depend on flow parameters and fluid properties such as the roughness of tieback's surface, and the presence of laminar or turbulent flow, the average velocity, the specific heat capacity, the thermal conductivity, the thermal expansion coefficient and the viscosity of the fluid inside the tieback. The convective heat transfer inside the tieback becomes more dominant compared to the other heat transfer mechanisms for higher mass flow rates. Hence more heat is lost to (production)

or incorporated from (injection) the formation through conductive means with lower mass flow rates. One way to obtain an overall heat transfer coefficient of the completion is by analysing wellhead flowing temperature logs.

Numerous assumptions would be necessary to complete a detailed heat transfer calculation considering all elements. Many thermal properties like heat transfer coefficients and thermal conductivities of all completion elements are not provided because they are not directly necessary for buckling analysis. An estimation or calculation of all the missing variables may lead to more significant errors and falsified results.

Given the vast number of influencing factors and the before mentioned assumptions leads to the conclusion that the temperature distribution and with it, the underlying heat transfer calculations is simplified. They only include the influence of the surrounding rock formations (thermal conductivity and thermal diffusivity), the specific heat capacity of reservoir or injection fluid, the depth, the tieback dimensions (radius of the most extended section to be considered representable for the whole depth), the mass flow rates and the elapsed time. No thermal resistance elements in-between are considered to be present. An excellent estimation of the expected temperature distribution with respect to depth can be expected since the resistance to heat transfer into the surrounding rock is the most significant.

Equation 5 has been presented to obtain the temperature distribution during production. For Equation 5, it is assumed that the inflowing water temperature at the reservoir is the same as the downhole reservoir temperature and that the inflow takes place at reservoir depth. Equally important is Equation 6 for the temperature distribution during the injection.

These solutions refer to an instantaneous moment of the heating or cooling process, a snapshot of the time-dependent temperature distribution. Equation 5 and Equation 6 show that the fluid temperature decreases from the bottom of the well up to the wellhead and increase in the other direction exponentially.

The mass flow rate is, together with the specific heat capacity of water, incorporated in diffusion depth D_{Diff}, which serves as a scaling factor for the temperature distribution functions. The diffusion depth is calculated equally for producing or injecting temperature distributions.

Another strong influence is made by the elapsed time in the heat conduction function of the formation $f(t)$. The transient function $f(t)$ has, especially for later times, a relatively weak influence and values change only very little. Calculating results with times below 7 days becomes increasingly inaccurate due to the nature of the transient function $f(t)$. Times equal to and greater than 30 days are considered to lead to a steady-state well. Every time a well is shut-in, the temperature distribution slowly begins to move toward the natural geothermal temperature profile outline, correlating with the findings of Equation 3 and Equation 4.

Reservoir parameter such as the thermal conductivity and thermal diffusivity of the surrounding formation are also playing their roles in the diffusion depth A and the transient function $f(t)$.

$$T_{Dn,Pro} = T_{Surface} + \left(\frac{dT}{dD}\right)_{Formation} * \left(D_{n,TVD} + D_{Diff}\right) - \left(\frac{dT}{dD}\right)_{Formation} * D_{Diff} *$$
$$e^{\frac{D_{n,TVD} - D_{Res,TVD}}{D_{Diff}}}$$

Equation 5

Where $T_{Dn,Pro}$ is the temperature at a depth n during production [°C], $T_{Surface}$ is the surface temperature [°C], $\left(\frac{dT}{dD}\right)_{Formation}$ is the linear geothermal temperature gradient of the formation [°C/m], $D_{n,TVD}$ is the TVD at depth n [m], D_{Diff} is the diffusion depth [m], $D_{Res,TVD}$ is the reservoir TVD [m].

$$T_{Dn,Inj} = T_{Surface} + \left(\frac{dT}{dD}\right)_{Formation} * \left(D_{n,TVD} - D_{Diff}\right) + \left(T_{Injection} - T_{Surface} + \right.$$
$$\left. \left(\frac{dT}{dD}\right)_{Formation} * D_{Diff}\right) * e^{\frac{-D_{n,TVD}}{D_{Diff}}}$$

Equation 6

Where $T_{Dn,Inj}$ is the temperature at a depth n during injection [°C], $T_{Surface}$ is the surface temperature [°C], $\left(\frac{dT}{dD}\right)_{Formation}$ is the linear geothermal temperature gradient of the formation [°C/m], $D_{n,TVD}$ is the TVD at depth n [m], D_{Diff} is the diffusion depth [m], $T_{Injection}$ is the injection water temperature at the wellhead [°C].

$$D_{Diff} = \frac{\dot{m} * c_W * f(t)}{2 * \pi * K_{Formation}}$$

Equation 7

Where D_{Diff} is the diffusion depth [m], $\dot{m}$ is the mass flow rate [kg/s], c_W is the specific heat capacity of water [J/kg°C], $f(t)$ is a dimensionless time-dependent heat conduction function of the formation [-], $K_{Formation}$ is the average thermal conductivity of the formation [W/m°C].

$$f(t) = -\ln\frac{r_{Tieback,O}}{2 * \sqrt{\kappa_{Formation} * time}} - 0,29$$

Equation 8

Where $f(t)$ is a dimensionless time-dependent heat conduction function of the formation [-], $r_{Tieback,O}$ is the outer radius of a representable tieback section [m], $\kappa_{Formation}$ is the average thermal diffusivity of the formation [m²/s], $time$ is the elapsed time since the well has been switched from its last state [s].

(Ramey 1962; Durrant and Thambynayagam 1986; Hagoort 2004; Bellarby 2009, 278–282; Grant and Bixley 2011, 118–119; DiPippo 2016, 158-161; Tóth and Bobok 2016, 181–194; Naterer 2018, 23–149; Stephan et al. 2019, 17-36 & 709-748 & 759-783 & 803-811; Forsberg 2021, 1-9 & 23-34 & 57-78 & 211-304)

Equation 5 to Equation 8 are used to obtain temperature distribution values for the shut-in, production and injection state in the MATLAB application with a minimum of 1 day elapsed time (30 to be recommended).

Visualisations of this chapter's findings can be seen in Figure 7 to Figure 11. Mass flow rate and time dependency have been calculated with the case study information provided by Erdwerk, which will be presented later in more detail.

Constant average values for the thermal conductivity, thermal diffusivity and specific heat capacity of water are assumed along with depth and under varying temperatures. The specific water heat capacity of 4100 [J/kg°C] (for production and injection). (Noack et al. 2012) investigated the geological area of interest in detail. An average formation thermal conductivity of 2 [W/mK] can be assumed. (Grant and Bixley 2011, 119) and (DiPippo 2016, 160) suggest that the thermal diffusivity of rocks do not vary greatly and that 1 $[10^{-6}m^2/s]$ is a representable value for many geothermal rocks.

The linear geothermal temperature gradient is calculated from the absolute reservoir temperature and the total reservoir TVD. Even though the tieback is not run until reservoir TVD (additional stainless-steel liner in place), we use this depth as starting and endpoint for a complete temperature distribution along with the depth. The tiebacks representable outer radius for the most extended section is 0,0889 [m] (from 7 [inch] OD), which also collides with the stainless-steel liner OD below the tieback.

For the simulation of a shut-in, a sparse almost non-existential mass flow rate of 0,001 [kg/s] has been used to obtain values for the shut-in temperature distribution after 30 [days] of elapsed time (Figure 11).
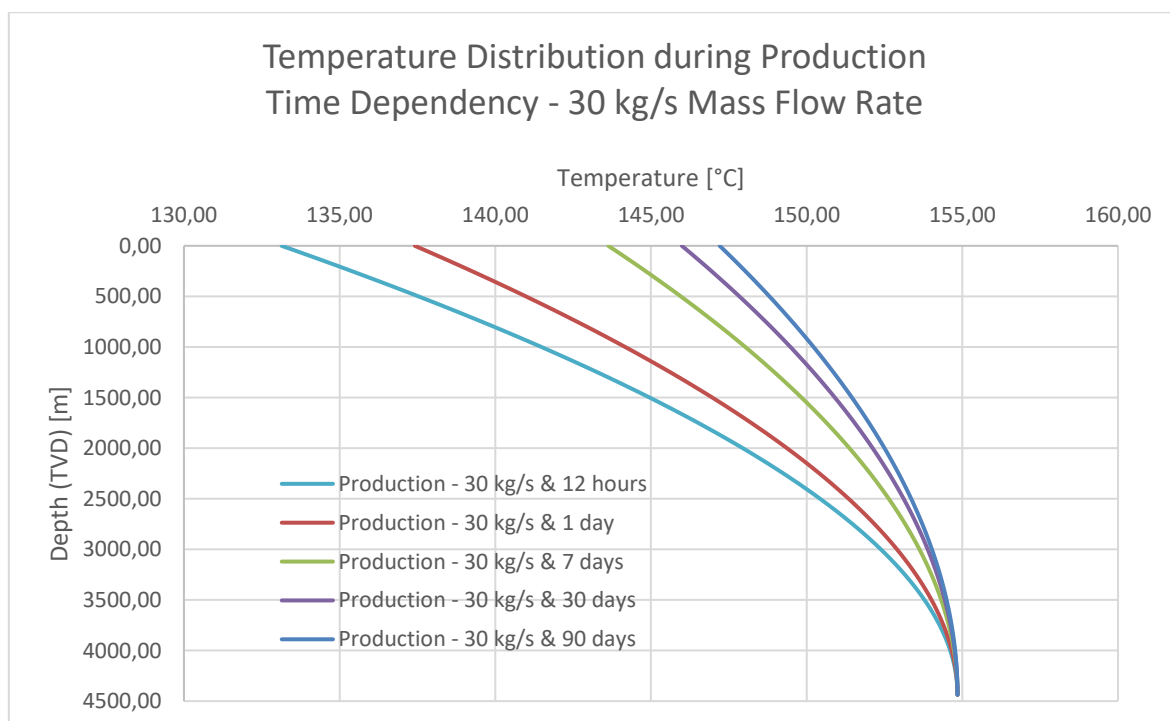

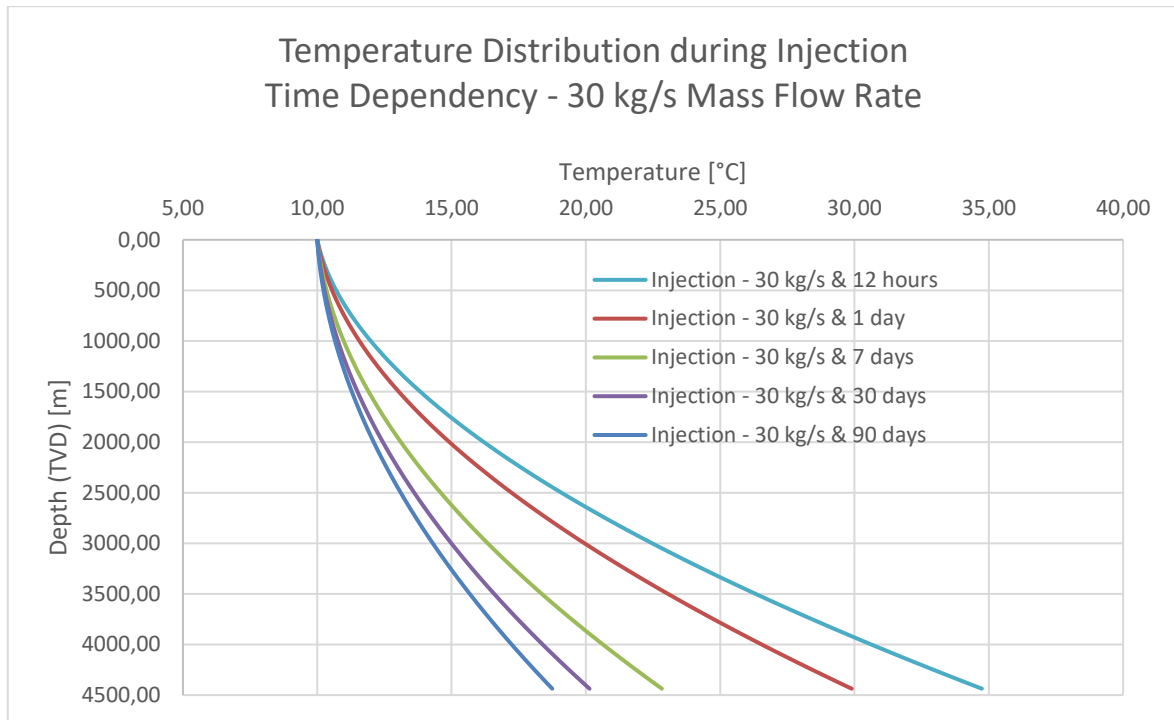Figure 7: Temperature distribution during production with varying times

Figure 8: Temperature distribution during injection with varying times
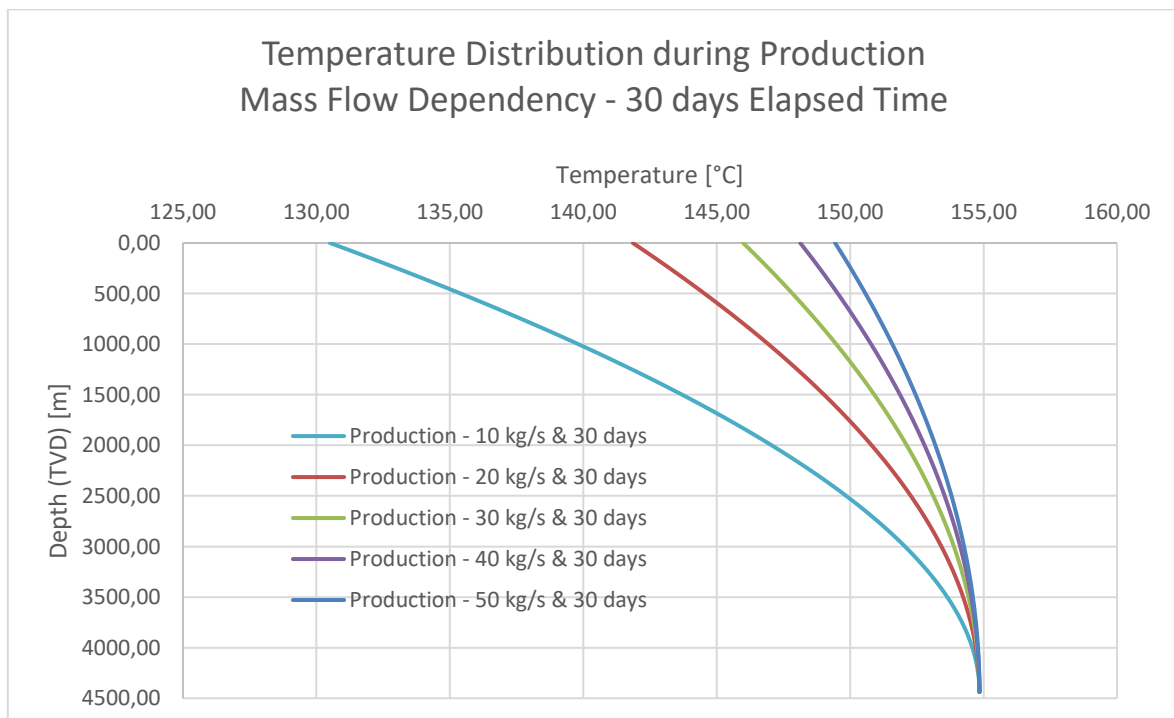

Figure 9: Temperature distribution during production with varying mass flow rates
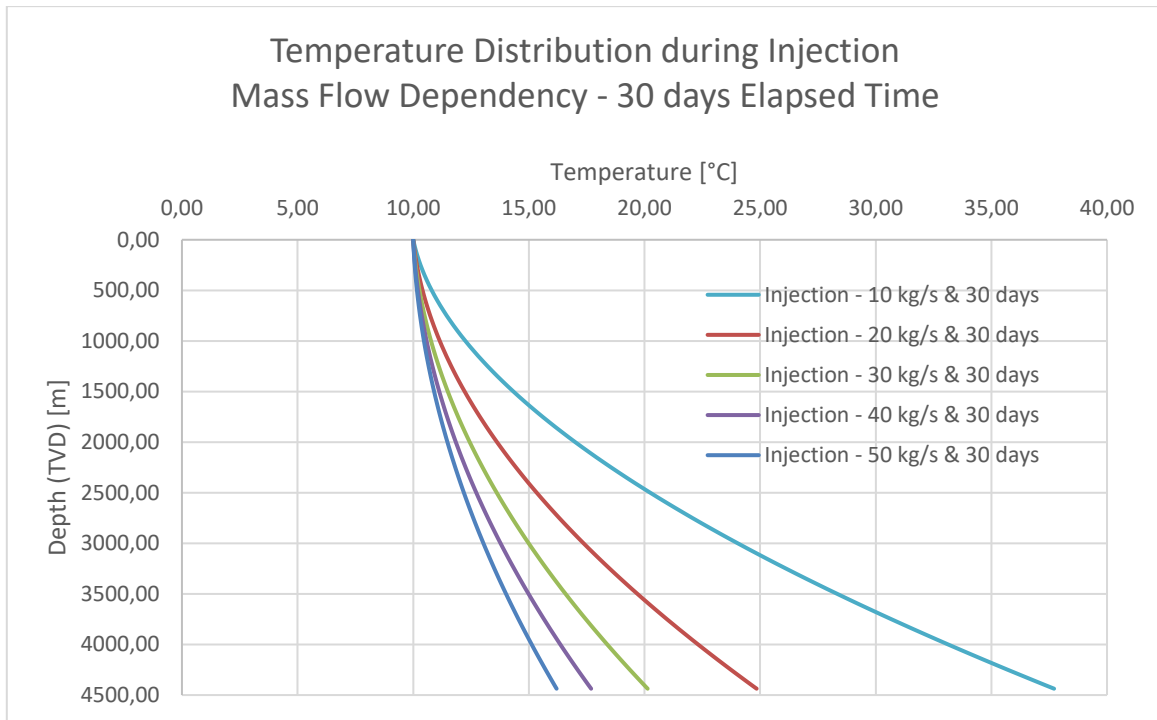
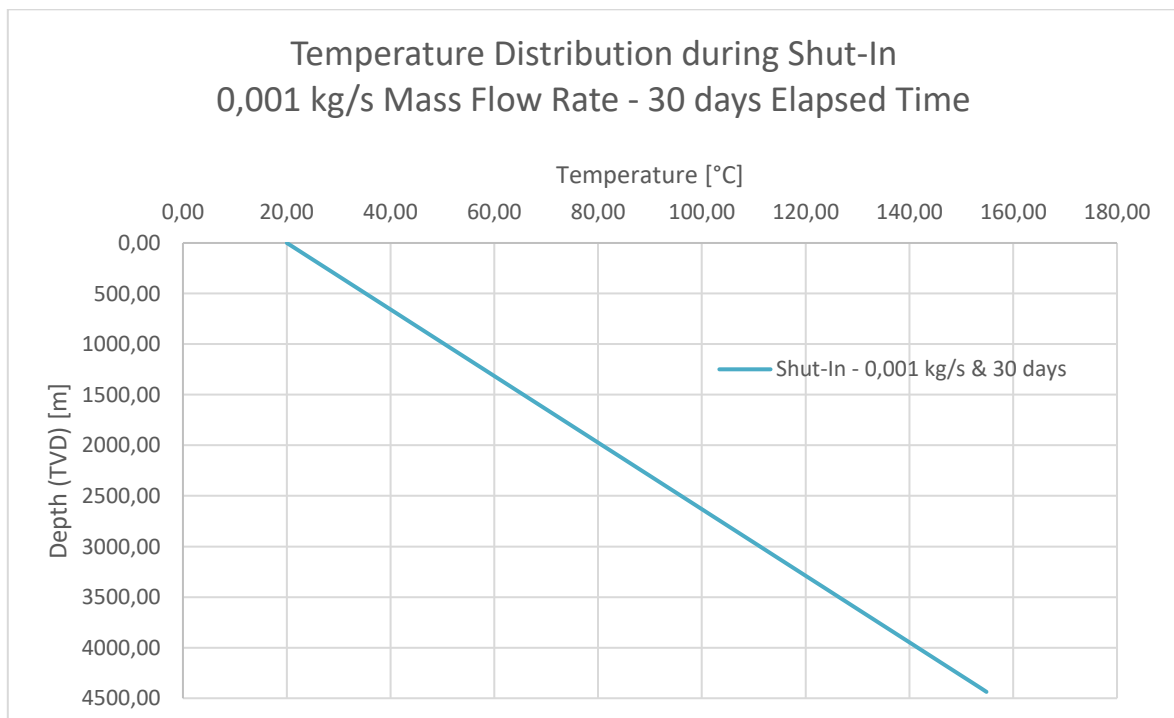Figure 10: Temperature distribution during injection with varying mass flow rates

Figure 11: Temperature distribution during Shut-In

2.5.3   Pressure Mechanics

A regular geothermal reservoir's pressure can be calculated with reasonable accuracy with a pressure gradient if representable values for the prevailing conditions are available. See Equation 9.

Alternatively, if no reliable pressure gradient is available, the reservoir pressure can be calculated using the reservoir brine's density.

The hydraulic water pressure gradient varies with the chemical composition, with the driving factors being the salinity and the content of dissolved solids contained in the water. A typical value for a water pressure gradient is suggested to be 0,45 [psi/ft], which is about 0,1018 [Pa/m]. The reservoir's brine density may vary under the prevailing conditions and needs to be assessed individually for each project.

By using TVD values to obtain hydrostatic pressures, the actual pressure at the depth is calculated, considering all possible deviations and inclinations.

Equation 9 and Equation 10 represent the most simplistic mathematical background to calculate the reservoir pressure in an undisturbed regular geothermal reservoir.

$$P_{Reservoir} = P_{Surface} + \left(\frac{dP}{dD}\right)_{Water} * D_{Res,TVD} \qquad\qquad \text{Equation 9}$$

Where $P_{Reservoir}$ is the reservoir pressure [Pa], $P_{Surface}$ is the surface pressure [Pa], $\left(\frac{dP}{dD}\right)_{Water}$ is the linear hydraulic water pressure gradient of the formation [Pa/m], $D_{Res,TVD}$ is the reservoir TVD [m].

$$P_{Reservoir} = P_{Surface} + \rho_{Brine} * g * D_{Res,TVD} \qquad\qquad \text{Equation 10}$$

Where $P_{Reservoir}$ is the reservoir pressure [Pa], $P_{Surface}$ is the surface pressure [Pa], ρ_{Brine} is the density of the brine inside the reservoir [kg/m³], g is the gravitational acceleration and equals 9,81 [m/s²], $D_{Res,TVD}$ is the reservoir TVD [m].

A more detailed approach to calculating the hydrostatic pressure has been presented by (Tóth and Bobok 2016). They suggest using a water density $\rho_{Water,Surface}$ under surface conditions and make use of the correlation introduced previously in Equation 1. As mentioned before, the water density decreases with an increasing temperature distribution along with the depth. By integration of Equation 1 with respect to the depth and surface pressure, Equation 11 is obtained. It is a good approximation and another more in-depth approach to calculate the reservoir pressure. It implies the underlying assumption that the reservoir is purely hydrostatic.

The pressure of an undisturbed regular geothermal reservoir is described in Equation 11. This equation can also be used with a minor modification to obtain the pressure distribution for a shut-in well if given sufficient time to equilibrize with the surrounding formation (Equation 12).

$$P_{Res,Temp} = P_{Surface} + \rho_{Water,Surface} * g * \left(D_{Res,TVD} - A_T * \left(\frac{dT}{dD}\right)_{Formation} * \right.$$
$$\left. \frac{D_{Res,TVD}^2}{2} - B_T * \left(\frac{dT}{dD}\right)_{Formation}^2 * \frac{D_{Res,TVD}^3}{3} \right)$$

Equation 11

Where $P_{Res,Temp}$ is the temperature-accounted pressure of an undisturbed reservoir [Pa], $P_{Surface}$ is the surface pressure [Pa], $\rho_{Water,Surface}$ is the density of water under surface conditions [kg/m³], g is the gravitational acceleration and equals 9,81 [m/s²], $D_{Res,TVD}$ is the reservoir TVD [m], $\left(\frac{dT}{dD}\right)_{Formation}$ is the linear geothermal temperature gradient of the formation [°C/m], A_T is a constant and equals $1,712 * 10^{-4}$ [1/°C], B_T is a constant and equals $3,232 * 10^{-6}$ [1/°C²].

$$P_{Dn,Shut,Temp} = P_{Surface} + \rho_{Water,Surface} * g * \left(D_{n,TVD} - A_T * \left(\frac{dT}{dD}\right)_{Formation} * \right.$$
$$\left. \frac{D_{n,TVD}^2}{2} - B_T * \left(\frac{dT}{dD}\right)_{Formation}^2 * \frac{D_{n,TVD}^3}{3} \right)$$

Equation 12

Where $P_{Dn,Shut,Temp}$ is the temperature-accounted pressure during shut-in [Pa], $P_{Surface}$ is the surface pressure [Pa], $\rho_{Water,Surface}$ is the density of water under surface conditions [kg/m³], g is the gravitational acceleration and equals 9,81 [m/s²], $D_{n,TVD}$ is the TVD at depth n [m], $\left(\frac{dT}{dD}\right)_{Formation}$ is the linear geothermal temperature gradient of the formation [°C/m], A_T is a constant and equals $1,712 * 10^{-4}$ [1/°C], B_T is a constant and equals $3,232 * 10^{-6}$ [1/°C²].

(Dake 1978, 1-10; DiPippo 2016, 141–147; Tóth and Bobok 2016, 93–105; Okotie and Ikporo 2019, 323-337)

With Bernoulli's general pressure equation and some adjustments to represent flow in a well we get Equation 13 and Equation 14. These equations satisfy the need to obtain absolute pressure at any depth within the producing (Equation 14) or injecting (Equation 13) well of an EGS. As already shown in the previous chapter, an injector and producer's temperature distribution approach the starting temperature after more extended periods. Thus, without significant errors, we can assume constant water density along with the depth from the surface to the bottom of the well and vice versa. The injector's water density is under surface conditions (may vary depending on the water temperature at the injection point). To obtain appropriate values for the water density of the heated water in the reservoir Equation 1 can be used.

The equations consider any applied wellhead pressure to an injector or bottomhole pressure of a producer, the water column's hydrostatic pressure (with temperature-reduced density for producer), and frictional pressure losses. Pressure losses in Equation 13 and Equation 14 are always denoted negative and are accumulative with greater depth. Their calculation is covered in the next chapter in more detail. The pressure that is considered to be the reservoir pressure of the EGS is denoted bottomhole pressure P_{Bottom} to not confuse it with the purely hydrostatic reservoir pressure of regular geothermal reservoirs.

For the sake of simplifying the investigation, we consider the previously mentioned mass and pressure balance. Thus, a geothermal doublet (one injection and one producer) is tapped in an ideal reservoir with perfect flow conditions. While investigating either the injection or production well, it can be assumed that the respective other well maintains mentioned mass and pressure balance.

$$P_{Dn,Injector} = P_{Wellhead} + \rho_{Water,Surface} * g * D_{n,TVD} - \Delta P_{Loss} \qquad \text{Equation 13}$$

Where $P_{Dn,Injector}$ is the pressure of an injector well at a depth n [Pa], $P_{Wellhead}$ is the wellhead pressure [Pa], $\rho_{Water,Surface}$ is the density of water under surface conditions [kg/m³], g is the gravitational acceleration and equals 9,81 [m/s²], $D_{n,TVD}$ is the TVD at depth n [m], ΔP_{Loss} is the pressure loss due to friction [Pa].

$$P_{Dn,Producer} = P_{Bottom} - \rho_{Water,Reservoir} * g * \left(D_{Res,TVD} - D_{n,TVD}\right) - \Delta P_{Loss} \qquad \text{Equation 14}$$

Where $P_{Dn,Producer}$ is the pressure of a producer well at a depth n [Pa], P_{Bottom} is the pressure at the bottom of the well [Pa], $\rho_{Water,Reservoir}$ is the density of water under reservoir conditions [kg/m³], g is the gravitational acceleration and equals 9,81 [m/s²], $D_{Res,TVD}$ is the reservoir TVD [m], $D_{n,TVD}$ is the TVD at depth n [m], ΔP_{Loss} is the pressure loss due to friction [Pa].

(Grant and Bixley 2011, 125–128; Watson 2013, 57-66; Tóth and Bobok 2016, 131-144; Bschorer 2018, 33–47)

2.5.4   Pressure Losses

According to Bernoulli, pressure losses demand that the fluid is incompressible. To calculate the pressure loss between two points of interest, it is beneficial that these two points have the same ID. If the tieback consists only of one section with one ID, this simplification is easily fulfilled. If a tapered completion is used and different IDs are subject to consideration, each section shall be calculated individually with the same simplification of equal IDs.

For the same ID, the flowing velocity v is equal between these points for a constant flow rate in a constant cross-sectional area (Equation 15). For a general pressure loss for a height h between two points, the relationship is described in Equation 16.

$$v = \frac{Q}{A_I} \qquad \text{Equation 15}$$

Where v is the flowing velocity of the fluid [m/s], Q is the flow rate [m³/s], A_I is the inside area of the tieback [m²].

$$\Delta P_{Loss} = \lambda * \frac{h}{ID} * \rho * \frac{v^2}{2} \qquad \text{Equation 16}$$

Where ΔP_{Loss} is the pressure loss due to friction [Pa], λ is the dimensionless friction factor [-], h is the height between the two points of interest where the pressure loss occurs [m], ID is the

inner diameter of the tieback [m], ρ is the density of the flowing fluid [kg/m³], v is the flowing velocity of the fluid [m/s].

To obtain the friction factor λ we must first introduce Reynold's number Re (Equation 17).

$$Re = \frac{v * ID * \rho}{\mu}$$
Equation 17

Where Re is the dimensionless Reynold's number [-], v is the flowing velocity of the fluid [m/s], ID is the inner diameter of the tieback [m], ρ is the density of the flowing fluid [kg/m³], μ is the dynamic viscosity of the flowing fluid [N*s/m²].

To obtain the friction factor λ is relatively easy for a laminar flow behaviour and $Re \leq 2300$ ().

$$\lambda = \frac{64}{Re}$$
Equation 18

Where λ is the dimensionless friction factor [-], Re is the dimensionless Reynold's number [-].

For higher Re values, a turbulent flow condition prevails, which is most frequently the case. We can finally introduce Colebrook's equation (Equation 19) which connects the friction factor λ with Reynold's number Re under turbulent flow. Besides Re, Colebrook's equation also depends on the roughness of the used tubular. λ is typically determined from Moody's friction factor diagram using the relative roughness (divided by the ID) and Re. In an almost fully automated MATLAB application, it is rather inconvenient to search for such values in a diagram. That's why λ can be obtained through Equation 19 by iteration. Usually, accurate results are obtained after 2 to 3 iterations.

Alternatively, Equation 20 can be used, which is a very close approximation of Equation 19 (Hibbeler and Yap 2017, 483).

$$\frac{1}{\sqrt{\lambda}} = -2 * \log\left(\frac{2,51}{Re * \sqrt{\lambda}} + \frac{\varepsilon/ID}{3,7}\right)$$
Equation 19

Where λ is the dimensionless friction factor [-], Re is the dimensionless Reynold's number [-], ε is the roughness of the tieback [m], ID is the inner diameter of the tieback [m].

$$\frac{1}{\sqrt{\lambda}} = -1,8 * \log\left(\frac{6,9}{Re} + \left(\frac{\varepsilon/ID}{3,7}\right)^{1,11}\right)$$
Equation 20

Where λ is the dimensionless friction factor [-], Re is the dimensionless Reynold's number [-], ε is the roughness of the tieback [m], ID is the inner diameter of the tieback [m].

Typical values for the roughness ε of steel pipes are ranging from 0,04 to 0,1 [mm] for new pipes, up to 0,40 [mm] for moderately rusted or encrusted and up to 3,00 [mm] for strongly

encrusted pipes. Pipes after a longer service life (cleaned) range from 0,15 to 0,20 [mm] (Stephan et al. 2019, 1357).

We only consider purely frictional pressure losses with perfect flow behaviour within the provided tubular dimensions. No changes or restrictions to the flow path caused due to corrosion, scaling, installed equipment, sudden changes in diameter (crossovers) or other effects that may play a diminishing role in the flow performance are to be considered. Pressure losses are incremental and increase steadily (for the same inside diameter) with the pipe's length.

(Grant and Bixley 2011, 125-128; DiPippo 2016, 227-230; Tóth and Bobok 2016, 131–144 & 213-221; Hibbeler and Yap 2017, 211-225 & 479-501; Bschorer 2018, 211-223; Stephan et al. 2019, 1353-1366; Longo et al. 2021, 389-395)

2.6 Steel Grade Selection in Geothermal Applications

Many different steel alloys are available for all sorts of industries. The ISO 11960 standard (*Specification for Casing and Tubing - API Specification 5CT - ISO 11960:2004*, Eighth Edition 2005. American Petroleum Institute and ISO) became a widely accepted and used reference for steel grades used in the oil & gas industry. The standard includes information about the manufacturing process & post-manufacturing processes like heat treatment, threading, testing mechanisms. It is further a useful reference for the minimum requirements of specific properties & the chemical composition, available sizes and dimensions among many other exciting and useful information.

The proposed steel grades of the API standard 5CT have been used countless times worldwide and are therefore well known to the Oil & Gas industry. Since they have been proven to hold up to the demanding circumstances in numerous projects, such as high temperature & pressure and perhaps corrosive environments, the geothermal industry came to use the same steel types in their projects. Therefore, some of these grades serve as pre-defined variables in the application.

Many steel grades are covered in detail by the API Standard 5CT. They are also partly used in the German guide for casing, tubing & liner calculations (*Leitfaden Futterrohrberechnung* 2006. Wirtschaftsverband Erdöl- und Erdgasgewinnung e.V.) and the (*Code of practice for deep geothermal wells* 2015. New Zealand Standard).

In the following chapters, we will discuss some aspects that may influence selecting the right steel type and grade, depending on the prevailing conditions. Still, for our investigation, we consider the here listed steel grades:

- J55
- K55
- L80
- N80

- C90
- C95
- P110
- Q125

2.6.1   Corrosion

Corrosion can pose a substantial threat to the integrity or performance of completion designs. Therefore, it is substantial to analyse all prevailing conditions and the possibility and likelihood of a change of these conditions while being in the planning phase of a geothermal project. This chapter gives a short introduction and overview of the different corrosion types applicable and most severe in geothermal applications, their influencing factors and the selection of the right steel for typical geothermal conditions, while not going into the underlying mechanisms of the different corrosion mechanics.

Corrosion typically requires three conditions:

- Metal
- Water or a saline solution (Electrolyte)
- A corrodent, which creates corrosion. For example, oxygen (O_2) or acids from carbon dioxide (CO_2) and hydrogen sulphide (H_2S).

The basic principle of corrosion is that the metal's surface contains anodes and cathodes, due to an electric potential difference. This difference can be caused by inhomogeneity in the grains such as variations in the composition and impurities within the metal structure, surface roughness, or films. The anode (less noble) emits electrons and reduces its metal mass at the anode's location. The cathode (nobler) naturally receives the electron. Less noble and nobler refers to the electric potential between two metals if connected through an electrolyte. The nobler metal with higher potential does not corrode while the less noble metal with a lower potential does corrode. The process of corrosion is illustrated in Figure 12. (Campbell 2008, 323–345; Bellarby 2009, 442–460)

(Lyons et al. 2015, 519, Chapter 4) provides a detailed table of reduction potentials and with it the knowledge which metals are likely to corrode.
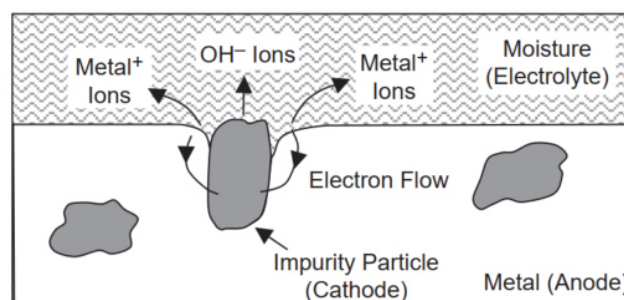

Figure 12: Electrolytic corrosion of steel (Campbell 2008, 324)

The corrosion types most often seen in deep geothermal applications include:

- Uniform corrosion
- Pitting corrosion
- Crack corrosion
- Stress corrosion cracking
    - Sulphide stress cracking
    - Chloride stress cracking
    - Ammonia stress cracking
- Hydrogen embrittlement
- Intergranular corrosion
- Galvanic corrosion
- Fatigue corrosion
- Erosion corrosion
- De-alloying
- Crevice
- Cavitation
- Microbiologically influenced corrosion

Influencing and driving factors of the different corrosion types are generally:

- pH values
- Temperature
- Hydrogen sulphide
- Carbon dioxide
- Ammonia
- Chloride
- Hydrogen
- Sulphate
- Oxygen
- Suspended solid materials
- Deposits

The ions chloride (Cl^-), hydrogen (H^+) and sulphate (SO_4^{-2}) have a strong corrosive effect at pH values <7, resulting in local corrosion phenomena such as stress cracking, crevice corrosion and pitting. Gas phases such as hydrogen sulphide, carbon dioxide and ammonia (NH_3) cause stress corrosion cracking and extensive material removal. Oxygen accelerates the corrosion of low-alloy and high-alloy steels. Heavy metals and heavy metal compounds are also corrosive. (Gunnlaugsson et al.; Kaya and HOŞHAN; Campbell 2008, 323–345; Bellarby 2009, 442–460; Bauer et al. 2014, 595–608; Wood Group Intetech Ltd 2017, 27-35 & 67-96; Nogara and Zarrouk 2018; Vallejo Vitaller et al. 2019)

The material costs rise sharply with a higher material value. For example, unalloyed steels (plain carbon steels) have relatively low material costs than duplex steels (ratio 1:7). However, if the duplex steel's longevity (higher material quality) is considered compared to unalloyed steels, the duplex steel is more advantageous.

Material quality is understood here as the higher resistance of a material to external influences such as corrosion and erosion. Alloy elements like chromium, for example, lead to this higher resistance to corrosive components of geothermal fluids. Chromium-nickel steels form a passivation layer due to the higher chromium content, which has an advantageous effect concerning the surface corrosion attack. Under dynamic loads, such as frequent start-ups and shutdowns of the geothermal system and the presence of a corrosive environment, high alloy steels such as duplex and super-duplex steels are advantageous. Superduplex steels are very suitable for local corrosion mechanisms such as pitting corrosion. They can also be used for temperatures up to 280 [°C]. If there is material removal by particles (erosion) in addition to corrosive attack, austenitic steels are advantageous. Nickel-based alloys are well suited in the higher temperature range. However, if there is a high chloride concentration in the geothermal fluid, corrosion signs can occur when using nickel-based alloys. Titanium alloys are very useful in terms of their corrosion resistance. Due to the high costs, this material usually is not used as tubular material.

Coatings are cost-effective, corrosion-resistant alternatives. Coated tubular are used up to a temperature range of approximately 200 [°C].

If pure corrosion occurs, as shown in Figure 13 on the left, low-alloy steels with inhibitors, low-alloy steels with coatings and high-alloy steels are ideal. If corrosion and erosion (Figure 13 on the right) occur together, coatings are not suitable. The coated surface is removed relatively quickly. High-alloy steel has the best cost-benefit ratio here. Due to the high investment costs, nickel-based alloys and austenitic steels are not economically attractive.

The legend for the letters a to f of Figure 13 is as follows:

- a – low alloy steel
- b – low alloy steel + coating
- c – low alloy steel + corrosion inhibitor
- d – high alloy steel
- e – nickel-based alloys
- f – austenitic steel

The service life of the tubular is shown on the x-axis ("Lebensdauer"), and the decreasing material cost is shown on the y-axis ("abnehmende Materialkosten"). The results of the calculation can be seen in the four quadrants. The ++ quadrant materials have the best cost-benefit ratio, whereas compared to the materials in the - - have the lowest service life at high material costs. (Bauer et al. 2014, 595–608)
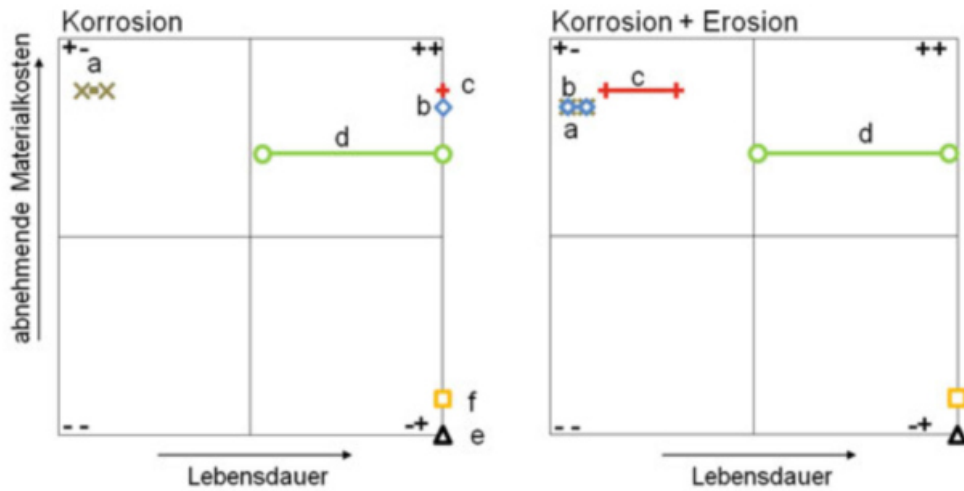
Figure 13: Material costs comparison and the service life for damage through corrosion and coupled corrosion and erosion (Modified from: Bauer et al. 2014, 606)

An increase in the chromium content has significant beneficial effects on the corrosion rates of well's completion at a lower temperature. At higher temperature steels with high chromium content corrode even faster than their low chromium content counterparts. Such effects can be seen in the following Figure 14. Even small chromium contents lead to a decreasing peak of the function and therefore lower corrosion rates.

The cost of corrosion-resistance is underlined by a cost assessment relative to plain carbon steel for different tubing material (per tonne) in Figure 15. (Bellarby 2009, 442-460)
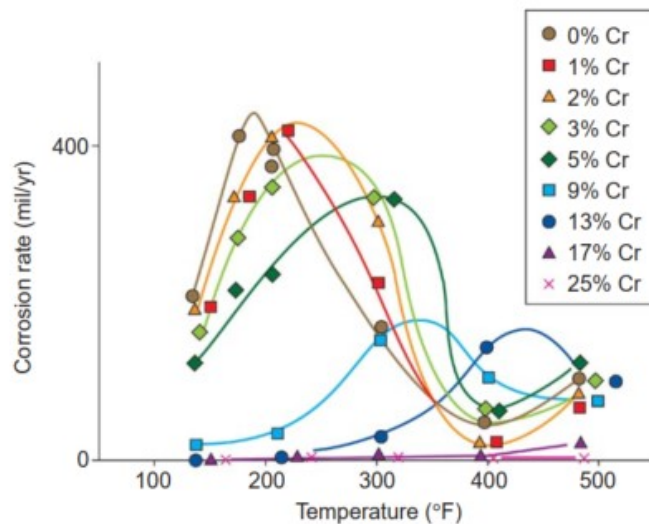

Figure 14: Corrosion rate as a function of chromium content (Bellarby 2009, 445)

Corrosion rate is typically measured in reduction of thickness per year [mm/year]. Here on 1 [mil/year] equals 0,0254 [mm/year].

Tubing	Approximate Cost Relative to Carbon Steel
L80 carbon steel	1
L80 1%Cr	1.05
Coated (e.g. phenolic epoxy) carbon steel	2
Fibreglass lined carbon steel tubing	3.5
L80 13Cr	3
Modified 13Cr steel (2Mo–5Ni)	5
22Cr duplex	8
25Cr duplex	10
2550 or 2035	20+
Titanium	10–20

Figure 15: Relative costs of different tubing materials (Bellarby 2009, 459)

2.6.2 Fatigue

Fatigue can imply the effect of two different phenomena. The first one being low cycle fatigue, which relates to steel being subjected to heavy cyclic loads which induce irreversible strains and lead to crack initiation and propagation. A low number of cycles is considered to be from magnitudes of 10 to 10^4. The second, and more applicable, fatigue is called high cycle fatigue and implies, as the name suggests, a high number of cyclic loads below the yield strength. A high number of cycles is considered to be in a range of 10^4 to 10^7 or even more. We denote high cycle fatigue (failure) as fatigue (failure) for this chapter. Fatigue failure occurs due to the reoccurring cyclic stresses applied to a tubular. A pipe is subject to failure caused by fatigue even if much lower stresses are applied repeatedly than on a single stress application failure.

Figure 16 shows how a load case under cyclic stresses may look like. The top graph refers to a fully reversed loading with the same amplitude (σ_a) between the maximum and minimum stress (σ_{max} & σ_{min}) and no additional stress applied. The second graph shows the same reversed loading with equal amplitude but with an applied tensile stress. This increases the mean stress (σ_m) measured from the neutral line (0 stress as reference). For a loading example under compressive stress the function would move below the neutral line. In real life conditions the maximum and minimum stress do not need to be equal and may depend on external circumstances. An increase in the mean stress will always cause a reduction in fatigue life (Figure 17).

The fatigue life is the number of cycles which are needed until failure occurs at a specified stress level. The fatigue strength is the stress below which failure does not occur. As the applied stress level is decreased, the number of cycles to failure increases. Normally, the fatigue strength increases as the static tensile strength increases.
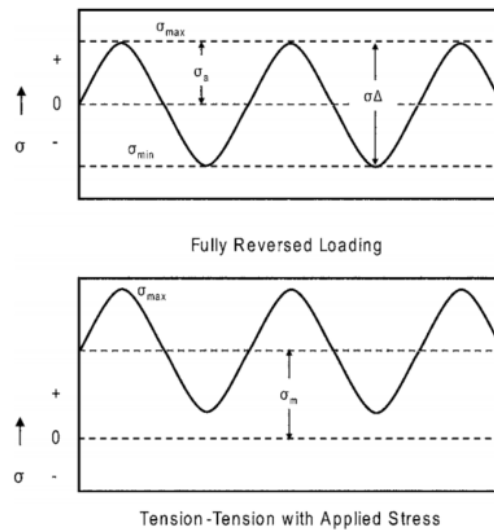
Figure 16: Cyclic stress with and without tension offset (Campbell 2008, 243)
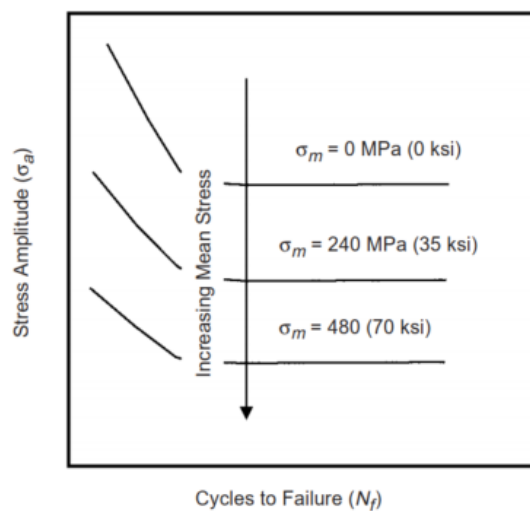

Figure 17: Effects of mean stress on fatigue life (Campbell 2008, 248)

In a geothermal application one must consider two factors with respect to fatigue failure. Firstly, the fatigue strength generally decreases with increasing temperatures. Secondly, often exerted thermal stresses caused by rapid changes in temperature are an influencing factor to fatigue failure. Such conditions may be prevailing in a geothermal system.

(Lemaitre and Desmorat 2005, 191-231 & 277-319; Krupp 2007, 3-37; Campbell 2008, 243–264; Teodoriu and Falcone 2009)

2.6.3   Creep

Elevated temperatures impact the mechanical properties of steels, and therefore the structural performance of wellbore tubular. Steel may be subject to time-dependent deformation such as creep when exposed to external loads at elevated temperatures. Numerous analysis has analysed steel tubular test specimen behaviour loaded with equal tensile loads while being subjected to different temperatures. The specimen subjected to higher temperatures are prone to fail after a particular exposure time. Depending on the type and grade of steel, failure can occur with stresses below the specified yield strength at temperatures about a third to a half of the steel's melting point. The exposure time needed to cause failure also depends on the steel. Creep is usually quantified in terms of creep or strain rate, which is the change of strain over time.

Creep typically shows up in three stages (Figure 18):

- Primary creep shows an initial elongation and is followed by a rapid decrease in creep rate with time.
- Secondary creep features a constant low creep rate.
- Tertiary creep is characterised by a rapid and drastic increase in creep rate, which leads to fracturing (rupture) of the steel.

In geothermal load conditions, it is common to have both creep and fatigue effects acting simultaneously. Combining these two effects may accelerate the onset of structural failure drastically. Caution must be exercised while designing and planning a geothermal well with respect to the right choice of steel grades and the operating temperatures, especially when it is subject to high-temperature conditions.

(Lemaitre and Desmorat 2005, 233-276; Campbell 2008, 265–278; Tao et al. 2020, 4–5)
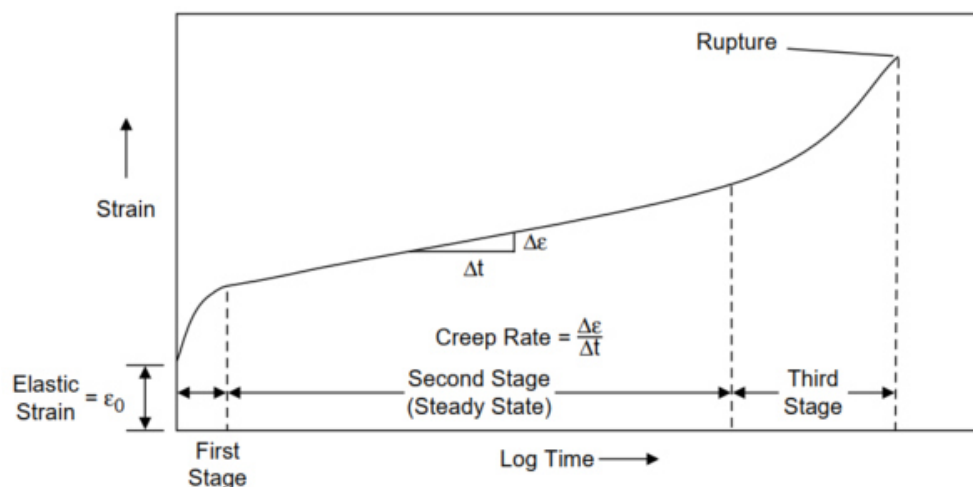

Figure 18: Typical creep curve (Campbell 2008, 266)

2.6.4 Steel properties at elevated temperatures

Steel features numerous properties and characteristics subject to change to a certain degree with a temperature change. The calculations governing the load, stress, buckling, and safety factor determination are also using some of these temperature-dependent properties.

We are only interested in the properties of the introduced steel grades at the beginning of this chapter, which is essential for our investigation. Namely, these are the modus of elasticity (Young's Modulus), the Poisson's Ratio, the yield strength and the thermal expansion coefficient.

A detailed analysis of the temperature dependency of some commonly used alloys in the geothermal industry is available. For others, it isn't easy to find publicly available detailed information.

Nevertheless, the deteriorating factors of the Young's Modulus, the Poisson's Ratio and the thermal expansion coefficient are covered by the German guide for casing, tubing & liner calculations (*Leitfaden Futterrohrberechnung* 2006. Wirtschaftsverband Erdöl- und Erdgasgewinnung e.V.) in Table 1.(Tao et al. 2020) has provided a detailed summary of deteriorating factors for the yield strength for a collection of steel grades. Some of them include the grades used in this investigation (Table 11). Another source of information is the (*Code of practice for deep geothermal wells* 2015. New Zealand Standard) which provides information for the yield strength, the tensile strength and the modulus of elasticity (Table 3).

Deterioration factors should be used with caution since they may vary between different pieces of literature and reports. Values for the deteriorated properties can be obtained by interpolating the provided deterioration factors and their corresponding reference temperature.

Steel Grade	Temperature Deration Points and Factors for Young's Modulus, Poission's Ratio and the Thermal Expansion Coefficient											
	Temp. Deration Point 1		Temp. Deration Point 2		Temp. Deration Point 3		Temp. Deration Point 4		Temp. Deration Point 5		Temp. Deration Point 6	
	T [°C]	Factor	T [°C]	Factor	T [°C]	Factor	T [°C]	Factor	T [°C]	Factor	T [°C]	Factor
J55	20,00	1,00	100,00	0,90	150,00	0,78	200,00	0,76	250,00	0,73	300,00	0,70
K55	20,00	1,00	100,00	0,90	150,00	0,78	200,00	0,76	250,00	0,73	300,00	0,70
L80	20,00	1,00	100,00	0,94	150,00	0,90	200,00	0,88	250,00	0,86	300,00	0,85
N80	20,00	1,00	100,00	0,80	150,00	0,75	200,00	0,74	250,00	0,74	300,00	0,73
C90	20,00	1,00	100,00	0,89	150,00	0,85	200,00	0,83	250,00	0,83	300,00	0,82
C95	20,00	1,00	100,00	0,89	150,00	0,85	200,00	0,82	250,00	0,80	300,00	0,79
T95	-	-	-	-	-	-	-	-	-	-	-	-
P110	20,00	1,00	100,00	0,94	150,00	0,91	200,00	0,89	250,00	0,87	300,00	0,86
Q125	20,00	1,00	100,00	0,94	150,00	0,92	200,00	0,89	250,00	0,87	-	-

Table 1: Deterioration factors for the Young's Modulus, Poisson's Ratio & Thermal Expansion Coefficient at different temperatures (Modified from: *Leitfaden Futterrohrberechnung* 2006. Wirtschaftsverband Erdöl- und Erdgasgewinnung e.V., 88)

Temperature Deration Points and Factors for the Yield Strength								
Steel Grade	Temp. Deration Point 1		Temp. Deration Point 2		Temp. Deration Point 3		Temp. Deration Point 4	
	T [°C]	Factor	T [°C]	Factor	T [°C]	Factor	T [°C]	Factor
K55	20,00	1,00	148,90	0,88	204,40	0,83	260,00	0,78
L80	20,00	1,00	148,90	0,88	204,40	0,83	260,00	0,78
N80	20,00	1,00	148,90	0,88	204,40	0,83	260,00	0,78
C90	20,00	1,00	148,90	0,93	204,40	0,89	260,00	0,86
C95	20,00	1,00	148,90	0,88	204,40	0,83	260,00	0,78
T95	20,00	1,00	148,90	0,93	204,40	0,89	260,00	0,86

Table 2: Deterioration factors for the Yield Strength at different temperatures (Modified from: Tao et al. 2020, 7)

Grade	Temperature (°C)						
	20	100	150	200	250	300	350
	API yield strength (factor)						
J55/K55	1.00	0.94	0.90	0.90	0.85	0.80	0.70
L80/C90/T95	1.00	0.96	0.92	0.90	0.88	0.85	0.81
	Tensile strength (factor)						
All grades	1.00	0.96	0.92	0.90	0.88	0.86	0.84
	Modulus of elasticity (10^3 MPa)						
All grades	210	205	201	197	194	190	185

Table 3: Deterioration factors for the Yield Strength, Tensile Strength & Young's Modulus at different temperatures (Modified from: *Code of practice for deep geothermal wells* 2015. New Zealand Standard, 23)

The temperature-dependent induced phenomena of steel or the deterioration of its properties are not accounted for automatically in this simple MATLAB model. They shall be subject to user supervision by adjusting the properties accordingly.

3 Load & Stress Analysis

An analysis of the occurring loads and stresses on an existing installation under different operational modes is critical to ensure the planned working conditions are not causing loads or stresses that could exceed the installed materials' limits. Even more so if the operation mode is changed for a well and the completion remains the same. The following chapters investigate the loads and stresses of an installed completion under varying working conditions (shut-in, production, injection and pressure tests). If the working conditions are not satisfied, a workover and change in the materials or completion design may be necessary. The operational parameters could also be adjusted to remain in the existing completion design's safety zone during the operation.

Usually, an installation is fixed at both ends, through the hanger at the wellhead and the packer at the bottom. The used packer and the installation type and procedure may provide additional axial tension or compression loads $F_{Setting}$ during the setting process.

A freely moveable completion design in a vertical direction can be engineered even if the installation is fixed at both ends. Suppose a completion is free to move, for example, due to the use of expansion joints or other expansion devices. In that case, it is allowed to compensate the acting loads with a change in length. In a freely moveable completion design, forces can only affect the tieback above where the force is applied. If a completion is restrained from movement or has reached its movement limit, applied loads affect both the tieback and the packer.

For this particular case, one of the driving factors is a change in the temperature during production or injection compared to the shut-in well. High pressures during injection must also be considered. These temperature & pressure-induced changes could eventually cause buckling of the tieback, which would aggravate the situation. During pressure tests, mainly the additional tension due to the force acting on the pressure testing plug and high pressures can be observed. A detailed load vs depth diagram is provided in the result section. (Bellarby 2009, 473–474, 507-509)

In a freely moveable design, forces can only affect the tieback above where the force is applied. (Bellarby 2009, 507-509)

For a profound investigation of axial loads and the resistance to failure, one must consider the joint strength of couplings such as short round thread coupling (STC), long round thread coupling (LTC) & BTC, and more in-depth aspects as the threads' makeup length, the cross-sectional area of the pipe under the last full thread. The joint strength is usually the yield strength of a casing connection in tension. Formulas for fracture strength of connections are also available but not used often. STC and LTC connections typically have a lower yield strength than the pipe.

Formulas for the calculations of the joint strength can be found in the API Standard 5C3. Still, one must additionally refer to API Standard 5B to get some of the necessary thread dimensions

for use in the formulas. There is one major complication with the use of joint strength. API does not address the strength of connections in compression, making an equal assessment under tension and compression very difficult. (Byrom 2015, 154–155)

3.1 Axial Loads

The following chapters go through the various loads acting along the tieback's length axis and the possible occurring length changes. Each chapter gives insight into the influencing factors and calculation procedure. Axial loads can contribute with a tensile or compressive element. Length changes manifest themselves as elongations (tieback is stretched) or contractions (tieback is compressed). All applicable forces and/or length changes must be summed up to a total axial load $F_{Axial,Total}$ and a total length change ΔL_{Total} to assess the conditions during operation fully. The total axial stress $\sigma_{Axial,Total}$ can be obtained by dividing the total axial load $F_{Axial,Total}$ by the smallest cross-sectional area $A_{Cross,Min}$ of the tieback.

By definition, tensile loads, stresses and elongations are positive, while compressive loads, stresses and contractions are negative.

(Bellarby 2009, 478; Kang et al. 2020)

3.1.1 Axial Strength

The axial strength $F_{Axial,Max}$ is not a force or load acting on a tieback but rather the quantification of how much axial force can be applied maximally before the yield strength Y_P is exceeded. The yield strength is temperature-dependent and may deteriorate with increasing temperature. Equation 21 for the axial strength only depends on the tieback's yield strength and cross-sectional area (depends on tieback ID & OD).

$$F_{Axial,Max} = (A_O - A_I) * Y_P \qquad \text{Equation 21}$$

Where $F_{Axial,Max}$ is the axial strength [N], $A_{Cross,Min}$ is the smallest cross-sectional area of the tieback [m²], A_O is the outside area of the tieback [m²], A_I is the inside area of the tieback [m²], Y_P is the yield strength of the tieback [Pa],

(Bellarby 2009, 478)

3.1.2 Weight of Tieback

The tieback's weight refers to its self-weight in air without acting pressures, flowing fluids or contact between the tieback and the enclosing casing. A tieback hung freely in a vertical well with its weight solely supported by the hanger at the wellhead is also transmitting the entire load due to the tieback's self-weight to the hanger. There is no load on the bottom of the tieback (neutral axial load). The tieback is in tension throughout the whole depth.

The tieback's entire weight force W (Equation 22) and the axial load due to its self-weight F_{Weight} (Equation 23) depend on the tieback's length and the mass per unit length $\frac{w}{l}$. The mass

per unit length is generally provided with the weight of the connection included. Varying connections are usually of insignificant effect and are ignored.

For vertical but deviated well the acting force can be split up into an acting axial force F_{Weight} and normal force $F_{N,Dev}$ (Equation 24). While a slightly deviated well does not significantly influence the relationship of the tieback's weight, it can become important for horizontal wellbores. $F_{N,Dev}$ is an import factor for the tieback-to-casing drag effect which we do not discuss further due to the assumption that only vertical wells with a low deviation are investigated.

The relationship to obtain the elongation due to the self-weight ΔL_{Weight} of a freely moveable tieback is shown in Equation 25. The elongation depends amongst other things on the modulus of elasticity, which is temperature-dependent and may deteriorate with increasing temperature.

Each section needs to be assessed separately for the load and elongation due to self-weight if tieback sections with different dimensions and mass per unit length or moduli of elasticity are present.

The total weight force of the tieback string in the air can be calculated with Equation 22.

$$W = \frac{w}{l} * MD * g \qquad\qquad \text{Equation 22}$$

Where W is the weight force of the tieback due to self-weight [N], $\frac{w}{l}$ is the mass per unit length of the tieback [kg/m], MD is the measured depth [m], g is the gravitational acceleration [m/s²].

For a vertical well, both straight vertically and deviated, the axial load due to the tieback string in air can be calculated with Equation 23.

$$F_{Weight} = \frac{w}{l} * TVD * g \qquad\qquad \text{Equation 23}$$

Where F_{Weight} is the load due to tieback self-weight in air in a wellbore [N], $\frac{w}{l}$ is the mass per unit length of the tieback [kg/m], TVD is the true vertical depth [m], g is the gravitational acceleration [m/s²].

The resulting normal force due to a vertical and slightly deviated wellbore is:

$$F_{N,Dev} = \frac{w}{l} * (MD - TVD) * g \qquad\qquad \text{Equation 24}$$

Where $F_{N,Dev}$ is the normal force due to tieback self-weight in air in a deviated wellbore [N], $\frac{w}{l}$ is the mass per unit length of the tieback [N/m], MD is the measured depth [m], TVD is the true vertical depth [m], g is the gravitational acceleration [m/s²].

$$\Delta L_{Weight} = \frac{L_{Tieback} * F_{Weight}}{2 * E * (A_O - A_I)}$$ Equation 25

Where ΔL_{Weight} is the elongation due to tieback self-weight in air [m], $L_{Tieback}$ is the length of the tieback (MD) [m], F_{Weight} is the load due to tieback self-weight in air in a wellbore, E is the modulus of elasticity of the tieback [Pa], A_O is the outside area of the tieback [m²], A_I is the inside area of the tieback [m²].
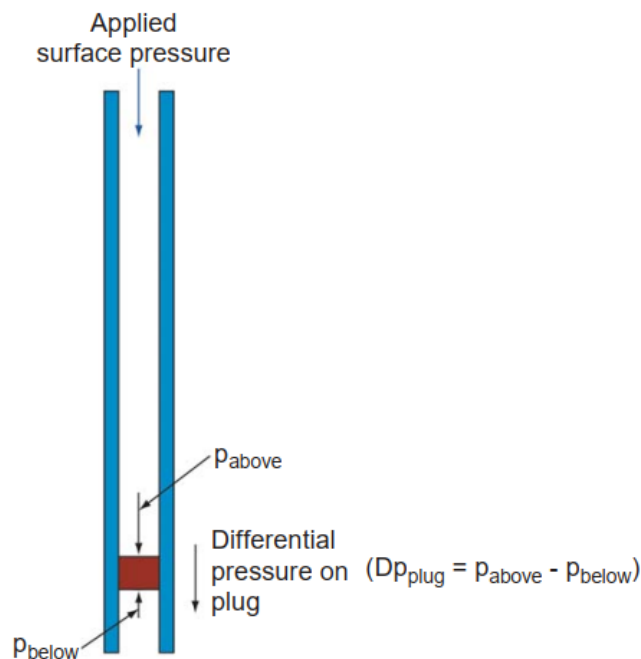
(Bellarby 2009, 479–480)

3.1.3 Buoyancy

Buoyancy is one of several piston forces that directly act in the direction of the axis, as opposed to indirect axial load changes due to radial acting forces.

Buoyancy describes the physical effect of fluid pressure acting on the bottom of an object exposed to it. In this case, it is the bottomhole pressure P_{Bottom} in the wellbore and the bottom of the free-hanging tieback. Pressure needs an area to act on, which is the cross-sectional area at the tieback's bottom. Since the fluid is acting below the tieback, the resulting buoyancy force $F_{Buoyancy}$ (Equation 26) is directed against the tieback string and it is compressive. Thus, it has a negative sign.

The buoyancy force acts like an offset on the surface and the bottom of the load profile, shifting it from the neutral axial load into compression at the bottom (the neutral axial load is at shallower depth).

$$F_{Buoyancy} = -P_{Bottom} * (A_{O,Bottom} - A_{I,Bottom})$$ Equation 26

Where $F_{Buoyancy}$ is the buoyancy force on the tieback's bottom [N], P_{Bottom} is the pressure at the bottom of the well [Pa], $A_{O,Bottom}$ is the outside area of the tieback at the bottom [m²], $A_{I,Bottom}$ is the inside area of the tieback at the bottom [m²].

(Bellarby 2009, 480–481)

3.1.4 Pressure Testing Plugs

Pressure testing plugs are also subject to piston forces. The plug is placed to seal within the tieback's inner area with fluid pressure applied to its upper cross-sectional area. Opposed to the pressure caused by the fluid on top is the pressure from the fluid below the plug. See Figure 19 for a schematic.

If the pressure acting on the plug's top is greater than the bottom pressure, which is usually the case during pressure tests, the resulting force F_{Plug} is tensile. Otherwise, for a more significant pressure at the bottom, it is compressive. A pressure test can cause significant tensile loads due to the tremendous pressures applied to the plug. The highest tensile load is close to the surface.

The force created through this pressure differential while preforming a pressure test with a fixed completion is described in Equation 27. For a free moving completion, the length change is described by Hook's law (Equation 28).

$$F_{Plug} = (P_{Above,Plug} - P_{Below,Plug}) * A_I$$
<div align="right">Equation 27</div>

Where F_{Plug} is the force due to a pressure differential on the plug [N], $P_{Above,Plug}$ is the pressure above the plug [Pa], $P_{Below,Plug}$ is the pressure below the plug [Pa], A_I is the inside area of the tieback [m²].

$$\Delta L_{Plug} = \frac{L_{Plug} * F_{Plug}}{2 * E * (A_O - A_I)}$$
<div align="right">Equation 28</div>

Where ΔL_{Plug} is the length change due to a pressure differential on the plug [m], L_{Plug} is the length from the surface to the plug (MD) [m], F_{Plug} is the force due to a pressure differential on the plug [N], E is the modulus of elasticity of the tieback [Pa], A_O is the outside area of the tieback [m²], A_I is the inside area of the tieback [m²].

(Bellarby 2009, 481–484; Kang et al. 2020)

Figure 19: Pressure Testing Plug (Bellarby 2009, 482)

3.1.5 Packer Piston Force

Piston forces acting on the packer or the bottom of the completion are caused due to the same mechanisms as the piston force on pressure testing plugs. The same principles applied to a pressure testing plug or packer also work for any additional completion part or installed equipment, which would seal the annulus and expose its area to differential pressure.

There is no pressure differential above and below the packer before the setting process, but this equilibrium is not maintained with changing operational conditions after the packer has been set.

For the packer piston force calculation (Equation 29), we can assume that the packer is set at the end of the completion string and is sealing tight between the casing and the tieback. That makes the area on which the pressures act upon the difference in the casing's inner diameter and the tieback's outer diameter at the packer setting depth. Suppose the packer is set at the bottom of the completion. In that case, the pressure above the packer is usually the hydrostatic pressure in the annulus between casing and tieback at the end of the tieback. The pressure below the packer is then the pressure at the end of the tieback.

For a free moving completion, the length change is described by Hook's law in Equation 30.

$$F_{Packer} = \left(P_{Above,Packer} - P_{Below,Packer}\right) * \left(A_{I,Casing,Packer} - A_{O,Tieback,Packer}\right) \quad \text{Equation 29}$$

Where F_{Packer} is the force due to a pressure differential on the packer [N], $P_{Above,Packer}$ is the annulus pressure above the packer [Pa], $P_{Below,Packer}$ is the pressure below the packer [Pa], $A_{I,Casing,Packer}$ is the inside area of the casing at the packer [m²], $A_{O,Tieback,Packer}$ is the outside area of the tieback at the packer [m²].

$$\Delta L_{Packer} = \frac{L_{Packer} * F_{Packer}}{2 * E * (A_O - A_I)} \quad \text{Equation 30}$$

Where ΔL_{Packer} is the length change due to a pressure differential on the packer [m], L_{Packer} is the length from the surface to the packer (MD) [m], F_{Packer} is the force due to a pressure differential on the packer [N], E is the modulus of elasticity of the tieback [Pa], A_O is the outside area of the tieback [m²], A_I is the inside area of the tieback [m²].

(Bellarby 2009, 481–484; Kang et al. 2020)

3.1.6 Crossovers

Pressures acting internally or externally on a fixed tieback generate forces $F_{Crossover}$ on crossovers from one diameter to another (Figure 20), since the change in diameters provides a surface area for the pressures to act. These forces are in opposite directions. The effect is a point load specifically acting at the crossover. Higher internal pressure is promoting compression, while higher external pressure promotes tension.

This force will be transferred up to the hanger at the wellhead if the completion is able to move freely in a vertical direction. For a fixed completion design, the force will be transferred to the wellhead hanger and the packer in proportion to the crossover's location and the tieback's stiffness above and below the crossover.

Most commonly crossovers occur at tapered completions where the upper section features a larger OD and ID than the lower section. For a regular crossover with this set-up, the acting

forces on the inside of the crossover are directed downwards causing a tension contribution and the upwards acting forces on the outside of the crossover cause a compression contribution. A reverse tapered crossover with smaller OD and ID in the upper section naturally has the force contributions pointing in the opposite direction, compressive on the inside and tensile on the outside. Crossovers with the same OD and only a change in ID have a smaller effect.

Another type of crossover within a completion may be expansion devices such as expansion joints, which can reduce acting forces and stress by allowing a certain degree of completion string movement. In some cases, the forces created through expansion devices can be significant. The possibility of expansion joint usage to counteract thermal expansion will be discussed in a later chapter. Expansion joints or other expansion devices may be simulated, but the change in diameters and the resulting crossover may vary substantially depending on the used tools which are not part of this investigation.

According to Hook's law, the length change due to a crossover in a freely moveable tieback is described in Equation 32. The length change will be an elongation for a tensile and a shortening for a compressive crossover force.

$$F_{Crossover} = P_O * \left(A_{O,2} - A_{O,1} \right) - P_I * \left(A_{I,2} - A_{I,1} \right) \qquad \text{Equation 31}$$

Where $F_{Crossover}$ is the force due to a crossover [N], P_O is the external pressure [Pa], $A_{O,1}$ is the outside area of the upper tieback section [m²], $A_{O,2}$ is the outside area of the lower tieback section [m²], P_I is the internal pressure [Pa], $A_{I,1}$ is the inside area of the upper tieback section [m²], $A_{I,2}$ is the inside area of the lower tieback section [m²].

$$\Delta L_{Crossover} = \frac{L_{Crossover} * F_{Crossover}}{2 * E * \left(A_{O,1} - A_{I,1} \right)} \qquad \text{Equation 32}$$

Where $\Delta L_{Crossover}$ is the length change due to a crossover [m], $L_{Crossover}$ is the length from the surface to the crossover (MD) [m], $F_{Crossover}$ is the force due to a crossover (MD) [N], E is the modulus of elasticity of the tieback [Pa], $A_{O,1}$ is the outside area of the upper tieback section [m²], $A_{I,1}$ is the inside area of the upper tieback section [m²].
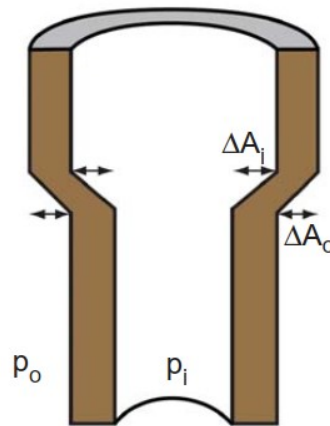
(Bellarby 2009, 484–487)

Figure 20: Crossover Example (Bellarby 2009, 484)

3.1.7 Ballooning

The ballooning effect describes an expansion or contraction of a pipe due to applied pressures on the inside and the outside of it (Figure 21). The ballooning effect depends on a material property called the Poisson's ratio v. In geothermal applications, ballooning plays a more significant role during injection of water in the reservoir or while fracturing the reservoir due to the high pressures needed.

For an axially loaded pipe in tension, a strain is generated. But not only axial strain but also radial compressive strain. This relationship can be reversed for an axial pipe in compression and a resulting radial expansion. The material property describing the radial strain to the axial strain is the Poisson's ratio v. It is temperature-depended. Thus, it can deteriorate with increasing temperature. Ballooning further depends on the pressure changes relative to the tieback in initial conditions (during shut-in).

For a fixed tieback, the pressure differences cause a resulting force $F_{Balloon}$. This force is tensile if the relative pressure change inside the tieback is more significant than the outside changes. Conversely, applying more external than internal pressure to the tieback results in a compressive force (Equation 33).

In a freely moveable tieback, an increase in applied internal pressure leads to a shortening of the tieback due to the shrinking effect while expanding. An increase in applied outside pressure leads to an elongation of the tieback due to the contraction. With Hook's law Equation 34 can be formulated.

One must pay special attention to the relationship between the just explained resulting load and length change. Usually, tension is related to elongation, while compression is related to shrinking. If the tieback is fixed in a rigid completion without movement, it wants to contract itself due to applied internal pressure but is held back. The tieback is then subject to the resulting load because of this phenomenon. Thus, leading to an induced tension to the tieback.

For applied external pressure, a compressive force is the outcome of the tieback being held back while it wants to expand.

If multiple sections with different dimensions, Poisson's ratios or moduli of elasticity are present, each section's ballooning effect must be calculated individually.

$$F_{Balloon} = 2 * v * (\Delta P_I * A_I - \Delta P_O * A_O)$$
<div align="right">Equation 33</div>

Where $F_{Balloon}$ is the force due to ballooning [N], v is the tieback's dimensionless Poisson's Ratio [-], ΔP_I is the internal pressure change [Pa], A_I is the inside area of the tieback [m²], ΔP_O is the external pressure change [Pa], A_O is the outside area of the tieback [m²].

$$\Delta L_{Balloon} = \frac{-L_{Balloon} * F_{Ballon}}{2 * E * (A_O - A_I)}$$
<div align="right">Equation 34</div>

Where $\Delta L_{Balloon}$ is the length change due to ballooning [m], $L_{Balloon}$ is the length of the tieback subject to the ballooning effect (MD) [m], F_{Ballon} is the force due to ballooning [N], E is the modulus of elasticity of the tieback [Pa], A_O is the outside area of the tieback [m²], A_I is the inside area of the tieback [m²].

(Bellarby 2009, 487–488; Kang et al. 2020)
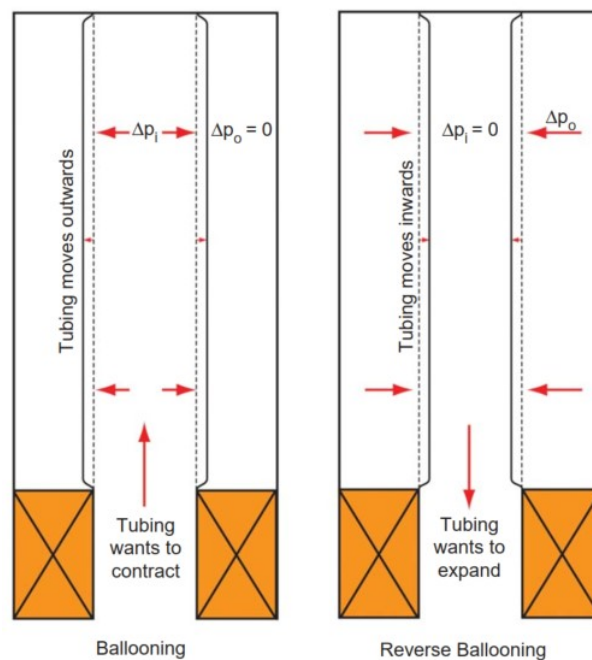
Figure 21: Ballooning and Reverse Ballooning Effect (Bellarby 2009, 488)

3.1.8   Temperature Changes

Changes due to temperature are probably the most influential factor in (almost) vertical wellbores used in geothermal applications due to hot water production from greater depth or cold-water injection at the surface. The same relationship between loads and length changes

explained previously for ballooning can be applied here. If the tieback wants to elongate due to higher temperatures in a rigid completion, it is held back, and compression is induced. On the other hand, if the tieback wants to shrink because of lower temperatures, a tensile force is induced.

The heating or cooling effect influences the induced forces F_{Temp} (Equation 35) for fixed completions and elongations or shortening ΔL_{Temp} (Equation 36) for free moveable completions. Cooling of the tieback leads to tensile forces or a reduction in length (contraction). On the other hand, heating of the tieback leads to compressive forces or increased length (elongation). The average change in temperature ΔT, which governs the magnitude of the force or length change, is measured from the initial to the load condition (change in the operational mode). Temperature profile during shut-in, production and injection and their influencing factors have been covered in previous chapters. We can use the earlier proposed relationships to obtain reference temperatures for the calculations of F_{Temp} and ΔL_{Temp}.

The thermal expansion of steel depends on a material property called the coefficient of thermal expansion α, which varies with the metallurgy and may vary even between manufacturers. The coefficient of thermal expansion is non-linear and temperature-dependent.

If multiple sections with different dimensions, coefficients of thermal expansion or moduli of elasticity are present, each section's response to a change in temperature must be calculated individually.

$$F_{Temp} = -\alpha * E * \Delta T * (A_O - A_I) \hspace{3cm} \text{Equation 35}$$

Where F_{Temp} is the force due to temperature differentials [N], α is the tieback's coefficient of thermal expansion [1/°C], E is the modulus of elasticity of the tieback [Pa], ΔT is the average change in temperature over the effected length [°C], A_O is the outside area of the tieback [m²], A_I is the inside area of the tieback [m²].

$$\Delta L_{Temp} = \alpha * \Delta T * L_{Temp} \hspace{3cm} \text{Equation 36}$$

Where ΔL_{Temp} is the elongation due to temperature differentials [m], α is the tieback's coefficient of thermal expansion [1/°C], ΔT is the average change in temperature over the effected length [°C], L_{Temp} is the length of the tieback subject to the temperature change (MD) [m].

(Bellarby 2009, 488–489; Kang et al. 2020)

3.1.9 Fluid Drag

Any fluid flowing through a pipe causes a drag due to a frictional pressure loss. The resulting drag force F_{Drag} (Equation 37) is directed in the flow direction of the fluid. Thus, during production, it causes a compressive and during injection a tensile force. The length change ΔL_{Drag} follows the flow's direction, thus shortening the tieback during production and

elongation during the injection (Equation 38). Since we already investigated the calculation of pressures losses previously, Equation 37 can be used with the total pressure loss ΔP_{Loss} (Equation 15 to Equation 20) or the frictional pressure loss gradient $\frac{\Delta P}{\Delta L}$ of the flow-through pipe. Both are always considered positive in Equation 37.

If multiple sections with different dimensions, moduli of elasticity or flow conditions are present, each section's fluid drag is determined separately.

The resulting force or length change due to fluid drag is smaller in most cases compared to the other influencing factors.

$$F_{Drag} = \pm \frac{\Delta P}{\Delta L} * A_I * L_{Drag} = \pm \Delta P_{Loss} * A_I \qquad \text{Equation 37}$$

Where F_{Drag} is the drag force due to flowing fluid [N], $\frac{\Delta P}{\Delta L}$ is the frictional pressure loss gradient [Pa/m], A_I is the inside area of the tieback [m²], L_{Drag} is the flowed through length (MD) [m], ΔP_{Loss} is the total pressure loss due to friction over the length L_{Drag} [Pa].

$$\Delta L_{Drag} = \frac{L_{Drag} * F_{Drag}}{2 * E * (A_O - A_I)} \qquad \text{Equation 38}$$

Where ΔL_{Drag} is the length change due to flowing fluid [m], L_{Drag} is the flowed through length (MD) [m], F_{Drag} is the drag force due to flowing fluid [N], E is the modulus of elasticity of the tieback [Pa], A_O is the outside area of the tieback [m²], A_I is the inside area of the tieback [m²].

(Bellarby 2009, 489–490)

3.1.10 Bending Stresses

There are two circumstances which can cause bending stresses (Equation 39). One reason could be the presence of doglegs in a borehole, which have been created during the drilling activities. It is also possible that the bending stresses are induced due to buckling, which also causes doglegs. The effects of buckling will be discussed in the following chapter. Bending stresses always occur in pairs of a positive and a negative magnitude. On the outside of the bend a tensile force is created, while a compressive force is introduced on the inside of the bend.

The bending stress is different on the outside and the inside of the bend, but also in different locations within the tieback's wall thickness. Equation 39 can be used to obtain the stress at different points through the pipe section by altering the tieback diameter to any value from the tieback ID to its OD (Figure 22). This methodology is required to calculate the triaxial failure criteria, which will be explained later on. For other calculations, the OD of the tieback is used to obtain the highest stresses.

Bending stresses are locally bound to the location of the bend in the well. Thus, unlike the previously discussed axial loads, the loads calculated through the bending stresses (Equation 40) are only valid strictly for the region where the doglegs are present. Bending stresses are therefore not affecting the load distribution in other locations other than they occur. The axial loads due to bending can be added to the load distribution with either a positive or negative sign. The assessment of axial loads in respect to bending can be made simpler by assuming the worst-case scenario. The positive tensile load is added to the existing tension. The additional tension is only of concern if the bend occurs at the uppermost part of the completion. In contrast, the negative compressive load is added to the existing compression (subtracted from the existing load). If a bend is present at the last well section, it causes an increase of the maximum compressive load applied to the completion. The latter case could significantly influence the structural integrity of the completion design.

Bending stresses do not directly create length changes unlikely the other axial loads.

$$\sigma_{Bending} = \pm \frac{E * OD}{2} * \frac{DLS}{30} * \frac{\pi}{180}$$

Equation 39

Where $\sigma_{Bending}$ is the bending stress due to doglegs [Pa], E is the modulus of elasticity of the tieback [Pa], OD is the outer diameter of the tieback [m], DLS is the dogleg severity in [°/30m].

$$F_{Bending} = \frac{\sigma_{Bending}}{A_O - A_I}$$

Equation 40

Where $F_{Bending}$ is the bending force due to the bending stress [N], $\sigma_{Bending}$ is the bending stress due to doglegs [Pa], A_O is the outside area of the tieback [m²], A_I is the inside area of the tieback [m²].

(Bellarby 2009, 490-491 & 515-516)
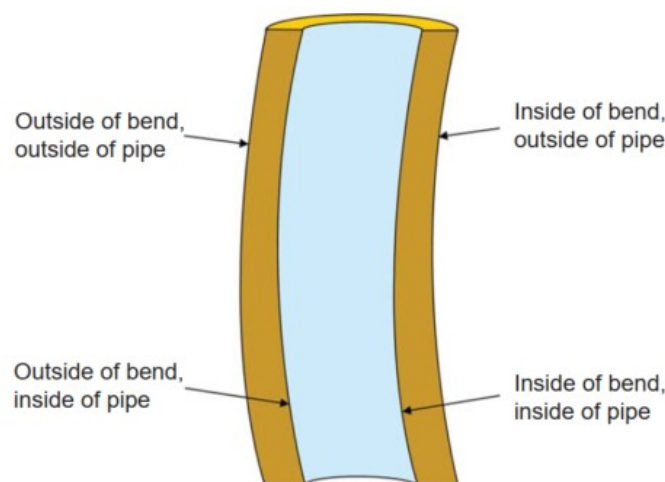
Figure 22: Stress locations in a bend (Bellarby 2009, 516)

3.2 Failure Criteria & Safety Factors

The API ratings to calculate the resistance against burst and collapse failure is described in the API BULLETIN 5C3. The following chapters go through the calculation process and the needed equations to obtain the burst and collapse ratings. Additionally, the influence of tension and compression on the burst and collapse ratings are discussed. In the end of this chapter, the triaxial approach is introduced in a short overview, which is the most in-depth rating taking stresses of all three axes into account altogether in the form of the Von Mises equivalent stress.

With the help of safety factors, the tieback's rating can be compared with its loads. A safety factor greater than 1 represents a rating that is greater than the load. Given that a failure is possible for each failure mechanism, the safety factor should be calculated for axial loads, burst, and collapse. Triaxial safety factors usually are only used in the most complex projects.

3.2.1 Burst

In comparison to axial or collapse failure, burst failures only require the failure of a very small piece of the tieback. Once a rupture occurs the entire integrity is compromised.

The burst rating can be calculated according to API BULLETIN 5C3 in Equation 41.

$$P_B = 0{,}875 * \left(\frac{2 * Y_P * t}{OD} \right) \qquad \text{Equation 41}$$

Where P_B is the burst rating [Pa], Y_P is the yield strength of the tieback [Pa], t is the wall thickness of the tieback [m], OD is the outer diameter of the tieback [m].

The factor 0,875 in the equation accounts for the wall thickness tolerance of API tubular. The value 0,875 is equal to a 12,5% reduction. This factor may be adjusted for other pipes or if the wall thickness has been verified through checks and measurements. Any alterations of the minimum wall thickness have an impact on the burst rating. For example, if a corrosion log indicates a minimum wall thickness of 60%, the tolerance in Equation 41 would be reduced to 0,6.

Equation 41 is based on the inner wall's circumferential stress (hoop stress) equalizing the yield stress at the point of failure. It assumes that the slenderness ratio is much greater than 1, a conservative assumption for thick-walled tubular.

The ratio of the tieback's outer diameter OD to the wall thickness t is called slenderness ratio and is an important ratio that is also needed for the collapse rating calculations.

(*Bulletin on Formulas and Calculations for Casing, Tubing, Drill Pipe, and Line Pipe Properties - API BULLETIN 5C3*, Sixth Edition 1994. American Petroleum Institute; Bellarby 2009, 509–510)

3.2.2 Collapse

Assessing the collapse rating is more complex than obtaining the burst rating. Collapse is an instability problem requiring the entire tieback body's yield around the circumference. The collapse rating depends on the tieback's diameter, wall thickness and more challenging to measure properties such as the ovality of the pipe. Four collapse modes are recognized by the API BULLETIN 5C3. These being yield strength $P_{C,Yp}$ (Equation 47), plastic $P_{C,P}$ (Equation 49), transitional $P_{C,T}$ (Equation 51) and elastic $P_{C,E}$ (Equation 53) collapse. Results of the collapse mode equations for a L80 tubing are presented in Figure 23.
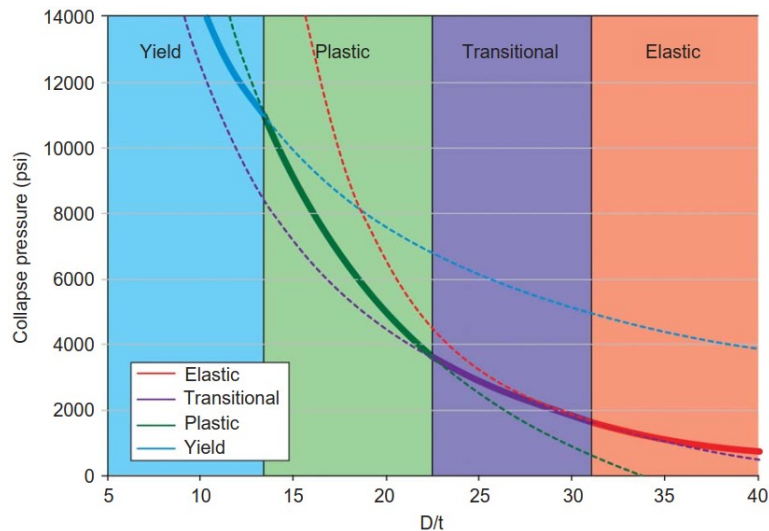
Figure 23: Collapse pressure as a function of slenderness for a L80 tubing
(Bellarby 2009, 512)

The right collapse mode is chosen by comparing the slenderness ratio of the tieback with the slenderness ratio ranges obtained by Equation 48, Equation 50 and Equation 52.

Dimensionless factors $A, B, C, F \,\&\, G$ (Equation 42 to Equation 46) are used to calculate the collapse ratings and the slenderness ratio ranges of the four collapse modes.

$$A = 2{,}8762 + 0{,}10679 * 10^{-5} * Y_P + 0{,}21301 * 10^{-10} * Y_P{}^2 - 0{,}53132 * 10^{-16} * Y_P{}^3$$

Equation 42

Where A is a dimensionless factor [-], Y_P is the yield strength of the tieback [Pa].

$$B = 0{,}026233 + 0{,}50609 * 10^{-6} * Y_P$$

Equation 43

Where B is a dimensionless factor [-], Y_P is the yield strength of the tieback [Pa].

$$C = -465{,}93 + 0{,}030867 * Y_P - 0{,}10483 * 10^{-7} * Y_P{}^2 + 0{,}36989 * 10^{-13} * Y_P{}^3$$

Equation 44

Where C is a dimensionless factor [-], Y_P is the yield strength of the tieback [Pa].

$$F = \frac{46{,}95 * 10^6 * \left(\frac{3 * B/A}{2 + (B/A)}\right)^3}{Y_P * \left(\frac{3 * B/A}{2 + (B/A)} - (B/A)\right) * \left(1 - \frac{3 * B/A}{2 + (B/A)}\right)^2}$$

Equation 45

Where F is a dimensionless factor [-], Y_P is the yield strength of the tieback [Pa], A is a dimensionless factor [-], B is a dimensionless factor [-].

$$G = \frac{F * B}{A}$$

Equation 46

Where G is a dimensionless factor [-], A is a dimensionless factor [-], B is a dimensionless factor [-], F is a dimensionless factor [-].

(*Bulletin on Formulas and Calculations for Casing, Tubing, Drill Pipe, and Line Pipe Properties - API BULLETIN 5C3*, Sixth Edition 1994. American Petroleum Institute; Bellarby 2009, 510–514)

3.2.2.1 Yield Collapse

The yield strength collapse (Equation 47) is the external pressure that generates stress equivalent to the minimum yield stress on the tieback inside wall.

$$P_{C,Yp} = 2 * Y_P * \left(\frac{(OD/t) - 1}{(OD/t)^2}\right)$$

Equation 47

Where $P_{C,Yp}$ is the yield strength collapse rating [Pa], Y_P is the yield strength of the tieback [Pa], OD is the outer diameter of the tieback [m], t is the wall thickness of the tieback [m].

Yield strength collapse occurs if the tieback's slenderness ratio is less than the maximum slenderness ratio for the yield strength collapse $(OD/t)_{Yp}$ of Equation 48.

$$(OD/t)_{Yp} = \frac{\sqrt{(A - 2)^2 + 8 * (B + C/Y_P)} + (A - 2)}{2 * (B + C/Y_P)}$$

Equation 48

Where $(OD/t)_{Yp}$ is the maximum slenderness ratio for the yield strength collapse [-], Y_P is the yield strength of the tieback [Pa], A is a dimensionless factor [-], B is a dimensionless factor [-], C is a dimensionless factor [-].

(*Bulletin on Formulas and Calculations for Casing, Tubing, Drill Pipe, and Line Pipe Properties - API BULLETIN 5C3*, Sixth Edition 1994. American Petroleum Institute; Bellarby 2009, 510–514)

3.2.2.2 Plastic Collapse

The minimum plastic collapse pressure is calculated with Equation 49.

$$P_{C,P} = Y_P * \left(\frac{A}{OD/t} - B \right) - C \qquad \text{Equation 49}$$

Where $P_{C,P}$ is the plastic collapse rating [Pa], Y_P is the yield strength of the tieback [Pa], A is a dimensionless factor [-], B is a dimensionless factor [-], C is a dimensionless factor [-], OD is the outer diameter of the tieback [m], t is the wall thickness of the tieback [m].

Plastic collapse occurs if the tieback's slenderness ratio is between the maximum slenderness ratio for the yield strength collapse $(OD/t)_{Yp}$ and the maximum slenderness ratio for the plastic collapse $(OD/t)_P$ of Equation 50.

$$(OD/t)_P = \frac{Y_P * (A - F)}{C + Y_P * (B - G)} \qquad \text{Equation 50}$$

Where $(OD/t)_P$ is the maximum slenderness ratio for the plastic collapse [-], Y_P is the yield strength of the tieback [Pa], A is a dimensionless factor [-], B is a dimensionless factor [-], C is a dimensionless factor [-], F is a dimensionless factor [-], G is a dimensionless factor [-].

(*Bulletin on Formulas and Calculations for Casing, Tubing, Drill Pipe, and Line Pipe Properties - API BULLETIN 5C3*, Sixth Edition 1994. American Petroleum Institute; Bellarby 2009, 510–514)

3.2.2.3 Transitional Collapse

The minimum collapse pressure for the transition zone between plastic and elastic is calculated with Equation 51.

$$P_{C,T} = Y_P * \left(\frac{F}{OD/t} - G \right) \qquad \text{Equation 51}$$

Where $P_{C,T}$ is the transitional collapse rating [Pa], Y_P is the yield strength of the tieback [Pa], F is a dimensionless factor [-], G is a dimensionless factor [-], OD is the outer diameter of the tieback [m], t is the wall thickness of the tieback [m].

Transitional collapse occurs if the tieback's slenderness ratio is between the maximum slenderness ratio for the plastic collapse $(OD/t)_P$ and the maximum slenderness ratio for the transitional collapse $(OD/t)_T$ of Equation 52.

$$(OD/t)_T = \frac{2 + (B/A)}{3 * B/A} \qquad \text{Equation 52}$$

Where $(OD/t)_T$ is the maximum slenderness ratio for the transitional collapse [-], A is a dimensionless factor [-], B is a dimensionless factor [-].

(*Bulletin on Formulas and Calculations for Casing, Tubing, Drill Pipe, and Line Pipe Properties - API BULLETIN 5C3*, Sixth Edition 1994. American Petroleum Institute; Bellarby 2009, 510–514)

3.2.2.4 Elastic Collapse

The minimum elastic collapse pressure is calculated with Equation 53.

$$P_{C,E} = \frac{46{,}95 * 10^6}{(OD/t) * \left((OD/t) - 1\right)^2}$$

Equation 53

Where $P_{C,E}$ is the elastic collapse rating [Pa], OD is the outer diameter of the tieback [m], t is the wall thickness of the tieback [m].

Elastic collapse occurs if the tieback's slenderness ratio is greater than the maximum slenderness ratio for the transitional collapse $(OD/t)_T$ of Equation 52.

(*Bulletin on Formulas and Calculations for Casing, Tubing, Drill Pipe, and Line Pipe Properties - API BULLETIN 5C3*, Sixth Edition 1994. American Petroleum Institute; Bellarby 2009, 510–514)

3.2.2.5 Equivalent External Pressure

API 5C3 derates collapse resistance for internal pressure. An equivalent external pressure P_{Equ} represents the influence of external and internal pressure while assessing collapse resistance. The area on which the internal pressure is acting is smaller than the area on which the external pressure acts. Thus, the internal pressure is reduced to account for this phenomenon.

The equivalent pressure can be caused by applying additional internal pressure or with the hydrostatic pressure in depth. The relationship in Equation 54 leads to higher collapse loads with depth, even though the differential pressure could remain the same.

$$P_{Equ} = P_O - \left(1 - \frac{2}{OD/t}\right) * P_I$$

Equation 54

Where P_{Equ} is the equivalent outside pressure for the collapse rating [Pa], P_O is the external pressure [Pa], P_I is the internal pressure [Pa], OD is the outer diameter of the tieback [m], t is the wall thickness of the tieback [m].

(*Bulletin on Formulas and Calculations for Casing, Tubing, Drill Pipe, and Line Pipe Properties - API BULLETIN 5C3*, Sixth Edition 1994. American Petroleum Institute; Bellarby 2009, 510–514)

3.2.3 Biaxial

Biaxial design means that axial stresses are considered in the calculations of burst and collapse ratings. Tension and compression affect the resistance of burst and collapse against failure differently. The response to an increase in either tensional or compressive loads is summarized in Table 4.

Increase in tensional loads →	Burst resistance is increased
	Collapse resistance is reduced
Increase in compressive loads →	Burst resistance is reduced
	Collapse resistance is increased

Table 4: Axial loads response to burst and collapse resistance

For the biaxial approach a so-called effective yield strength Y_{Pa} is used to measure the above-listed effects on the burst and collapse resistances. To calculate the effective yield strength for the collapse resistance under tension or the collapse resistance under compression Equation 55 is used. To calculate the effective yield strength for the burst resistance under tension or the burst resistance under compression Equation 56 is used. The convention of tensile stresses being positive and compressive stresses being negative is accounted for in the equations.

$$Y_{Pa} = Y_P * \left(\sqrt{1 - 0,75 * \left(\frac{\sigma_{Axial,Total}}{Y_P} \right)^2} - \frac{\sigma_{Axial,Total}}{2 * Y_P} \right) \qquad \text{Equation 55}$$

Where Y_{Pa} is the effective yield strength of the tieback [Pa], Y_P is the yield strength of the tieback [Pa], $\sigma_{Axial,Total}$ is the total axial stress [Pa].

$$Y_{Pa} = Y_P * \left(\sqrt{1 - 0,75 * \left(\frac{\sigma_{Axial,Total}}{Y_P} \right)^2} + \frac{\sigma_{Axial,Total}}{2 * Y_P} \right) \qquad \text{Equation 56}$$

Where Y_{Pa} is the effective yield strength of the tieback [Pa], Y_P is the yield strength of the tieback [Pa], $\sigma_{Axial,Total}$ is the total axial stress [Pa].

The above equations show that a reducing factor is calculated under the square root for any kind of axial load (tension or compression). A second factor is added or subtracted depending on the sign of the axial load and the desired effective yield strength. The influence of tension on the effective yield strength used to obtain the biaxial collapse rating is more severe than the effect of compression. Conversely, compression's influence is more dominant than tension when calculating the effective yield strength for the biaxial burst rating.

To obtain the burst resistance with the influence of the axial loads Y_P must be substituted by the corresponding Y_{Pa} in Equation 41.

To obtain the collapse resistance with the influence of the axial loads Y_P must be substituted by the corresponding Y_{Pa}. Equation 42 to Equation 46 are used to calculate the dimensionless factors A, B, C, F & G. After that the slenderness ratio ranges must be found through Equation

48, Equation 50 and Equation 52. With the slenderness ratio of the tieback, the corresponding collapse resistance can then be calculated.

(*Bulletin on Formulas and Calculations for Casing, Tubing, Drill Pipe, and Line Pipe Properties - API BULLETIN 5C3*, Sixth Edition 1994. American Petroleum Institute; Bellarby 2009, 510–514)

3.2.4   Triaxial

Analysing the failure criteria individually for axial, burst and collapse loads is sufficient in most design cases. Considering axial stresses for burst and collapse resistance ratings is a first step in the right direction to a more accurate assessment. Nevertheless, it is not the most accurate approach since the acting stresses in all three axes (Figure 24) (axial σ_{Axial}, radial σ_{Radial} and tangential σ_{Tan}) interact with each other and may have mitigating or aggravating influences. The combination of these three stresses is the so-called triaxial stress. The most accurate determination of resistance against failure is achieved through the triaxial analysis. This approach is more complicated and usually only used in the most rigorous designs. The triaxial analysis is typically done by commercial software and is not part of the MATLAB application due to its complexity.

A widely accepted yielding criterion is the Huber-Hencky-Mises yield stress. The yield stress is abbreviated as Von Mises equivalent (VME) stress. Yielding occurs when the VME stress exceeds the yield strength of the tieback. No reduction in the yield strength is necessary since all stresses are considered. The VME stress is based on the maximum distortion energy theory and is calculated from the axial, radial and tangential stresses while ignoring torque (Equation 57). The VME stress reaches a maximum either on the inside or the outside of a pipe, but never at any point within the wall of the pipe. The peak VME stress is used as a reference for the yielding criteria.

$$\sigma_{VME} = \frac{1}{\sqrt{2}} * \sqrt{(\sigma_{Axial} - \sigma_{Tan})^2 + (\sigma_{Tan} - \sigma_{Radial})^2 + (\sigma_{Radial} - \sigma_{Axial})^2} \qquad \text{Equation 57}$$

Where σ_{VME} is the Von Mises equivalent stress [Pa], σ_{Axial} is the axial stress [Pa], σ_{Radial} is the radial stress [Pa], σ_{Tan} is the tangential stress [Pa].

The contributions to the axial loads have been discussed in detail and can be applied here. The axial stress is constant across the tieback's cross-sectional area if no bends are present or bending is ignored. If bends are present and ought to be considered, axial loads must be calculated for the inside and the outside of the bend and from the inside to the outside of the pipe as well.

Applying tension or external pressure to a tubular tends to reduce its diameter by stretching the pipe if allowed to move. On the other hand, applying compression or internal pressure suggests an increase in diameter as the pipe would be contracted. Combining these phenomena generates higher stresses than either the pressure or axial loads alone. The

relationship is shown in Lame's equations (Equation 58 and Equation 59). The variable A_X must be substituted for the inside area A_I or outside area A_O of the tieback to obtain the maximum radial and tangential stress. Together with the maximum axial stress, the peak VME stress can finally be calculated.

$$\sigma_{Radial} = \frac{P_I * A_I - P_O * A_O}{A_O - A_I} - \frac{(P_I - P_O) * A_I * A_O}{(A_O - A_I) * A_X} \qquad \text{Equation 58}$$

Where σ_{Radial} is the radial stress [Pa], P_I is the internal pressure [Pa], A_I is the inside area of the tieback [m²], P_O is the external pressure [Pa], A_O is the outside area of the tieback [m²], A_X is a variable to insert A_I or A_O [m²].

$$\sigma_{Tan} = \frac{P_I * A_I - P_O * A_O}{A_O - A_I} + \frac{(P_I - P_O) * A_I * A_O}{(A_O - A_I) * A_X} \qquad \text{Equation 59}$$

Where σ_{Tan} is the tangential stress [Pa], P_I is the internal pressure [Pa], A_I is the inside area of the tieback [m²], P_O is the external pressure [Pa], A_O is the outside area of the tieback [m²], A_X is a variable to insert A_I or A_O [m²].

(Bellarby 2009, 510–514)
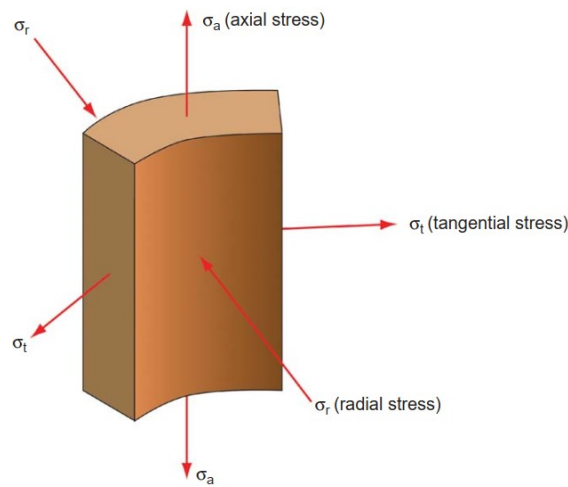
Figure 24: Stress components of the triaxial analysis (Bellarby 2009, 514)

3.2.5 Safety Factors

Safety factors for axial loads (tension and compression) SF_A, burst SF_B and collapse SF_C (Equation 60 to Equation 62) are obtained by dividing the corresponding resistance rating with its load under operating condition. The axial rating is the axial strength $F_{Axial,Max}$ while the burst rating P_B and collapse rating P_C must be calculated, as shown in the following chapters.

For the triaxial safety factor SF_T the yield strength Y_P is used as a rating against the Von Mises equivalent stress σ_{VME}.

Design factors are the minimum required safety factors which need to be maintained to deem a completion safe to use. Commonly used design factors can be found in Figure 25. Design factors may vary between companies or even projects and completion parts.

$$SF_A = \frac{F_{Axial,Max}}{F_{Axial,Total}} = \frac{Y_P}{\sigma_{Axial,Total}} \qquad \text{Equation 60}$$

Where SF_A is the axial (tension and compression) safety factor [-], $F_{Axial,Max}$ is the axial strength [N], $F_{Axial,Total}$ is the total axial load [N], Y_P is the yield strength of the tieback [Pa], $\sigma_{Axial,Total}$ is the total axial stress [Pa].

$$SF_B = \frac{P_B}{P_{I,Max} - P_{O,Max}} \qquad \text{Equation 61}$$

Where SF_B is the burst safety factor [-], P_B is the burst rating [Pa], $P_{I,Max}$ is the maximum internal pressure [Pa], $P_{O,Max}$ is the maximum outside pressure [Pa].

$$SF_C = \frac{P_C}{P_{Equ}} \qquad \text{Equation 62}$$

Where SF_C is the collapse safety factor [-], P_C is the collapse rating [Pa], P_{Equ} is the equivalent outside pressure [Pa].

$$SF_T = \frac{Y_P}{\sigma_{VME}} \qquad \text{Equation 63}$$

Where SF_T is the triaxial safety factor [-], Y_P is the yield strength of the tieback [Pa], σ_{VME} is the Von Mises equivalent stress [Pa].

Failure Mode	Design Factor
Burst	1.1–1.25
Collapse	1.0–1.1
Axial (tension and compression)	1.3–1.6
Triaxial	1.2–1.3

Figure 25: Common completion design factors (Bellarby 2009, 521)

(*Bulletin on Formulas and Calculations for Casing, Tubing, Drill Pipe, and Line Pipe Properties - API BULLETIN 5C3*, Sixth Edition 1994. American Petroleum Institute; Bellarby 2009, 509–523)

3.3 Load Scenarios

After analysing all the possible loads and length changes and introducing the various failure criteria, it is time to define the circumstances under which they may act.

This investigation considers a realistic approach to determine the axial loads and/or length changes. The determination of said loads and length changes is somewhat different for all the operation modes. It also depends if the tieback is restrained from movement or is allowed to move freely in a vertical direction. The user data is supposed to have maximum influence on the calculations.

Conservative worst-case as well as realistic load scenarios are used to obtain the resistance against burst and collapse. During normal operations, these circumstances should usually not arise. Nevertheless, it is wise to use worst-case scenarios to calculate the possibly occurring maximum loads to ensure the completion design holds even against the worst conditions.

3.3.1 Shut-In (Initial Conditions)

The shut-in case refers to the initial conditions while the tieback is being installed. During the initial conditions, the tieback floats freely inside the casing, which is filled with water. The outside and inside pressure are equal since the initial conditions refer to before any packer has been set. Further, the initial conditions refer to a state where the temperature of the water inside and outside of the tieback as well as the tieback itself are in equilibrium with the linear temperature caused by an average geothermal gradient.

To determine the worst-case burst load, an annulus pressure of zero $P_O = 0$ along with the entire completion depth shall be used. For the assessment of a realistic burst load, the actual maximum outside pressure in the annulus must be used $P_{O,Max}$. The inside pressure shall be the maximum at the end of the completion $P_{I,Max}$.

For the worst-case collapse load, an internal pressure of zero $P_I = 0$ along with the entire completion depth must be used as a reference. Realistic collapse load is determined with the equivalent outside pressure P_{Equ} (Equation 54) taking into account the maximum internal pressure $P_{I,Max}$ and the the maximum outside pressure at the bottom of the completion $P_{O,Max}$.

The following conditions must be taken into account to determine all applicable axial loads:

The water temperature distribution inside the tieback shall be a linear function matching the formation's geothermal gradient. If multiple gradients were used to obtain the reservoir temperature, a linear approximation must be used.

The water column's hydrostatic pressure inside the tieback during shut-in shall be in equilibrium with the formation pressure at the bottom of the well without any excess pressure at the wellhead. Thus, the maximum inside pressure is equal to the temperature-accounted reservoir pressure for an undisturbed reservoir at the tieback's end depth $P_{I,Max} = P_{Dn,Shut,Temp}$ (Equation 12).

The annulus pressure distribution during shut-in is equal to the water pressure distribution inside the tieback.

The load due to the weight of the tieback F_{Weight} shall be accounted for buoyancy $F_{Buoyancy}$ with the pressure at the bottom of the well.

The piston force acting on the packer F_{Packer} or the resulting length change ΔL_{Packer} is zero because there is no pressure differential acting on the packer.

If applicable to the completion design, any crossover loads $F_{Crossover}$ or length changes $\Delta L_{Crossover}$ caused by a tampered tieback shall be calculated with the pressures at the location of the crossover.

No ballooning loads $F_{Balloon}$ or length changes $\Delta L_{Balloon}$ due to relative pressure differentials are present since the shut-in servers as the reference case with initial conditions.

There are no temperature loads F_{Temp} or length changes ΔL_{Temp} due to a temperature differential (initial conditions).

No drag force F_{Drag} or length change due to drag ΔL_{Drag} is applicable since the hydrostatic water column inside the tieback remains static.

Any present initial doglegs from drilling activities shall be accounted for with the resulting bending loads F_{Bend}. Bending loads are to be added or subtracted to achieve maximum tensile and compressive loads on the bend's applicable length.

3.3.2 Production

To determine the worst-case burst load, an annulus pressure of zero $P_O = 0$ along with the entire completion depth shall be used. For the assessment of a realistic burst load, the actual maximum outside pressure in the annulus must be used $P_{O,Max}$. The inside pressure shall be the maximum at the end of the completion $P_{I,Max}$. The required bottomhole pressure from which the pressure at the bottom of the tieback is deducted considering frictional pressure losses and the difference in depth is subject to user input.

For the worst-case collapse load, an internal pressure of zero $P_I = 0$ along with the entire completion depth must be used as a reference. Realistic collapse load is determined with the equivalent outside pressure P_{Equ} (Equation 54) taking into account the maximum internal pressure $P_{I,Max}$ and the the maximum outside pressure at the bottom of the completion $P_{O,Max}$.

The following conditions must be taken into account to determine all applicable axial loads.

The temperature distribution of the hot water inside the tieback during production shall be governed by Equation 5, Equation 7 & Equation 8.

The water pressure distribution inside the tieback during production shall take into account the reduced density due to heat $P_I = P_{Dn,Producer}$ (Equation 14). The inside pressure must be accounted for the pressure losses described in Equation 15 to Equation 20.

The annulus pressure distribution $P_{Dn,Annulus}$ during production shall be obtained with a constant annulus fluid density. No additional applied pressure (except surface pressure) or pressure losses are applicable to the annulus pressure.

The load due to the weight of the tieback F_{Weight} shall be accounted for buoyancy $F_{Buoyancy}$ with the pressure at the bottom of the well.

The piston force acting on the packer F_{Packer} or the resulting length change ΔL_{Packer} needs to be considered.

If applicable to the completion design, any crossover loads $F_{Crossover}$ or length changes $\Delta L_{Crossover}$ caused by a tampered tieback shall be calculated with the pressures at the location of the crossover.

Ballooning loads $F_{Balloon}$ or length changes $\Delta L_{Balloon}$ due to relative pressure differentials in respects to the shut-in base case are to be considered.

Temperature loads F_{Temp} or length changes ΔL_{Temp} due to hot water inside the tieback during production must be considered.

Pressure loss calculations shall be used to calculate the drag force F_{Drag} or length change due to drag ΔL_{Drag}.

Any present initial doglegs from drilling activities shall be accounted for with the resulting bending loads F_{Bend}. Bending loads are to be added or subtracted to achieve maximum tensile and compressive loads on the bend's applicable length.

3.3.3   Injection

To determine the worst-case burst load, an annulus pressure of zero $P_O = 0$ along with the entire completion depth shall be used. For the assessment of a realistic burst load, the actual maximum outside pressure in the annulus must be used $P_{O,Max}$. The inside pressure during injection is equal to the maximum pressure at the end of the completion $P_{I,Max}$ including any applied pressure at the wellhead and frictional pressure losses.

For the worst-case collapse load, an internal pressure of zero $P_I = 0$ along with the entire completion depth must be used as a reference. Realistic collapse load is determined with the equivalent outside pressure P_{Equ} (Equation 54) taking into account the maximum internal pressure $P_{I,Max}$ and the the maximum outside pressure at the bottom of the completion $P_{O,Max}$.

The following conditions must be taken into account to determine all applicable axial loads.

The temperature distribution of the cold water inside the tieback during production shall be governed by Equation 6, Equation 7 & Equation 8. The injection water temperature at the surface may vary.

The water pressure distribution inside the tieback during injection shall be obtained by using the density under surface conditions $P_I = P_{Dn,Injector}$ (Equation 13). Any additional applied pressure at the wellhead must be considered. The inside pressure must be accounted for the pressure losses described in Equation 15 to Equation 20.

The annulus pressure distribution $P_{Dn,Annulus}$ during injection shall be obtained with a constant annulus fluid density. No additional applied pressure (except surface pressure) or pressure losses are applicable to the annulus pressure.

The load due to the weight of the tieback F_{Weight} shall be accounted for buoyancy $F_{Buoyancy}$ with the pressure at the bottom of the well.

The piston force acting on the packer F_{Packer} or the resulting length change ΔL_{Packer} needs to be considered.

If applicable to the completion design, any crossover loads $F_{Crossover}$ or length changes $\Delta L_{Crossover}$ caused by a tampered tieback shall be calculated with the pressures at the location of the crossover.

Ballooning loads $F_{Balloon}$ or length changes $\Delta L_{Balloon}$ due to relative pressure differentials in respects to the shut-in base case are to be considered.

Temperature loads F_{Temp} or length changes ΔL_{Temp} due to cold water inside the tieback during injection must be considered.

Pressure loss calculations shall be used to calculate the drag force F_{Drag} or length change due to drag ΔL_{Drag}.

Any present initial doglegs from drilling activities shall be accounted for with the resulting bending loads F_{Bend}. Bending loads are to be added or subtracted to achieve maximum tensile and compressive loads on the bend's applicable length.

3.3.4   Pressure Test

Pressure tests to test and verify the completion design's integrity are to be conducted with pressure testing plugs at the bottom of the tieback.

To determine the worst-case burst load, an annulus pressure of zero $P_O = 0$ along with the entire completion depth shall be used. For the assessment of a realistic burst load, the actual maximum outside pressure in the annulus must be used $P_{O,Max}$. The maximum inside pressure $P_{I,Max}$ during a pressure test is present at the pressure testing plug. It is equal to the hydrostatic pressure at the plug at the bottom of the tieback plus any applied wellhead pressure without pressure losses (no flowing fluid).

For the worst-case collapse load, an internal pressure of zero $P_I = 0$ along with the entire completion depth must be used as a reference. Realistic collapse load is determined with the

equivalent outside pressure P_{Equ} (Equation 54) taking into account the maximum internal pressure $P_{I,Max}$ and the the maximum outside pressure at the bottom of the completion $P_{O,Max}$.

The following conditions must be taken into account to determine all applicable axial loads.

The water temperature distribution inside the tieback during pressure tests shall be the same as during initial conditions in shut-in.

The water pressure distribution inside the tieback during pressure tests shall be the temperature-accounted pressure of the shut-in case plus any applied wellhead pressure without pressure losses (no flowing fluid).

The annulus pressure distribution $P_{Dn,Annulus}$ during pressure tests shall be obtained with a constant annulus fluid density.

The load due to the weight of the tieback F_{Weight} shall be accounted for buoyancy $F_{Buoyancy}$ with the pressure at the bottom of the well.

The piston force acting on the pressure testing plug F_{Plug} or the resulting length change ΔL_{Plug} needs to be examined.

The piston force acting on the packer F_{Packer} or the resulting length change ΔL_{Packer} needs to be considered.

If applicable to the completion design, any crossover loads $F_{Crossover}$ or length changes $\Delta L_{Crossover}$ caused by a tampered tieback shall be calculated with the pressures at the location of the crossover.

Ballooning loads $F_{Balloon}$ or length changes $\Delta L_{Balloon}$ due to relative pressure differentials in respects to the shut-in base case are to be considered.

Temperature loads F_{Temp} or length changes ΔL_{Temp} are not applicable since the temperature distribution does not change between shut-in and load case.

No pressure loss calculations need to be considered for the drag force F_{Drag} or length change due to drag ΔL_{Drag} because only static pressure is applied at the wellhead (no flowing fluid).

Any present initial doglegs from drilling activities shall be accounted for with the resulting bending loads F_{Bend}. Bending loads are to be added or subtracted to achieve maximum tensile and compressive loads on the bend's applicable length.

4   Buckling Analysis

Buckling is a phenomenon of structural deformation for elements that are thin in comparison to their length. Under normal circumstances, buckling requires compressive forces. While investigating buckling in an uncemented tieback, there is a further complication due to the presence of internal P_I and external P_O pressures.

Buckling is calculated differently for vertical and deviated wellbores. In context with buckling the term deviated wellbores refers to a wellbore with a constant inclination angle θ. Buckling in deviated wells depends on the pipe contact force and thus on the degree of inclination. Both vertical and deviated buckling calculations are presented throughout this chapter.

Suppose the wellbore subject to the investigation is deviated only in particular sections of the well's trajectory and not continuously over the entire length. If the latter is the case, the MATLAB model will determine an average constant inclination angle in respect to the vertical with $\cos\theta = \frac{TVD}{MD}$. The average inclination angle will then be used to simulate a deviated wellbore for the buckling assessment. Any inclination angle lower than 3 [°] shall lead to the usage of equations associated with a purely vertical wellbore.

Buckling could complicate the situation of a completion because of various reasons. It can induce high doglegs which then further cause bending stresses. The bending stresses can cause local maxima in axial compression and tension where the bends are located, causing reduced biaxial and triaxial safety factors. Especially the maximum axial compression increases with buckling occurring at the bottom of the well. Buckling can lead to a contraction of the tieback if it is allowed to move freely. If the doglegs are significant, they can limit access through the tieback for any tools that may be desired to use. Buckling also creates a torque on connections which in extreme cases can unscrew them.

A small thought model shall help to understand the characteristics of buckling (Figure 26). Even in a vertical wellbore, a small deviation to the vertical tieback creates a bend. The internal pressure acts on both sides of the tieback's bend. Due to the nature of a bend, the internal area A_I. on the outside of the bend is larger than on the inside. The resulting sideway forces are not equal because of this uneven distribution of internal area created by a bend. The sideways forces with different magnitudes are aggravating the severity of the initial bend. Thus, compressive loads and internal pressure will promote the onset of buckling. External pressure and tensile loads are diminishing the tendency of the onset of buckling. All these findings are represented in a newly introduced effective axial load $F_{Axial,Eff}$ (Equation 64).

$$F_{Axial,Eff} = F_{Axial,Total} + (P_O * A_O - P_I * A_I) \hspace{3cm} \text{Equation 64}$$

Where $F_{Axial,Eff}$ is the effective axial load [N], P_O is the external pressure [Pa], A_O is the outside area of the tieback [m²], P_I is the internal pressure [Pa], A_I is the inside area of the tieback [m²].

(Mitchell 2006; Bellarby 2009, 491–500)
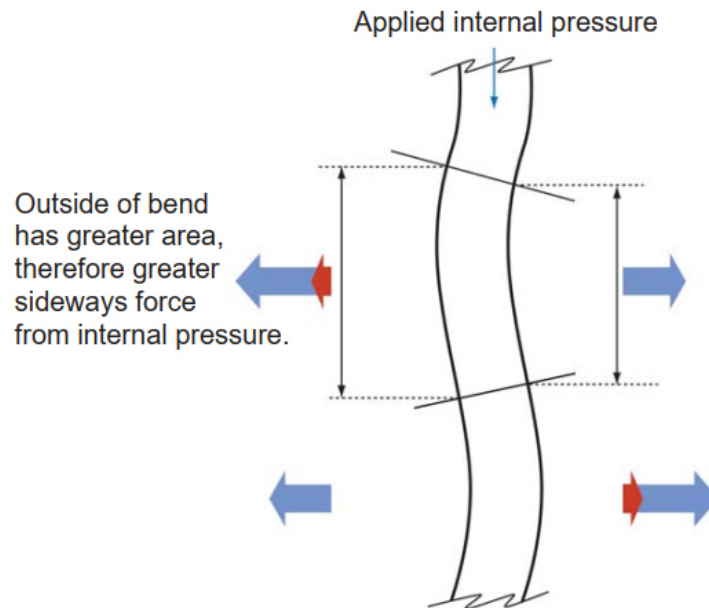
Figure 26: Effect of internal pressure on buckling (Bellarby 2009, 492)

The onset of buckling tends to occur if the effective axial load $F_{Axial,Eff}$ is less than a critical force F_C. If the effective axial load is greater than the critical force, no buckling tends to occur. Equation 64 shows that buckling could occur to a tieback even if it is entirely under tension if the inside pressure is high enough.

The critical force calculations (Equation 68 to Equation 71) result in positive values, but the critical force itself is compressive by nature. For this reason, the critical force has a minus sign in the overview of the buckling's onset criteria in Table 5. (Bellarby 2009, 491–500)

$F_{Axial,Eff} < -F_C$	Buckling will tend to happen
$F_{Axial,Eff} > -F_C$	Buckling will not tend to happen

Table 5: Buckling onset

There are two modes of buckling that are widely recognized. The first being sinusoidal buckling (a in Figure 27) and the second being helical buckling (b in Figure 27). Sinusoidal buckling manifests itself in an approximately "S" shape. Nevertheless, sinusoidal or lateral buckling as it is also called is not a real sinusoid. Helical buckling as the name suggests describes a helical deformation. One can imagine a corkscrew as a fair comparison. Each mode has its critical force with the sinusoidal critical force being lower than the helical.

Furthermore, there are different critical forces for non-deviated vertical wellbores and deviated wellbores. Critical forces in vertical wells usually are small compared to their counterparts in highly deviated wells. (Bellarby 2009, 491–500)
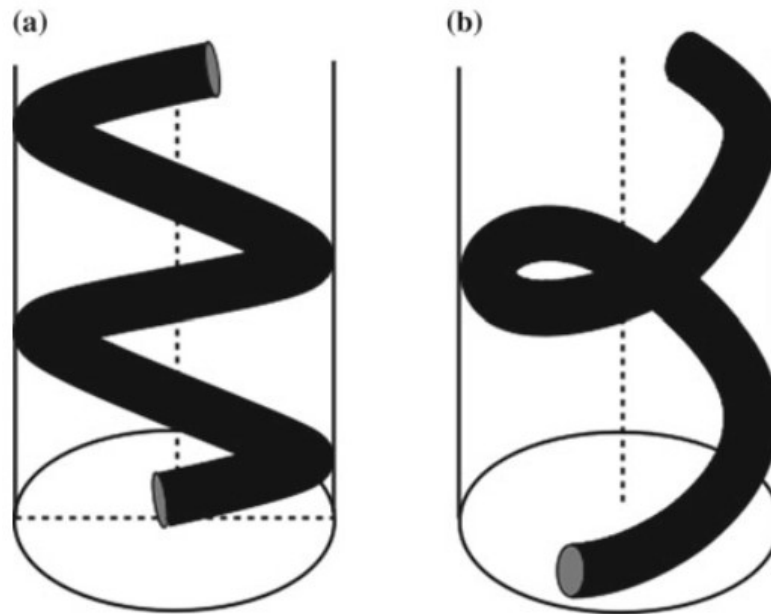
Figure 27: The two buckling modes – sinusoidal and helical (Jaculli and Mendes 2018, 11)

Literature often refers to the likelihood or tendency of the onset of buckling. It is not guaranteed that buckling will not occur if the effective axial force is greater than the critical force, especially if the forces are similar in magnitude. The onset of buckling has been covered by multiple authors and often different factors governing the onset and switch from sinusoidal to helical buckling (and back) are added to the same equations leading to different results. (Cunha 2004)

For the equations of the following chapters, three more variables are needed. The first is the moment of inertia I. It can be obtained through Equation 65. Suppose multiple sections are present in the completion design (crossovers). In that case, the moment of inertia of the bottom has to be used since the bottom is the reference point where the effective axial load and the critical force(s) are compared.

$$I = \frac{\pi}{64} * (OD^4 - ID^4)$$
Equation 65

Where I is the moment of inertia of the tieback [m⁴], OD is the outer diameter of the tieback [m], ID is the inner diameter of the tieback [m].

The second is the buoyed weight w_B of the tieback, which is a force per unit length and can be calculated with Equation 66. If multiple sections are present (crossovers), the total force due to weight in air of the entire completion string can be used to obtain an average buoyed weight.

$$w_B = \frac{W - F_{Buoyancy}}{MD}$$
Equation 66

Where w_B is the effective buoyed weight of the tieback [N/m], W is the entire weight force of the tieback due to self-weight [N], $F_{Buoyancy}$ is the buoyancy force on the tieback's bottom [N], MD is the measured depth [m].

The third is the radial clearance, which is the difference in the casing's ID and the tieback's OD (Equation 67). The bottom's radial clearance has to be used even if the tieback passes through multiple casing sections and may features crossovers since the bottom is the reference point where the effective axial load and the critical force(s) are compared.

$$r_C = ID_{Casing} - OD$$ Equation 67

Where r_C is the radial clearance [m], ID_{Casing} is the inside diameter of the casing [m], OD is the outer diameter of the tieback [m].

(Mitchell 2006; Bellarby 2009, 491–500)

Connectors (couplings and tool joints) should have some impact on the buckling of a tubular. For example, the connector OD may be as much as 50% bigger than the pipe body OD. As a result, the connector's radial clearance can be significantly smaller compared to the radial clearance of the pipe itself. The buckling phenomena have been studied intensively in the last years, but little attention has been given to connectors' influence in that regard. Applied torque to the tubular also influences buckling. A pipe under torque may buckle while being entirely under tension. The contact force between pipe and wellbore can be increased or decreases, depending on the torque direction. Considering connectors and torque to the buckling investigation adds another degree of complexity, especially in deviated and horizontal wellbores. (Mitchell and Miska 2006)

There are unsolved problems when considering tapered completions strings. One would expect modifications to the solution for a uniform pipe body, joining two helically buckled strings with different geometry and maybe even mechanical properties. Lubinski suggested a stacked solution, meaning that each completion string is treated as a separate string with a helical pitch. Lubinski's solution is only valid away from the boundary conditions (the crossover), and the solution is therefore unknown at the point of the crossover as indicated in Figure 28. Another approach by Hammerlindl is a discrepancy to Lubinski's approach because it can only be applied to sections with the same radial clearance. Which means Hammerlindl's solution only applies to sections with the same diameters and therefore not to a tapered completion string. Studies have shown that changing the radial clearance produces oscillatory behaviour in the helix pitch, contradicting the conventional solutions.

The question remains: "What is the pipe's behaviour at the crossover point between two strings with different dimensions?". The problem of a tapered string regarding buckling analysis still needs resolution. (Mitchell 2005, 2006)
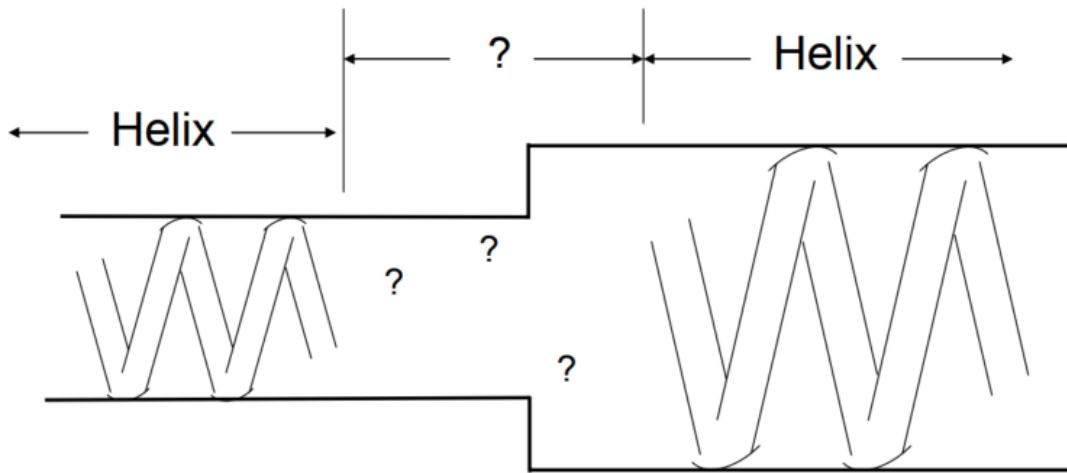
Figure 28: Tapered string problem (Mitchell 2006)

4.1 Buckling in a vertical non-deviated Wellbore

In a vertical non-deviated wellbore, the two critical forces for sinusoidal $F_{C,S}$ and helical buckling $F_{C,H}$ are described by Equation 68 and Equation 69, respectively.

The critical forces for sinusoidal and helical buckling are directly connected to the moment of inertia and the buoyed weight of the tieback. Thus, larger diameter and/or wall thickness leads to a more significant critical force and will reduce buckling risk.

The critical force for helical buckling is more than double in magnitude than the sinusoidal critical force. Thus, more compression would be needed to cause helical buckling. There may be a window in which a tieback starts to buckle under sinusoidal but not helical buckling. A change in the axial loads or more applied internal pressure could then cause the tip over to helical buckling.

$$F_{C,S} = 1,94 * \sqrt[3]{E * I * w_B{}^2} \qquad \text{Equation 68}$$

Where $F_{C,S}$ is the critical force for sinusoidal buckling [N], E is the modulus of elasticity of the tieback [Pa], I is the moment of inertia of the tieback [m⁴], w_B is the buoyed weight of the tieback [N/m].

$$F_{C,H} = 4,05 * \sqrt[3]{E * I * w_B{}^2} \qquad \text{Equation 69}$$

Where $F_{C,H}$ is the critical force for helical buckling [N].

(Bellarby 2009, 491–500)

4.2 Buckling in a deviated Wellbore

In a deviated wellbore Equation 70 and Equation 71 can be used to calculate the critical force for sinusoidal $F_{C,S}$ and helical buckling $F_{C,H}$. A smaller tieback OD for the same casing ID would create a significantly lower critical force and a higher likelihood to buckling, due to the influence on the moment of inertia I and the radial clearance r_C. The factor $1{,}41{\sim}1{,}83$ in Equation 71 presents the previously mentioned uncertainty when sinusoidal buckling may switch to helical buckling in a deviated wellbore. The factor will be subject to user input within the limits of 1,41 and 1,83 through the graphical user interface (GUI) in the MATLAB application.

$$F_{C,S} = \sqrt{\frac{4 * E * I * w_B * \sin\theta}{r_C}}$$

Equation 70

Where $F_{C,S}$ is the critical force for sinusoidal buckling [N], E is the modulus of elasticity of the tieback [Pa], I is the moment of inertia of the tieback [m⁴], w_B is the buoyed weight of the tieback [N/m], θ is the inclination of the well [°], r_C is the radial clearance [m].

$$F_{C,H} = 1{,}41{\sim}1{,}83 * \sqrt{\frac{4 * E * I * w_B * \sin\theta}{r_C}}$$

Equation 71

Where $F_{C,H}$ is the critical force for helical buckling [N].

Buckling, especially in deviated wellbores, is further complicated because the switch from sinusoidal to helical buckling does not occur under the same loads as the reverse switch from helical to sinusoidal buckling. More complicated in-depth investigations are needed in curved wellbores and if connections ought to be considered. It is important to note that Equation 70 and Equation 71 are based on simplifications that would lead to a result of zero for a vertical wellbore with zero inclination.

(Bellarby 2009, 491–500)

4.3 Length changes due to Buckling

When buckling occurs the tieback will be shortened, but buckling does not result in elongation in length, which is different from previously induced effects throughout this thesis. There is a neutral point, where, below this point, buckling occurs and no buckling occurs above it. If the compressive force which causes buckling is too high it is possible that the result of the neutral point would lead to a length longer than the tieback. For that reason, first the neutral point must be calculated (Equation 72) and then the appropriate equation used to determine the reduction in length. Equation 73 is used if the value of the neutral point is smaller than the total tieback length and Equation 74 is used if the value is greater. One of the variables in Equation 72 and Equation 73 is the packer bore area A_P. If no information about the packer is available the outside diameter of the tieback shall be used instead.

$$n = \frac{A_P * \left(P_{I,Packer} - P_{Above,Packer}\right)}{(w_T + w_I - w_O)}$$
Equation 72

Where n is the neutral point below which buckling occurs [m], A_P is the packer bore area [m²], $P_{I,Packer}$ is the inside pressure of the tieback at the packer [Pa], $P_{Above,Packer}$ is the annulus pressure above the packer [Pa], w_T is the linear weight of the tieback [N/m], w_I is the linear weight of the fluid inside the tieback [N/m], w_O is the linear weight of the fluid in the annulus [N/m].

$$\Delta L_{Buck} = \frac{r_C{}^2 * A_P{}^2 * \left(P_{I,Packer} - P_{Above,Packer}\right)^2}{-8 * E * I * (w_T + w_I - w_O)}$$
Equation 73

Where ΔL_{Buck} is the shortening due to buckling [m], r_C is the radial clearance [m], A_P is the packer bore area [m²], $P_{I,Packer}$ is the inside pressure of the tieback at the packer [Pa], $P_{Above,Packer}$ is the annulus pressure above the packer [Pa], E is the modulus of elasticity of the tieback [Pa], I is the moment of inertia of the tieback [m⁴], w_T is the linear weight of the tieback [N/m], w_I is the linear weight of the fluid inside the tieback [N/m], w_O is the linear weight of the fluid in the annulus [N/m].

$$\Delta L'_{Buck} = \Delta L_{Buck} * \frac{L_{Tieback}}{n} * \left(2 - \frac{L_{Tieback}}{n}\right)$$
Equation 74

Where $\Delta L'_{Buck}$ is the shortening due to buckling of the entire tieback [m], ΔL_{Buck} is the shortening due to buckling [m], $L_{Tieback}$ is the length of the tieback (MD) [m], n is the neutral point below which buckling occurs [m].

If multiple sections are present in a tieback string the linear weight of the tieback w_T can be determined with the total load due to self-weight in air and the depth (Equation 75).

$$w_T = \frac{W}{MD}$$
Equation 75

Where w_T is the linear weight of the tieback [N/m], W is the entire weight force of the tieback due to self-weight [N], MD is the measured depth [m].

The linear weight of the water inside the tieback w_I at the packer location can be calculated with Equation 76 assuming that the density of the reservoir water is representable for the density at the packer.

$$w_I = \rho_{Water,Reservoir} * A_I * g$$
Equation 76

Where w_I is the linear weight of the fluid inside the tieback [N/m], $\rho_{Water,Reservoir}$ is the density of water inside the tieback under reservoir conditions [kg/m³], A_I is the inside area of the tieback [m²], g is the gravitational acceleration [m/s²].

The linear weight of the water inside the annulus w_O at the packer location can be calculated with Equation 77 assuming that the density of the water in the annulus is the same as the density of the reservoir.

$$w_O = \rho_{Water,Annulus} * A_O * g$$ Equation 77

Where w_O is the linear weight of the fluid in the annulus [N/m], $\rho_{Water,Annulus}$ is the density of water inside the annulus [kg/m³], A_O is the outside area of the tieback [m²], g is the gravitational acceleration [m/s²].

(Lyons et al. 2015, 489, Chapter 4; Kang et al. 2020)

4.4 Helix Angle and induced Doglegs

Buckling is limited by contact of the tieback with the casing. Thus, some degree of buckling can be tolerated. The severity of buckling is dependents on the radial clearance r_C but also the helix angle, which is obtained differently for sinusoidal and helical buckling. For the helical buckling mode, the $Pitch$ describes the distance from the centre of one maximum of the bend to the next one on the same side.

The helix angle is not constant through the "S" shape of sinusoidal buckling and therefore a maximum helix angle $\theta_{Helix,Max}$ (Equation 78) needs to be calculated. However, the helix angle θ_{Helix} (Equation 79) is constant for helical buckling, as long as connections and end effects are ignored.

To calculate the pitch first the helix angle of the bend θ_{Helix} during helical buckling must be determined. The pitch is then obtained through Equation 80.

The resulting DLS due to buckling (Equation 81) depends on the helix angle and the radial clearance. The DLS creates local bending stresses according to Equation 39. The tieback will permanently become like a corkscrew if the bending stresses exceed the yield stress of the tieback.

$$\theta_{Helix,Max} = \frac{1,1227}{\sqrt{2 * E * I}} * F_{Axial,Eff}^{0,04} * \left(F_{Axial,Eff} - F_{C,S}\right)^{0,46}$$ Equation 78

Where $\theta_{Helix,Max}$ is the maximum helix angle for sinusoidal buckling [rad/m], E is the modulus of elasticity of the tieback [Pa], I is the moment of inertia of the tieback [m⁴], $F_{Axial,Eff}$ is the effective axial load [N], $F_{C,S}$ is the critical force for sinusoidal buckling [N].

$$\theta_{Helix} = \sqrt{\frac{F_{Axial,Eff}}{2 * E * I}}$$ Equation 79

Where θ_{Helix} is the helix angle for helical buckling [rad/m], E is the modulus of elasticity of the tieback [Pa], I is the moment of inertia of the tieback [m⁴], $F_{Axial,Eff}$ is the effective axial load [N].

$$Pitch = \frac{2 * \pi}{\theta_{Helix}}$$ Equation 80

Where $Pitch$ is the distance from one maximum of the bend to the next one on the same side during helical buckling [m], θ_{Helix} is the helix angle for helical buckling [rad/m].

$$DLS = \frac{180 * 30}{\pi} * r_C * \theta_{Helix,Max}^2 = \frac{180 * 30}{\pi} * r_C * \theta_{Helix}^2$$ Equation 81

Where DLS is the dogleg severity [°/30m], r_C is the radial clearance [m], $\theta_{Helix,Max}$ is the maximum helix angle for sinusoidal buckling [rad/m], θ_{Helix} is the helix angle for helical buckling [rad/m].

(Bellarby 2009, 491–500)

4.5 Torque due to Buckling

Torque promotes buckling, but the reverse effect is also correct. Buckling promotes torque which under extreme circumstances could unscrew connections or risk an over-torquing. Torque induced from buckling is small and often ignored. Nevertheless, suppose the tieback would be small and/or the radial clearance r_C large the buckling-induced torque can be significant compared to the make-up torque of the tieback's connections. The torque τ in Equation 82 can have a positive or a negative sign, like the bending stresses before. The sign depends on the selection of the counter-clockwise or clockwise helix angle.

$$\tau = \pm \frac{F_{Axial,Eff} * r_C^2 * \beta}{2 * \sqrt{1 - r_C^2 * \beta^2}}$$ Equation 82

Where τ is the buckling-induced torque [Nm], $F_{Axial,Eff}$ is the effective axial load [N], r_C is the radial clearance [m], β is a variable to calculate the buckling-induced torque [m⁻¹].

$$\beta = \sqrt{\frac{-F_{Axial,Eff}}{2 * E * I}}$$ Equation 83

Where β is a variable to calculate the buckling-induced torque [m⁻¹], $F_{Axial,Eff}$ is the effective axial load [N], E is the modulus of elasticity of the tieback [Pa], I is the moment of inertia of the tieback [m⁴].

(Bellarby 2009, 491–500)

4.6 Mitigation Methods

Buckling can be mitigated through a couple of standard measurements. Expansion devices can reduce stresses on packers and the tieback because they allow compensating for axial loads with a change in length. In horizontal but even more so in deviated and horizontal wells, centralizers could provide an additional mitigation option by stiffening the string. Applying tension during the tieback setting could potentially help keep the entire string under tension, avoiding buckling as a result.

4.6.1 Expansion Devices

Expansion devices can be used to reduce loads on packers and tubular, mainly for loads caused by thermal changes. They compensate the loads with a change in length. (Mitchell 2007)

(Bellarby 2009) suggests that expansion devices have three principal configurations, listed below. Nonetheless, many different builds featuring different operational conditions and functionalities are available from various manufacturers.

1. The polished bore receptacle (PBR) has multiple seals which are connected to the male upper section. The seals can therefore be recovered during a workover. The PBR can be run in two trips or run pinned together with shear pins or more commonly a shear ring.
2. The expansion joint is essentially an upside-down PBR; with the female section above the male section, the seals connect to the female section. As with a PBR, the sections can be run on a single trip and pinned together or separately. Some expansion joints can have allowable seal strokes up to 12 meters.
3. The slip joint is designed to no-go after both excess upward and downward movement. Conversely, all PBRs and expansion joints are designed to no-go after excess downward movement; most are designed to disengage with excess upward movement.

(Bellarby 2009, 576–578)

The assessment of loads and possible length changes introduced throughout this thesis implies the use of expansion devices. This mitigation method is an option of the MATLAB model, without further specification which expansion device is used. A complete expansion and reduction in length are possible in the MATLAB application to indicate how much the tieback's total elongation or contraction under different load scenarios would be.

4.6.2 Centralizer

Using a centralizer stabilizes the tieback in the middle of the casing. Buckling can be mitigated by strategic placement of centralizers to decrease the annular clearance.

Regarding the radial clearance between the ID of the casing and the OD of the tieback, a centralizer does not have much impact in a purely vertical well, where one can assume that radial clearance remains constant along with the depth of the wellbore.

However, curved, deviated, and horizontal wells are exposed to sections where the tieback is likely to contact the surrounding casing. Centralizers can maintain a constant radial clearance, given that enough centralizers are installed. Centralizers would therefore also decrease the contact forces acting on the tieback. However, the contact between the casing and the centralizers is still given, and the contact forces are then acting on said centralizers. Figure 29 illustrates the change in contact forces and radial clearance by using centralizers. (Sanchez et al. 2012)
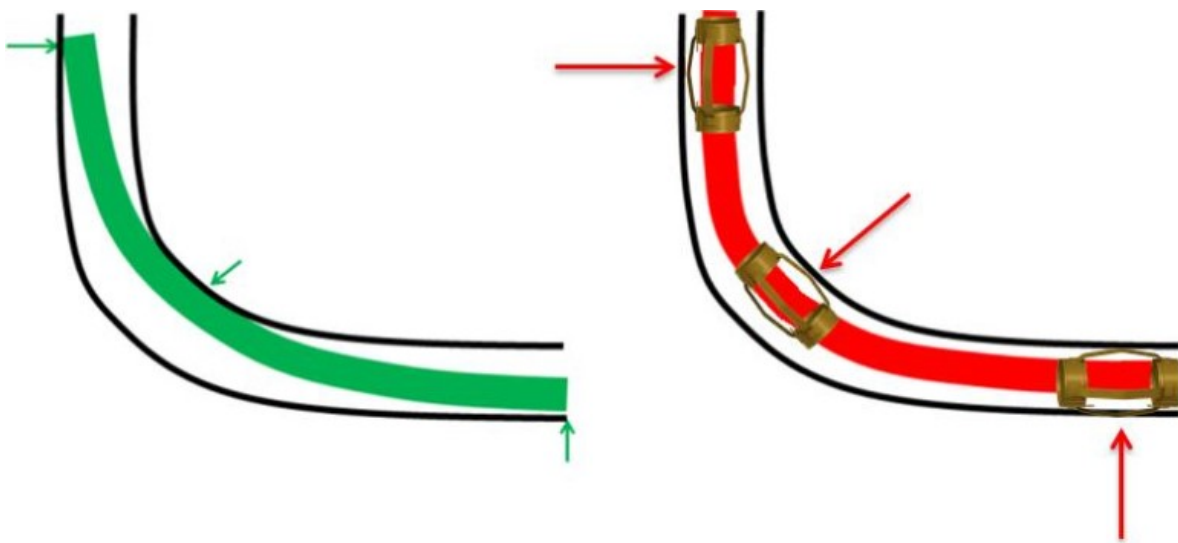
Figure 29: Effect of centralizers on contact forces and radial clearance
(Sanchez et al. 2012)

4.6.3 Tieback under Pre-Tension

The tieback can be suspended so that the temperature & pressure-related changes in axial loads or length during subsequent production or injection can be compensated. Suppose temperature changes due to hot water production are the most significant contribution to the compressive axial force. If these changes can be anticipated and the resulting compression calculated, additional tension can be applied to the tieback to counteract the compression and preventing buckling in the process. Of course, one must consider the additional tension for the failure criteria of the tieback as well. During the tieback setting, additional preload could be applied through a packer or at the wellhead, for example. (*Leitfaden Futterrohrberechnung* 2006. Wirtschaftsverband Erdöl- und Erdgasgewinnung e.V., 50)

Additional tension can also be applied to the load and buckling calculations in the MATLAB model.

5 Case Study

The company (Erdwerk GmbH) has provided information on a case study with a sample completion from a well for the buckling investigation at hand. Erdwerk advises on geological, hydrogeological, geothermal, energetic and drilling-related issues as an independent planning office. Their headquarters are located in Munich, Germany. Nonetheless, they are planning and monitoring the implementation of deep-geothermal projects in many parts of Europe.

The data is supposed to help develop the application and determine results for a real project as a reference. While the provided information serves as a good start to develop and test the application and its functionality, it is not based entirely on the sample completion from Erdwerk. Erdwerk's sample completion can be used as good as any other well with a tieback installation up to the surface. A tieback or tieback liner runs from the wellhead within the casing completion string(s). A tieback may be required for different reasons, such as higher pressure resistance during flow and pressure tests and if high reservoir and/or injection pressures can be expected. They can also be used as a remedy if a section of a casing string has lost integrity and for other treatments or purposes. Tiebacks are often not cemented as it is the case for this sample well.

5.1 Well Completion

Figure 30, provides a sketch of the case study's sample well completion at the end of this chapter.

The first three casing sections are cemented to the surface followed by a casing liner section and an open-hole section without casing at the end of the wellbore. Table 6 summarizes the hole and casing diameters with respect to their setting depths.

Start Depth (MD) [m]	End Depth (MD) [m]	Hole Diameter [in]	OD [in]	w/l [lb/ft]	t [in]	ID [in]
0,00	60,00	36	26			
0,00	850,00	23	18 5/8	87,50	0,435	17,755
0,00	2410,00	17 1/2	13 3/8	72,00	0,514	12,347
2310,00	3910,00	12 1/4	9 7/8	62,80	0,625	8,625
3910,00	4437,00	8 3/8				

Table 6: Hole and casing diameters of the case study well (Erdwerk GmbH)

No exact details about the used steel grades, nominal linear mass, wall thickness, inner diameter or connection type have been provided for the casing sections. Some of the above-mentioned details are assumed for the calculations, according to the corresponding values in the API table of Appendix A. Most important are the IDs for the innermost casing section, encasing the annulus around the tieback string. The casing sections' structural integrity is not part of this investigation and is assumed to be intact and modelled, keeping best practice in mind.

The tieback runs from the surface to an MD of 3886 meters (not shown in Figure 30). It consists of two sections with a reducing diameter from the upper to the lower section. It features the same L80 steel grade and BTC connections. The connection between the tieback sections is

made seamless with a connection piece. Thus, it allows assuming that the tieback is one continuous string only with two sections and different dimensions for all following calculations. The tieback (both sections) features a coating which is not specified further. Table 7 summarizes the tieback's dimensions and properties with respect to each section's MD.

Start Depth (MD) [m]	End Depth (MD) [m]	Steel Grade	OD [in]	w/l [lb/ft]	t [in]	ID [in]
0,00	700,00	L80	9 5/8	53,500	0,545	8,535
700,00	3886,00	L80	7	32,000	0,453	6,094

Table 7: Dimension and properties of the tieback sections (Erdwerk GmbH)

Figure 3 shows that an additional 7 [inch] stainless-steel liner runs from the end of the tieback all the way down to bottom hole at 4437 meters MD. The stainless-steel liner is necessary due to the highly corrosive media present in the reservoir.

The stainless-steel liner or any other liner that may be attached to or installed after the tieback is also not part of the investigation. Therefore, the stainless-steel liner is neglected for the buckling analysis and other calculations. The completion is assumed to have an open-hole section without liner, through which reservoir fluids are flowing towards the tieback or injection water pumped through the tieback in the open-hole section.

The annulus above the end of the tieback is sealed off from the fluid at the wellbore's bottom. The means used to create the annulus barrier was not specified further. Standard completion equipment would be a packer, for example. The annulus fluid between the tieback and the innermost casing string can be assumed to be regular freshwater with a density of 1000 [kg/m³] for this case.

Erdwerk has provided the information that this particular tieback string can move freely in a vertical direction.

The uncemented tieback is assumed to be hung in tension from the liner top and not supported at the shoe in compression. (*Code of practice for deep geothermal wells* 2015. New Zealand Standard, 31)

Any other indications of completion components in Figure 30 are not relevant to the investigation and are therefore neglected. (Erdwerk GmbH)
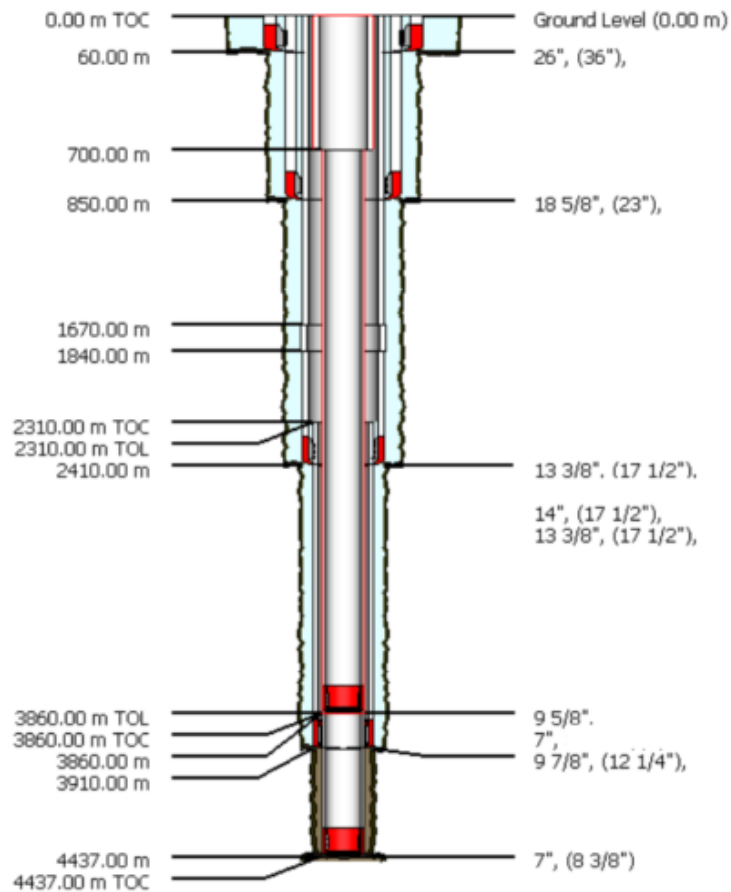
Figure 30: Sample well completion (Erdwerk GmbH)

The abbreviations TOC and TOL in Figure 3 refer to Top of Cement and Top of Liner, respectively.

5.2 Given Parameters & Properties

Other essential information has been provided to create a working model for comprehensive buckling analysis. Table 8 shows the stratigraphy of the target area. While it has no direct impact to the investigation at hand or influence in the MATLAB model, it is useful additional information and reference to where the presented sample well is located and which geological strata are present. All depths of the following Table 8, Table 9 and Figure 31 are TVD.

Stratigraphy	Top Boundary [m]	Bottom Boundary [m]
Lias	333,00	651,00
Keuper	651,00	1244,00
Muschelkalk	1244,00	1552,00
Buntsandstein	1552,00	2370,00
Zechstein	2370,00	3881,80
Rotliegend	3881,80	4230,00
Volcanics	4230,00	4294,00

Table 8: Stratigraphy in the target area (Erdwerk GmbH)

Table 9 shows the expected temperature gradients concerning the previous presented geological strata in Table 8. Besides the temperature gradients, the cumulative temperature around the target depth can be seen in the table. A strong correlation between a lower geothermal temperature gradient and the geological strata "Zechstein", which in this case is present as halite and the "Volcanics" strata is present in the provided data from (Erdwerk GmbH).

Start Depth [m]	End Depth [m]	Temp. Gradient [°C/km]	Cum. Temperature [°C]
0,00	0,00	-	10,00
0,00	333,00	42,85	24,27
333,00	651,00	33,50	34,92
651,00	1244,00	48,12	63,46
1244,00	1552,00	36,86	74,81
1552,00	2370,00	44,45	111,17
2370,00	3881,80	18,63	139,34
3881,80	4230,40	32,76	150,76
4230,40	4294,00	11,70	151,50
4294,00	4580,00	11,70	154,85

Table 9: Expected temperature gradients and cumulative temperature in the target area (Erdwerk GmbH)

Figure 31 indicates the expected hydraulic pore pressure and fracture pressure gradients, essential for planning the drilling activities and the casing setting depths. "Zechsteinsalze" in Figure 31 refers to the halite strata present in the region of interest.
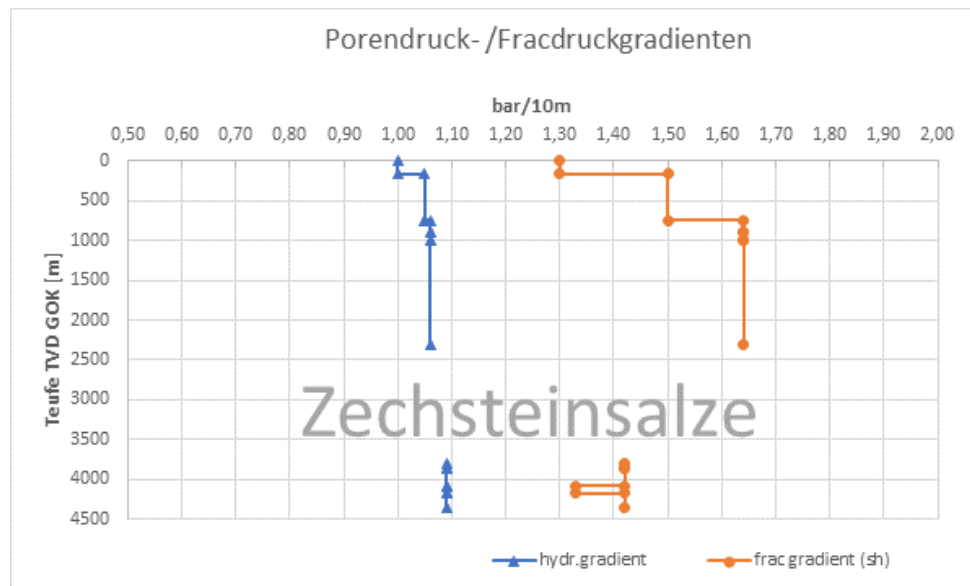
Figure 31: Hydraulic pore and fracture pressures in the target area (Erdwerk GmbH)

The full borehole path plan exported from the Landmark Solutions software can be found in Table 10. While not all information provided here is necessary to develop a working model to

analyse an uncemented tieback's buckling behaviour, it is presented here for the sake of completion. VS and DLS stand for Vertical Section and Dogleg Severity, respectively.

MD [m]	TVD [m]	Inclination [°]	Azimuth [°]	Easting [m]	Northing [m]	X [m]	Y [m]	VS [m]	DLS [°/30m]
0,00	0,00	0	242	0	0	405939,5	5862432,5	0	0
900,00	900,00	0	242	0	0	405939,5	5862432,5	0	0
1020,00	1019,10	12	242	-11,1	-5,9	405928,5	5862426,6	12,5	3
2176,10	2150,00	12	242	-223,2	-118,7	405716,3	5862313,8	252,8	0
2356,10	2328,70	0	242	-239,8	-127,6	405699,7	5862305	271,6	2
4192,5	4165	0	242	-239,8	-127,6	405699,7	5862305	271,6	0
4437,5	4410	0	242	-239,8	-127,6	405699,7	5862305	271,6	0

Table 10: Borehole path (Erdwerk GmbH)

Additionally, one simplification has been mentioned that could be used for the production case:

- While producing hot water, a maximum reservoir temperature of 155 [°C] could be assumed constant along with the completion's depth until the surface.

Furthermore, more details for the injection procedure have been provided:

- The injection water temperature is 10 [°C] at the surface.
- The maximum pressure at the wellhead during injection is 590 [bar].

6   MATLAB Application

The MATLAB Application featuring a GUI has been developed with the MATLAB App Designer. Setting up the initial GUI is relatively intuitive and straightforward thanks to the extensive component library. Generating a user interface is done by using the drag and drop environment. With the easy-to-handle component browser, specific parameters can be set directly without the necessity to code anything yet.

This Application is made with MATLAB's Auto-Reflow option in a two-panel style. Auto-Reflow optimises the viewing experience by automatically adjusting the size, location, and visibility of the app content in response to screen size, orientation, and platform. The GUI elements are linked to a flexible grid layout instead of a simple orientation governed by pixel values, which also changes depending on the application size but keep its proportions and settings. This feature allows for even more accurate adjustments and a better viewing experience. If a screen is too small to view all elements fully, scroll bars will automatically scroll through the user interface. The right panel with spaces for visual interpretations and text adjusts to the remaining screen size if the left panel is shown fully.

The user needs to install the standalone MATLAB Runtime to run the program. If MATLAB is not installed on the target or computer which is supposed to run the application or the installed MATLAB version has not the same version than the one used to compile the program the user needs to install the standalone MATLAB Runtime to run the program. (MathWorks 2020)

The program shows, whether or not sinusoidal or helical buckling occurs and visualises the occurring loads, stresses, torque, temperatures and pressures along with the depth of the tieback during production, injection and pressure test activities. The user must adjust parameters to fit the scenarios. Given design factors have to be verified against a worst-case and realistic load scenario to determine if the completion at hand is fit for usage. All results are presented in a user-friendly manner in written and plot form.

The term numerical results will be used in the following chapters, which related to all calculated values covering the following aspects of the investigation:

- Reservoir temperature and bottomhole pressure calculations
- Heat transfer calculations and temperature distribution of the water column inside the tieback
- Pressure losses and pressure distribution of the water column inside the tieback
- Loads, stresses and torque on tieback
- Buckling analysis
- Failure prediction calculations (Safety factors)

During the design and programming of the application literature from the following authors has proven to be very informative and useful: (Sizemore and Mueller 2014; Hahn and Valentine 2019; Parkeh 2020)

6.1 Quick Start Guide and Overview

The following quick start guide and overview of the MATLAB application's intended use and its functionality are meant to ensure a user-friendly experience while operating the application. The instructions are also available directly in the application in PDF format as long as the file is saved in the program directory.

The user can choose if the system is in a shut-in (initial state), production, injection or pressure test state. It is vital to understand how the set-up of the application works. A geothermal doublet (one producer and one injector) is assumed to be tapped in an ideal reservoir, maintaining mass and pressure balance. The spacing between the wells is sufficient to assume constant downhole temperatures. Depending on the chosen mode of operation, one of the two wells, either producer or injector, is being simulated (except shut-in and pressure test).

It must be decided if the completion design wants to be assessed with a freely moveable tieback in the vertical direction due to expansion devices or a rigid completion which restrains movement. Both cases are realized with a tieback installation fixed at the surface and the bottom with the annulus sealed off. Note that the application's intended use is with one tieback string made of the same steel grade throughout. Crossovers can be added to the tieback and will be accounted for in the model.

If the application simulates the initial conditions during shut-in, no user input is required regarding temperature and pressure parameters. The program determines all necessary values. While simulating an injector, the wellhead pressure and injection water temperature are subject to user input. On the other hand, if the application simulates a producer, the program will load a value for the bottomhole pressure referenced to the shut-in bottomhole pressure to initiate the pre-calculations. The bottomhole pressure during production is subject to user input, while other pressures and temperature-related values are obtained automatically. The model requires positive wellhead pressure during production. Thus, appropriate bottomhole values must be chosen. During pressure test operations, a pressure test plug is installed at the bottom of the tieback, which is accounted for in the load calculations. The applied pressure at the wellhead is the only user input parameter during pressure tests.

The program then runs a series of pre-calculations while the input data is simultaneously being uploaded and inserted by the user. These pre-calculations are smaller but essential calculations done by the program in the background. Some pre-calculations are visible on the GUI and can be adjusted by the user. After the user has verified all custom input data and pre-defined values (for example, surface pressure), the program executes its core calculations. A realistic approach representing all user parameters as good as possible has been chosen to determine the axial loads and/or length changes. Worst-case and realistic load scenarios are used to verify the tieback's resistance against burst and collapse failure while considering the influence of the axial loads (biaxial design) and the chosen design factors. The onset and outcome of buckling are analysed and integrated into the calculations.

Finally, all the calculated temperatures, pressures, loads, safety factors and buckling assessments can be displayed and exported as numerical results or as plots.

The following points must be considered at all times:

1. The instructions must be read thoroughly and carefully before intending to operate the application to avoid any confusions later on.
2. To ensure the MATLAB application runs correctly download and install the MATLAB runtime for version R2020b from https://www.mathworks.com/.
3. The tooltips can be considered for additional more detailed descriptions and messages of value ranges for number boxes.
4. Changes are updated instantly on the input summary text area on the right panel. Please verify all changes made in this area before attempting to run the application.
5. Generally, manual changes of input parameters and some pre-calculated values are allowed. Other pre-calculated values are part of the underlying functions, and their results cannot be changed directly by the user but must be adjusted through the influencing factors instead.
6. The Menu on the top hand side of the application features additional information and options.
     a. Info:
          - Download: Possibility to download templates for preliminary data set files in a Microsoft Excel format, which are ready to be filled with user data. Further, a table with the pre-defined steel grades and references of the temperature influence on the material properties can be accessed.
          - Export: Option to export the input summary and the numerical results in an Excel file. Numerical results become available after the program has been run at least once.
          - About: Information about the Project, MATLAB version, Author and Copyright can be seen.
     b. Instructions: Opens the step-by-step instructions.
     c. Useful Links: Lets the user quickly access external webpages with useful information.
          - Properties of Water: Search online for properties of water (density, specific heat capacity and dynamic viscosity) with varying temperatures and pressures.
7. Mode of Operation: The mode of operation needs to be chosen from the drop-down list. Some user interface elements only become editable if a particular state is selected.
     a. Shut-In (Initial Conditions)
     b. Production after Shut-In
     c. Injection after Shut-In
     d. Pressure Test after Shut-In
8. Preliminary Data: Upload the preliminary data sets and verify surface conditions.

- Temperature Gradient
- Borehole Path
- Tieback Dimensions
- Casing Dimensions
- Surface Temperature [°C]
- Surface Pressure [barA]

Press the corresponding button then select and upload the right excel file which contains the desired data. Download the templates before and use them to make sure the information is entered correctly. The exact format needs to be maintained. Otherwise, the application is not able to process the data correctly.

9. Geological & Reservoir Parameter: Insert and verify geological and reservoir related variables.
   a. Reservoir Temperature [°C]
   b. Thermal Conductivity [W/m°C] (average value and constant along with depth)
   c. Thermal Diffusivity [10^{-6}m²/s] (average value and constant along with depth)

10. Shut-In (Initial Conditions): Verify all shut-in related variables for the initial conditions.
    a. Bottomhole Temperature [°C]
    b. Bottomhole Pressure [barA]
    c. Wellhead Temperature [°C]
    d. Wellhead Pressure [barA]

- The bottomhole temperature is the reservoir temperature.
- The bottomhole pressure is the temperature accounted for hydrostatic pressure of the water column inside the tieback.
- The wellhead temperature is approaching surface conditions with a linear geothermal temperature gradient function after 30 days of a shut-in (pre-set).
- The excess wellhead pressure is assumed to be 0 with the well in equilibrium with the formation.

11. Injection: Insert and verify all injection-related parameters.
    a. Wellhead Temperature [°C]
    b. Wellhead Pressure [barA]
    c. Water Density [kg/m³]
    d. Mass Flow Rate [kg/s]
    e. Elapsed Time [days]
    f. Specific Heat Capacity [J/kg°C] (constant along with depth)
    g. Dynamic Viscosity [cP] (constant along with depth)
    h. Bottomhole Temperature [°C]
    i. Bottomhole Pressure [barA]

- The wellhead temperature of the injection water needs to be inserted.
- The applied wellhead pressure during injection needs to be inserted.
- The bottomhole temperature is a function of the reservoir parameters, the injection water's mass flow rate and specific heat capacity and the elapsed time.
- The bottomhole pressure is a function of the injection water's mass flow rate, density and dynamic viscosity and the pipe or coating roughness

12. Production: Insert and verify production-related variables.
    a. Bottomhole Temperature [°C]
    b. Bottomhole Pressure [barA]
    c. Water Density [kg/m³]
    d. Mass Flow Rate [kg/s]
    e. Elapsed Time [days]
    f. Specific Heat Capacity [J/kg°C] (constant along with depth)
    g. Dynamic Viscosity [cP] (constant along with depth)
    h. Wellhead Temperature [°C]
    i. Wellhead Pressure [barA]

- The bottomhole temperature of the production water is equal to the reservoir temperature.
- The bottomhole pressure of the production well is subject to user input.
- The wellhead temperature is a function of the reservoir parameters, the production water's mass flow rate and specific heat capacity and the elapsed time.
- The wellhead pressure is a function of the production water's mass flow rate, density and dynamic viscosity and the pipe or coating roughness

13. Pressure Test: Insert and verify pressure test-related variables.
    a. Wellhead Pressure [barA]
    b. Pressure at Plug [barA]
    c. Wellhead Temperature [°C]
    d. Temperature at Plug [°C]

- The applied wellhead pressure during pressure tests needs to be inserted.
- The pressure at the plug is the temperature accounted for hydrostatic pressure (like in the shut-in case) plus any applied wellhead pressure.
- The wellhead temperature is approaching surface conditions, exactly like in the shut-in case.
- The temperature at the plug is the shut-in temperature at the bottom of the tieback.

14. Steel Grades: The pre-defined set of properties of the used steel grade can be seen and verified in the input summary text area on the right panel. The following steel properties of all pre-defined streel grades can be viewed by simply selecting the name of the steel grade from the drop-down list:
    a. Minimum Yield Strength [MPa]
    b. Minimum Tensile Strength [MPa]
    c. Modulus of Elasticity (Young's Modulus) [GPa]
    d. Poisson's Ratio [-]
    e. Coefficient of Thermal Expansion [10^{-6}/°C]
    f. Coating / Pipe Roughness [mm]

Please note that only one set of values per steel grade can be saved and used within the program. For example, two "L80" steel grades with a different pipe roughness value for each is not possible. Nevertheless, if a custom steel type is desired (which for example may be very similar to a pre-defined type but the latter is used as well) you can choose the "Custom" option (up to two) from the drop-down list. "Custom" options

have the "J55" values pre-set. Changes to the pre-defined steel grades' values can only be made if the used steel grade is "Custom 1" or "Custom 2".

15. Annulus Fluid: Insert the annulus fluid properties between the casing and the tieback.
    a. Annulus Fluid Density [kg/m³] (constant along with depth)
16. Design factors: Verify the desired design factors applied to the completion.
    a. Tension
    b. Compression
    c. Burst
    d. Collapse
17. Additional Information & Settings: Choose additional information and settings if desired.
    a. Checking "Free Tieback String" indicates that the completion is freely able to move vertically. The none-checked option automatically means that the tieback is restrained from movement in a vertical direction.
    b. "Measuring Interval" for calculated data points per meter for all applicable calculations. The default value is 10 meters (upper limit) with the lower limit being 1 meter.
    c. "Setting Force [N]" gives the option to include an additional setting force (tension or compression) which acts on the tieback.
    d. "Helical Buckling Onset in a deviated Well" allows the user to adjust the factor that governs the onset of helical buckling in a deviated wellbore. Values must be between 1,41 and 1,83.
18. Run: The button on the top right corner of the left panel starts the calculation process after verifying all input parameters have been entered correctly. One must note that before each run, the previous results are erased. Therefore, it is important to export those before rerunning the application with different input data. The numerical results are written in the corresponding text area, and the plots become available. The GUI input mask is disabled.
19. Reset: This button resets all results and disables the plot panel. It enables the GUI input mask and allows the user to change input parameters and/or the operation mode.
20. Right Panel: On the right-hand side panel, three tabs can be found on the top with text output and visual interpretations:
    a. Input Summary: Displays a live view of all uploaded, pre-defined & pre-calculated values in a multiline text area.
    b. Numerical Results: Shows the calculated numerical results in a sorted manner in a multiline text area once the program has been run at least once.
    c. Plots: Shows all plots in a multipurpose diagram after the program has been run at least once. Choose an option from the drop-down list at the top of the tab to cycle through plots, and the diagram updates automatically. MATLAB automatically provides user-friendly functionalities for the plots, such as zoom functions and the possibility to export the plot as PDF or picture files such as JPG or PNG.
        • Water Temperature
        • Water Pressure

- Tieback Loads

6.2 Graphical User Interface - Layout & Functionality

Table 18 in Appendix B gives a detailed insight into all used GUI components and how the functionality is explained to a user with the tooltips.

All the input area of the GUI is concentrated on the left Auto-Reflow panel of the application. The GUI consists of multiple containers in which components that belong to the same set of functionalities are grouped. The containers are arranged in the supposed order of user interaction from top to bottom (except the "Reset" and "Run" buttons in the top right corner). The input section is shown in Figure 32.

Figure 32: MATLAB GUI Input – Panel overview (MATLAB R2020b)

6.2.1 Output

All the output area of the GUI is concentrated on the right Auto-Reflow panel of the application. The GUI consists of three tabs in which a summary of all input data, the numerical results and plots are being displayed.

The first tab features a multiline text area where a summary of all uploaded, inserted, pre-defined & pre-calculated values is shown. This summary is updated live as soon as values are being added or changed.

The numerical results tab features the same text area and shows results as soon as the program has been run at least once. The results are sorted and displayed in a way to ensure good readability for the user.

Figure 33 shows the GUI of the first and second tab "Input Summary" and "Numerical Results. The picture is cropped at the bottom to reduce its space.
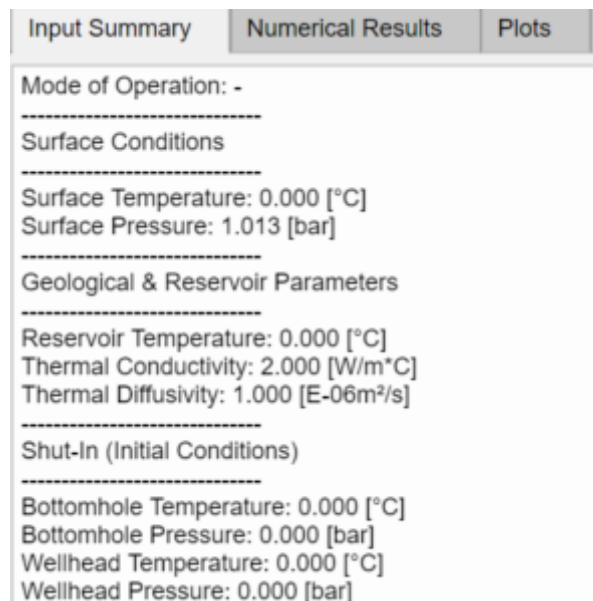
Figure 33: MATLAB GUI Output – Text area of input summary and numerical results (MATLAB R2020b)

The third tab contains a multipurpose diagram and a drop-down list to choose options. To choose one of the options shown in Figure 34, select the desired option from the drop-down list, the plot then changes accordingly including axis, descriptions and data points. All plots will become available after the program has been run at least once.
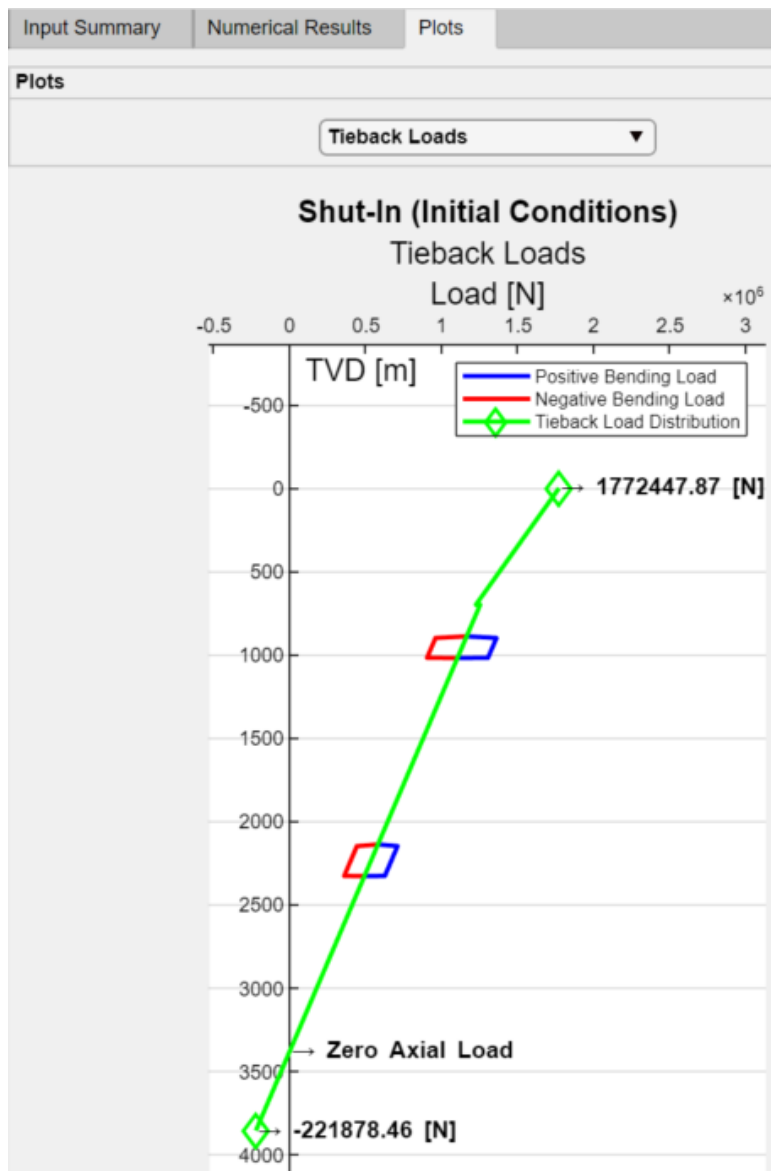
Figure 34: MATLAB GUI Output – Plots (MATLAB R2020b)

6.2.2   Menu

The menu on the application's top left-hand side and its functions have been explained before in the step-by-step instructions. Figure 35 shows how the menu looks. Submenus are not shown in figures, to avoid adding depth to the thesis.
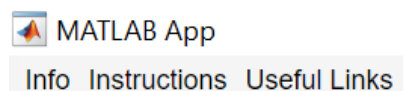
Figure 35: MATLAB GUI Menu (MATLAB R2020b)

6.3 Preliminary Data Sets

Preliminary data sets are an essential means of user dictated input, which is needed to run the application correctly. One must upload the data sets precisely as intended and described in the following chapters. Otherwise, wrong information may be produced, or the program would not process the information at all. In the pre-made excel files that are available for download through the application, all the formulae are already put in place. Only the values need to be added, and the table is expanded to how many entries are needed.

6.3.1 Temperature Gradient

Perhaps the most vital variable to know in a geothermal reservoir is its temperature. The required data set follows a simple pattern for each section, including the temperature gradient. A little modification, in the beginning, accounts for the current surface temperature. All depths have to be given in meter [m], the temperature gradient in degree Celsius per Kilometre [°C/Kilometre] and the cumulative (and surface) temperature in degree Celsius [°C]. Table 11 shows how the data sets need to be set up with a short description below.

In the first row, the start and depth are kept to zero, and the temperature gradient is not valid because only an absolute surface temperature is present. The last column of the first row represents the absolute surface temperature. If not explicitly stated otherwise, a surface temperature of 20 [°C] can safely be assumed.

The second row begins with a start depth of zero since naturally, meaning zero elevation (not measured against a level but in the local area). From the third row on until the maximum of needed sections is reached the table works the same way. Each section's start depth is equal to the previous section's end depth, and no values need to be added here. The section end depth and temperature gradient are the only user input values.

Each section's total cumulated temperature equals the sum of the previous section's temperature and the temperature increase through the temperature gradient of the section multiplied with the section depth, which is equal to the section end depth minus the start depth.

Start Depth [m]	End Depth [m]	Temp. Gradient [°C/km]	Cum. Temperature [°C]
0,00	0,00	-	Surface Temperature
0,00	End Depth Section #1	Gradient Section #1	Total Temperature #1
Start Depth Section #1	End Depth Section #2	Gradient Section #2	Total Temperature #2
Start Depth Section #2	End Depth Section #3	Gradient Section #3	Total Temperature #3
Start Depth Section #3	End Depth Section #4	Gradient Section #4	Total Temperature #4
Start Depth Section #4	End Depth Section #5	Gradient Section #5	Total Temperature #5

Table 11: Temperature gradient preliminary data set

6.3.2 Borehole Path

The second preliminary data set includes a small portion of the borehole path data, which is usually available after the path design and calculations have been finished. MD and TVD have

to be given in meter [m], the Inclination in degree [°] and the DLS in degree per 30 meters [°/30m]. Those four values are sufficient, and a more detailed set of data about the borehole path and geometry is not required. Table 12 shows how the data sets need to be set up with a short description below.

The first column always describes the MD of the corresponding borehole section end, while the second column describes the TVD of each section. The third column describes the section's inclination with respect to the vertical. The fourth column describes the occurring DLS in said sections. Values should be taken from external borehole design and calculation programs, for example, Landmark Solutions.

MD [m]	TVD [m]	Inclination [°]	DLS [°/30m]
MD End of Section #1	TVD End of Section #1	Inclination Section #1	Dog Leg Severity Section #1
MD End of Section #2	TVD End of Section #2	Inclination Section #2	Dog Leg Severity Section #2
MD End of Section #3	TVD End of Section #3	Inclination Section #3	Dog Leg Severity Section #3
MD End of Section #4	TVD End of Section #4	Inclination Section #4	Dog Leg Severity Section #4
MD End of Section #5	TVD End of Section #5	Inclination Section #5	Dog Leg Severity Section #5

Table 12: Borehole path preliminary data set

6.3.3   Tieback Dimensions

The third preliminary data set includes information about the dimensions and steel grade used in the tieback string and its length. The Excel template can be used to insert data for a tieback composed of only one section with no change in dimensions but also for a tapered design with multiple sections. Due to the nature of habit in the industry and the majority of available data primarily being published in imperial units, these units were used for the tieback. Table 13 shows how the data sets need to be set up with a short description below.

The first two columns always describe the end depth of the corresponding tieback section's MD & TVD in [m] and the third row is a drop-down list where the user can choose one of the steel grades introduced in the next chapter. Two custom values are also available if the desired steel grade is not one of the listed ones (Steel specific values need to be verified in the program afterwards). Only a value from this list is a valid option. Otherwise, an error message is displayed in the Excel file. Columns four to seven refer to the Outer Diameter (OD) [in], Nominal Linear Mass (w/l) [lb/ft], Wall Thickness (t) [in] and Inner Diameter (ID) [in] of the tieback section.

The Excel file contains a second sheet with a modified table from the standard for Specification for Casing and Tubing - API Specification 5CT / ISO 11960 including outer diameters, nominal linear masses, wall thicknesses and calculated inner diameters. This sheet's sole purpose is to make the user input as easy as possible since the table can be filtered and the needed values can be copied and pasted afterwards in the first sheet again. The full table can be seen in Appendix A.

End Depth (MD) [m]	End Depth (TVD) [m]	Steel Grade	OD [in]	w/l [lb/ft]	t [in]	ID [in]
MD End of Section #1	TVD End of Section #1	J55	▾ D in Section #1	w/l in Section #1	t in Section #1	ID in Section #1
MD End of Section #2	TVD End of Section #2	K55	OD in Section #2	w/l in Section #2	t in Section #2	ID in Section #2
MD End of Section #3	TVD End of Section #3	N80	OD in Section #3	w/l in Section #3	t in Section #3	ID in Section #3
MD End of Section #4	TVD End of Section #4	L80	OD in Section #4	w/l in Section #4	t in Section #4	ID in Section #4
MD End of Section #5	TVD End of Section #5	C90	OD in Section #5	w/l in Section #5	t in Section #5	ID in Section #5
			Choose Steel Grade! Please choose a steal grade from the dropdown menu.			

Table 13: Tieback dimensions preliminary data set

6.3.4   Casing Dimension

The fourth and last preliminary data set includes information about the casing dimensions and setting depths. It is very similar to the previous data set of the tieback but not steel grades and only MD indications are necessary.

In Table 14 the first two columns always describe the start and end depth of the corresponding casing section's MD in [m]. Columns three to six refer to the Outer Diameter (OD) [in], Nominal Linear Mass (w/l) [lb/ft], Wall Thickness (t) [in] and Inner Diameter (ID) [in] of the tieback section.

The values for the nominal linear masses, wall thicknesses and calculated inner diameters can again be copied from the second sheet of the Excel file.

Start Depth (MD) [m]	End Depth (MD) [m]	OD [in]	w/l [lb/ft]	t [in]	ID [in]
MD Start of Section #1	MD End of Section #1	OD in Section #1	w/l in Section #1	t in Section #1	ID in Section #1
MD Start of Section #2	MD End of Section #2	OD in Section #2	w/l in Section #2	t in Section #2	ID in Section #2
MD Start of Section #3	MD End of Section #3	OD in Section #3	w/l in Section #3	t in Section #3	ID in Section #3
MD Start of Section #4	MD End of Section #4	OD in Section #4	w/l in Section #4	t in Section #4	ID in Section #4
MD Start of Section #5	MD End of Section #5	OD in Section #5	w/l in Section #5	t in Section #5	ID in Section #5

Table 14: Casing dimensions preliminary data set

6.4   Pre-Defined Steel Grades

Values of all pre-defined steel grades can be found in Table 15. The "Custom 1" and "Custom 2" values are set-up with the values from the J55 grade. Pre-defined steel properties are meant to be constant along with the completion depth.

The Young's modulus or modulus of elasticity, the Poisson's ratio, and thermal expansion coefficient are taken from the German guide for casing, tubing & liner calculations (*Leitfaden Futterrohrberechnung* 2006. Wirtschaftsverband Erdöl- und Erdgasgewinnung e.V.). The minimum yield and tensile strength for the steel grades are taken from (*Specification for Casing and Tubing - API Specification 5CT - ISO 11960:2004*, Eighth Edition 2005. American Petroleum Institute and ISO).

The average steel pipe roughness for all steel grades is taken as 0,2 [mm].

Steel Grade	Min. Yield Strength [MPa]	Min. Tensile Strength [MPa]	Young's Modulus [GPa]	Poisson's Ratio [-]	Expansion Coeff. [E-06/°C]
J55	379,00	517,00	206,84	0,30	12,40
K55	379,00	655,00	206,84	0,30	12,40
L80	552,00	655,00	215,00	0,28	12,70
N80	552,00	689,00	206,84	0,30	12,40
C90	621,00	689,00	206,84	0,30	12,40
C95	655,00	724,00	206,84	0,30	12,40
P110	758,00	862,00	215,00	0,28	12,70
Q125	862,00	931,00	215,00	0,28	12,70
Custom 1	379,00	517,00	206,84	0,30	12,40
Custom 2	379,00	517,00	206,84	0,30	12,40

Table 15: Pre-defined Steel Grades (*Specification for Casing and Tubing - API Specification 5CT - ISO 11960:2004*, Eighth Edition 2005. American Petroleum Institute and ISO, 87; Modified from: *Leitfaden Futterrohrberechnung* 2006. Wirtschaftsverband Erdöl- und Erdgasgewinnung e.V., 88)

Some steel grades like the L80, for example, are available in different types and with varying chemical compositions. L80 steel is available as 1, 9Cr and 13Cr version. The increase in chromium does not change previously mentioned properties. Therefore, even if different steel types within the same grade are used in a well's completion design, the same properties can be applied. Applicable for the steel grades and types from the API Standard 5CT. Table 16 shows the difference in the compositions of the L80 steel alloys.

(*Specification for Casing and Tubing - API Specification 5CT - ISO 11960:2004*, Eighth Edition 2005. American Petroleum Institute and ISO)

Steel Grade	Type	C [%]		Mn [%]		Mo [%]		Cr [%]		Ni [%]	Cu [%]	P [%]	S [%]	Si [%]
		min.	max.	min.	max.	min.	max.	min.	max.	max.	max.	max.	max.	max.
L80	1	-	0,43	-	1,90	-	-	-	-	0,25	0,35	0,03	0,03	0,45
L80	9Cr	-	0,15	0,30	0,60	0,90	1,10	8,00	10,00	0,50	0,25	0,02	0,01	1,00
L80	13Cr	0,15	0,22	0,30	0,25	1,00	1,10	12,00	14,00	0,50	0,25	0,02	0,01	1,00

Table 16: Chemical composition of L80 steel alloys with mass fractions (%).(Modified from: *Specification for Casing and Tubing - API Specification 5CT - ISO 11960:2004*, Eighth Edition 2005. American Petroleum Institute and ISO, 86)

Properties of different coupling types such as STC, LTC and BTC are not part of this evaluation and corresponding information is omitted.

6.5 Application Workflow

This chapter aims to illustrate the overall workflow of the MATLAB application and the workflows of processes that are being used to determine the numerical results. The dependency of the mathematical functions used to derive the numerical results on their input parameters is also illustrated. Figure 36 shows the overall workflow of the program.
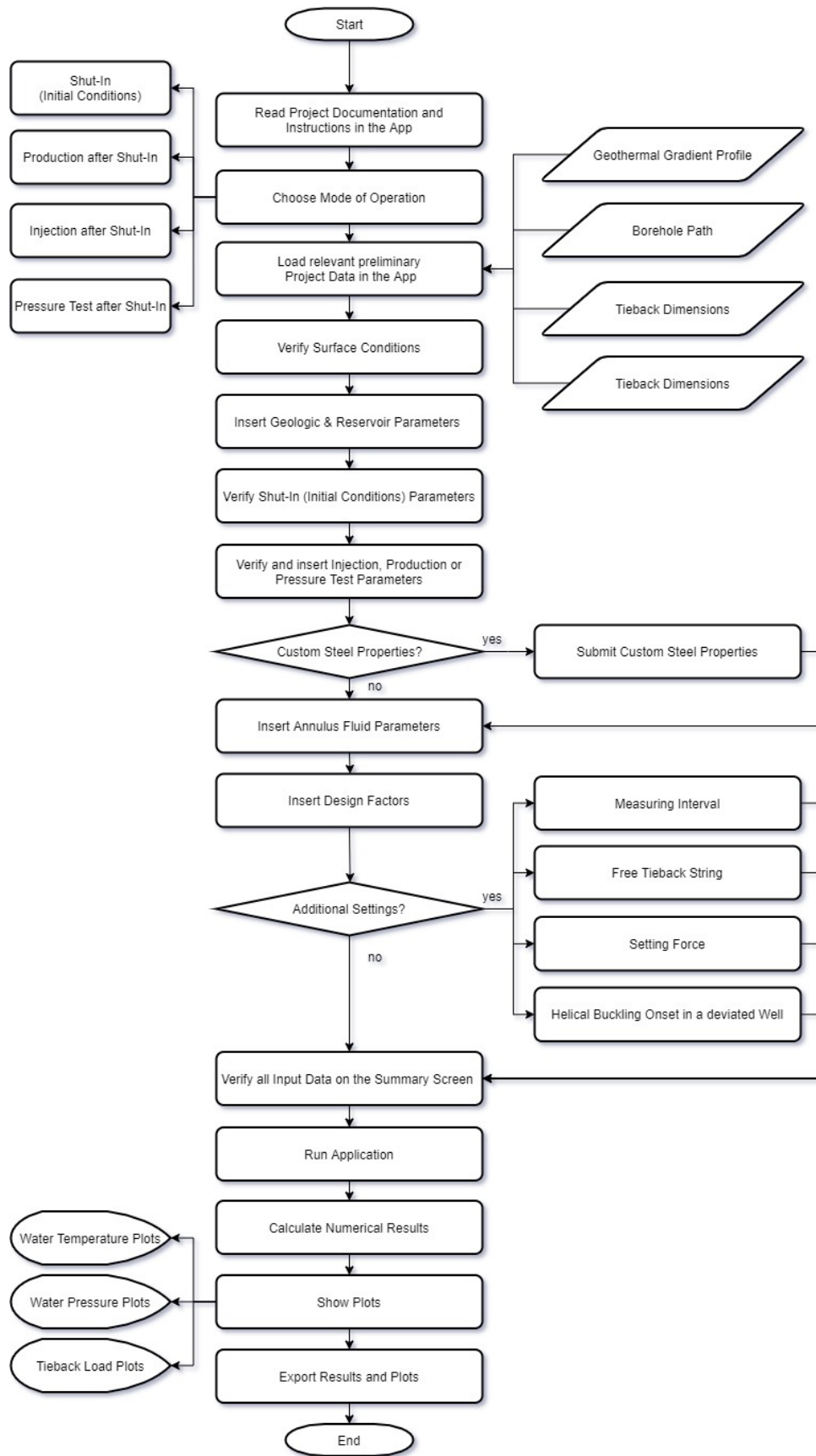
Figure 36: MATLAB application workflow

6.5.1 Calculation of Numerical Results

The numerical results are essentially the results of all the calculations and investigations in the MATLAB application. They are also the foundation for all visualisations in the form of plots and are among the most critical parts of the application's output. The results depend entirely on the chosen mode of operation and the input parameters. To calculate the system's states four individual level of calculations have been defined to obtain the numerical results during shut-in, production and injection state and pressure testing. The shut-in state calculations are always run first to achieve some kind of system initiation that allows comparison with the following scenarios with the same starting parameters. The shut-in state calculations calculated output serves as new input for either the production, injection or pressure test state calculations.

Figure 37 shows the process workflow of the different operational mods.
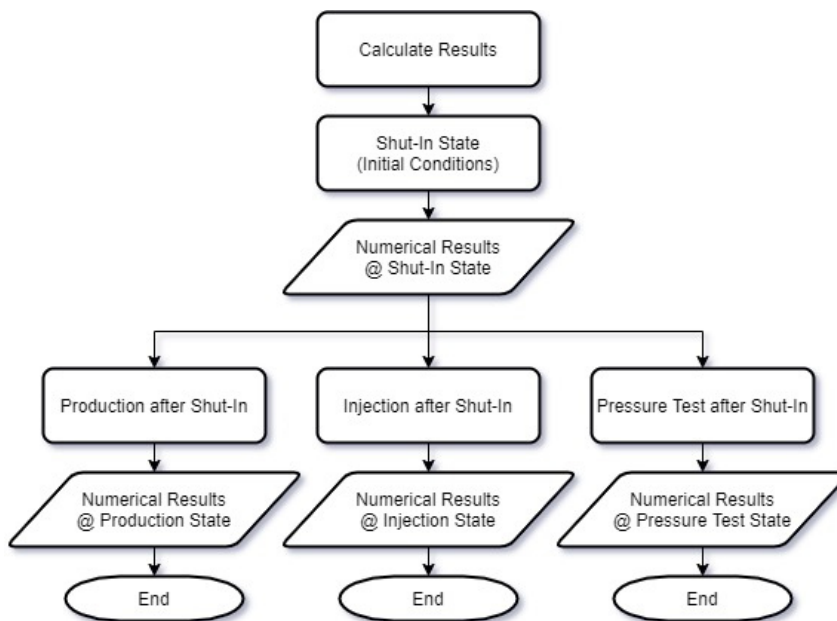
Figure 37: Calculation of numerical results workflow

6.5.2 Mathematical Functions

Mathematical functions are the heart of the calculations done by the program. The program is designed to reuse most of the mathematical functions as often as possible with different input values depending on the selected mode of operation. For example, the mathematical function governing the pressure loss calculations is valid during injection and production activities. This way, a maximum number of different scenarios can be simulated while keeping the programming effort comparatively low. Using said functionality also means that the previously mentioned functions to calculate the numerical results in the shut-in, production, injection and pressure test state are very similar since most of the mathematical and physical background overlaps and the mathematical functions are just being recalled within them.

Each mathematical function has a different purpose and needs a different set of input parameters to fulfil its purpose. Some of them can only be calculated after another mathematical function has delivered its results.

A measuring interval is introduced for mathematical functions depending on the completion's depth. The temperature distribution of the hydrostatic column inside the tieback is an example of this mathematical depth dependency. The measuring interval dictates how many data points and output values of the mathematical functions are being calculated per meter. The upper limit and at the same time the set standard value is 10 meters by default, while the lower limit is 1 meter. The user can change the interval through the GUI.

Appendix C shows the more complex functions with numerous input parameters. Smaller mathematical functions with fewer input parameters are not illustrated.

6.6 Art of Programming

This chapter provides insight into some of the essential aspects of programming and how to efficiently and correctly write code for a smoothly running and crash-proof program.

6.6.1 Naming of GUI Components & Variables

When designing a GUI, it is essential not to overload the interface while maintaining all essential parts easily accessible. On the front-end, it is a balance between a clean overview with short and self-explaining names & descriptions and a helpful tooltip function on top of the application's functionality.

On the back-end, however, it is crucial to name all GUI components and later on all the variables so that they are easily identified while coding the program's functionality. The key is only to have unique names. Especially if one or more components have the same or a very similar name and/or purpose. The naming of GUI components and variables is crucial, and at the same time, an easily achievable step before the process of coding can start correctly.

MATLAB automatically names components with the name of the said component plus the type of the component. For example, the editable number box with the label "Elapsed Time [days]" of the production section is named "ElapsedTimedaysEditField". The editable number box with the label "Elapsed Time [days]" of the injection section is automatically named "ElapsedTimedaysEditField_2". MATLAB ignores any may occurring special characters and exponents in its auto-naming process. While it is good practice to name all GUI elements uniquely, the naming is often not unique due to space reasons or simply because the component is easy to assign for the user. The component names then need to be changed to avoid confusion later on during the programming process.

An easy way to quickly identify similar elements is to add a keyword before the name. It is typically advised to keep the names simple and not use units within the names. Continuing the example from before the names would then be "ProductionElapsedTimeEditField" and "InjectionElapsedTimeEditField" respectively.

Figure 38 shows a part of the component browser with some of the renamed component names.
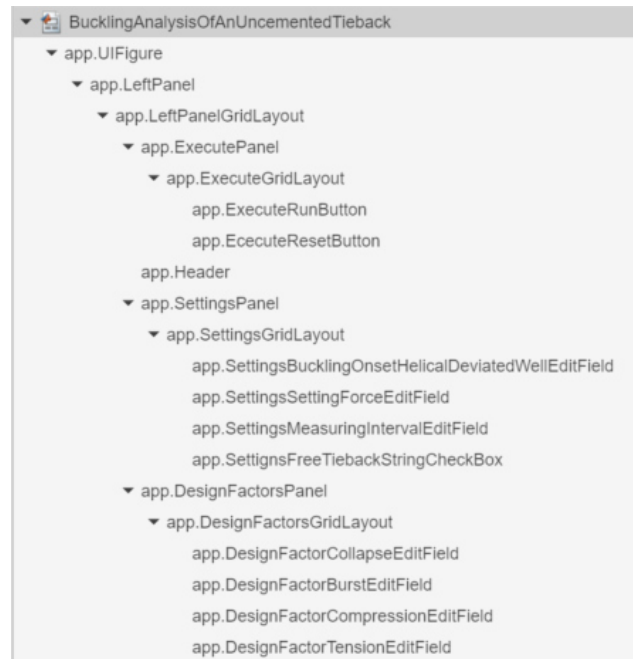
Figure 38: MATLAB Component Browser Section (MATLAB R2020b)

Figure 39 shows some of the program's used variables and how they are named to be unique.

Figure 39: MATLAB Variables (MATLAB R2020b)

6.6.2   Functions

Much code can be reused at multiple points within the program. Therefore, it is standard procedure to write functions. Functions are specific code lines that are meant to fulfil a specific purpose, such as a calculation or drawing a plot, and are usually saved in a separate file. It also allows adjustment and correction of certain functionalities more easily without tampering with the main code structure. Functions can be accessed at any point within the main code. This way of programming allows maintaining a clean code environment since the reusable code is only written once and not repeated in each section of the program where it has been used. Depending on the program's size, it can lead to significant improvements in performance and decrease the application size, besides the fact that the programming process is faster for the programmer.

Functions always have the same structure. They are being recalled in the main code and given input parameters (may vary from only one to many) and deliver output parameters (may also vary from only one to many). The output parameters can then be stored in the main code variables to be used further within the program.

6.6.3   Global Variables

Usually, each function has its own set of local variables used to carry out the tasks. Using local variables is perfectly fine as long as the calculated output is not used in other code parts. If the latter is the case, it may be better to define variables as global. Global variables can be accessed and modified throughout the whole program code in all different functions. Caution must be exercised because easy access to variables also means that they may be overwritten with wrong information if the program code is not perfectly organized. Using the MATLAB App Designer to create a graphical interface, the underlying code uses so-called properties instead of global variables. Properties can be used in the same way as global variables. Nevertheless, they are much more complex than global variables because they contain object data, and additional settings and functionalities can be defined. (MathWorks 2020)

6.6.4   Crash-proof Programming

A significant part of coding is to catch all possibly occurring errors and let the user precisely know what the error is and how to correct them. A simple message, such as "Error. Please try again" may prevent the program from crashing. At the same time, they do not give any indication whatsoever what the problem may be. It could be missing information that the user forgot to upload or insert or internal errors which are entirely unrelated to any user interaction.

Therefore, it is vital for the person who writes the program code to be able to think him- or herself through the exact workflow order in which the code is executed. The programmer must anticipate at which point errors may occur, regardless of whether those may be caused by human error or internal issues. This thought process is significant for setting up variables correctly and implementing mathematical background functions and calculations.

The standard procedure of such an error-catch-mechanism is a simple "if-else" structure on different levels. The outermost level prevents the program from crashing or delivering wrong information if any unforeseen or unthought-of errors occur. Successively more "if-else" structures are wrapped within each other to narrow down to more specific errors. Finally, reaching the innermost layer with the most specific messages. Such error reporting structures make the testing process a lot easier since the person who writes the code knows precisely where the error lays while testing and the program does not frequently crash on top of that.

In the best-case scenario, a user would never see any error messages that are not caused directly by human error, because an error message about internal errors would indicate a faulty segment of code.

A lot of errors can be prevented by setting up the user interface with the appropriate settings and limits for values that can be entered. Disabling parts of the GUI and restricting thereby the user interaction when they are not needed is an additional way of error prevention.

6.6.5 Executable Program Files

MATLAB gives its developers the option to easily compile the GUI including all code and functions in an executable (.exe) file that can run on every Windows and Mac computer without installing the full MATLAB. The standalone MATLAB runtime needs to be installed to run the .exe file made by the MATLAB compiler on the target computer if said computer does not run the same MATLAB version or none at all. The runtime can be found through the search function on https://www.mathworks.com/. The MATLAB runtime installs a set of shared libraries that are essential for executing the compiled application. The installed MATLAB runtime must have the same version as the MATLAB in which the application was compiled earlier!

(MathWorks 2020)

6.7 Assumptions & Simplifications

Throughout this document, numerous assumptions have been mentioned which are necessary to give this application a work frame that is both, close to real-life conditions and at the same time also simplified enough to be able to run the calculations without bottlenecks and unnecessary complications. The assumptions should not have any or at least meagre impact compared to real-life conditions. Some of the purposefully overlooked conditions can be overruled by user input if more accurate reference data is available. Other assumptions and simplifications cannot be implemented in this version of the program.

- The water within the reservoir is only present in liquid form and during the production process, the reduction of pressure is not sufficient to cause the water to flash to steam. During the injection process, the pressures are high enough and temperatures too low to cause a steam flash event. Hence, only a one-phase liquid flow is present in the system.

- No transient geological effects influence the production or injection process, such as the reservoir's cooling/heating and reservoir pressure decline/incline in time. The geological and reservoir related flow properties remain constant. Reservoirs are to be seen as an ideal without significant changes while the system is being investigated.

- The flow of hot reservoir water causes heat transfer during production or cold injection water. The heat transfer features transient behaviour due to the surrounding formation. Any evaluation of the water column's temperature inside the tieback, the tieback itself or any other completion element is only done after the system has had sufficient time to reach a steady-state.

- The properties of the surrounding formation, such as thermal conductivity and thermal diffusivity, are considered to be constant and representable for all present formation sections. Used average values shall be chosen to represent the whole range of all surrounding formation sections.

- No transient pressure response (for example, after beginning to produce or inject water) is considered within the calculations. Further, the mass and pressure balance inside the reservoir is maintained due to an injector-producer couple. All the injected water reaches the producer due to an optimized flow path.

- No scaling occurs along the water-bearing tubular where the production or injection fluid is being transported or any other completion element exposed to it. There is no high enough quantity of minerals in the reservoir water and/or the change in temperature, pressure or pH-value during reservoir water production is not substantial enough to form precipitations. Furthermore, the injection water is assumed to be filtered sufficiently on the surface that scaling does not occur along with the depth (also no chemical reactions in the reservoir).

- No corrosion occurs along the water-bearing tubular where the production or injection fluid is being transported or any other completion element exposed to it, even if highly corrosive media is present. All tubular with direct contact to corrosive media shall have adequate means of corrosion control. The steel selection has been carried out carefully to diminish the effects of corrosion.

- The properties of reservoir and injection water, such as dynamic viscosity, specific heat capacity, are considered constant along with the depth for simplification purposes. Used values shall be chosen to represent the whole range of expected temperatures in the system. Thus, average values between the expected temperature at the wellhead and the reservoir must be chosen.

- The properties of steel alloys are subject to change due to temperature variations (for example, the deterioration of Young's Modulus), but the program does not automatically account for these changes. Changes can be introduced by the user if deemed necessary to resemble the temperature dependence of steel alloys.

- No material creep (failure) affects the completion materials at hand even though the steel alloys might be subjected to elevated temperatures for considerable periods.

- No fatigue (failure) is present at any point of the completion due to possibly occurring cyclic loads at elevated temperatures.

- No restriction of the flow path and alteration of the flow regimes are present. Any existing tools or equipment (gravel packs, sand filter, valves, sensors, pumps, or others) installed at any point of the flow path are being neglected for calculation purposes.
- All and any equations presented in this document and implemented in the MATLAB application are considered state of the art research from official publications of the recent years. Thus, they can be applied to the problem at hand.
- A worst-case and realistic load scenario has been analysed in terms of acting loads on the tieback string and the verification of the desired design factors. The influence of axial loads on the burst and collapse resistances is considered. Coupling types (STC, LTC, BTC) are not considered in the failure criteria evaluations.

7   Results

The case study has been subject to extensive testing and analysis with the MATLAB application. Due to the vast possibilities of possible outcomes and the given choices to modify the parameters to the user's need, only a view selected examples will be presented.

The shut-in case with the tieback in its initial condition will be discussed as well as two production cases with different bottomhole pressures. Two injection cases will be shown with a medium and the maximum injection pressure of 590 [bar]. One pressure testing case will be presented with an applied wellhead pressure at the surface.

Each case (except shut-in) will be investigated with the tieback being fixed in a rigid completion and the resulting loads and a freely moveable variation allowing to compensate all occurring forces with a change in length. If a length change compensates all forces, the load condition will essentially remain as in the initial state.

The buckling analysis is of primary interest and makes it essential to discuss the acting loads on the tieback and the total change in length if the completion allows for free movement in the vertical direction. Moreover, the verification of safety factors shall be discussed.

The case study's used completion design with a crossover at 700 meters depth will be incorporated in the calculations as a separate section where all forces at the crossover depth or below it will be applied to the upper section. A result of this separate calculation of forces combined with the upper section's different dimensions is a distorted load profile. This distortion is amplified during load cases with various forces acting on the tieback. Especially for load cases with high axial tension such as injection or pressure tests, a significant maximum tension is the result of the crossover calculations.

Safety factors for tension, compression, burst and collapse have been calculated. Due to the present crossover, the tension and compression will be assessed individually for each section, and then the lowest value displayed.

A biaxial approach to obtain the influence of axial loads on burst and collapse failure was conducted. If the tieback is entirely under tension or compression, assessing the biaxial safety factors is relatively easy. On the other hand, if the tieback is subject to both tension and compression, the MATLAB application uses the maximum tension and compression values to determine if the tieback is dominantly under tension or compression. Using said methodology to determine the influential axial load for the biaxial ratings, no determination of the biaxial safety factors is possible if the tieback is subject to tension and compression to equal parts. Assessments of biaxial safety factors are done for the entire tieback string and not per section.

Furthermore, each burst and collapse failure has been investigated against a worst-case and a realistic scenario. Due to the amount of calculated data, not all findings can be presented, and only realistic burst and collapse safety factors are shown.

Additional bending loads due to buckling are taken into consideration when calculating the safety factors for tension, compression and the biaxial approach. If the maximum values of tension and/or compression are increased due to buckling it will have an influence on said safety factors.

One inconvenience with the calculation of biaxial safety factors for burst and collapse must be noted. Due to the mechanics of Equation 55 and Equation 56, high axial loads can lead to negative and even complex numbers. Numerically this means no solution can be found, and the yield strength may be reduced to a minimum. However, it is subject to user interpretation if burst or collapse would occur under high axial loads taking all other influencing factors like inside and outside pressure into consideration.

The temperature distribution during shut-in, production and injection has been discussed extensively before and results shown in Figure 7 to Figure 11 are representable for the values obtained through the MATLAB program.

Only one pressure distribution of the shut-in case will be presented since all cases show a similar linear function.

Since all cases refer to the same sets of preliminary data, some values like the geological and reservoir parameters are equal for all cases. These are shown in Figure 40 below.

Geological & Reservoir Parameters					
Reservoir Temperature [°C]	152.86	Thermal Conductivity [W/m*C]	2.00	Thermal Diffusivity [E-06m²/s]	1.00

Figure 40: Geological and reservoir parameters of the case study analysis.

Furthermore, the surface temperature is 10 [°C] and the surface pressure is 1,013125 [bar].

All load cases (except shut-in) use an annulus water density of 1000 [kg/m³].

The same Design Factors are used during all investigations (Figure 41):

Design Factors							
Tension	1.60	Compression	1.60	Burst	1.25	Collapse	1.10

Figure 41: Design factors of the case study analysis.

Additionally, the measuring interval and factor for the helical buckling onset in a deviated wellbore are equal for all cases. No tieback setting force during the installation process after the initial state is used.

Figure 42: Additional settings of the case study analysis.

The axial strength values for each section of the tieback have been obtained. Naturally, the upper section with a greater cross-sectional area has a higher axial strength.

Figure 43: Axial strength of upper and lower section.

7.1 Shut-In (Initial Conditions)

As a small recap, the shut-in or initial case refers to the condition the tieback is in while being hung freely in tension from the wellhead before the final installation and setting of a packer or any other sealing device. Any changes to the tieback that may have affected it before, such as changes from surface conditions, are not of interest. The tieback is not subject to any pressure differentials between inside and outside pressure since it is surrounded by the same fluid (no packer set). The temperature of the water and the tieback itself follows a linear slope of an average geothermal gradient. The only forces acting on the tieback are piston forces (buoyancy) on the cross-sectional area at the bottom of the tieback, and the crossover's outside area and of course, the load due to its self-weight.

During the shut-in case analysis, any occurring initial bends from the drilling process are considered with their respective bending loads, which can be seen in the load diagram. If the bending loads influenced the maximum tension or compression, the MATLAB application would incorporate these findings and adjust the safety factors accordingly. For the case study, the initial bends and associated DLS do not significantly influence the load diagram and do not change the safety factors. No Buckling occurs during the initial conditions.

The pre-calculated bottomhole pressure and temperature are as follows:

Figure 44: Pre-calculated bottomhole pressure and temperature during initial conditions.

The numerical results obtained from the program are presented below. Generally, all design factor requirements are fulfilled during the initial conditions.

One must note the compression at the bottom of the tieback due to the buoyancy effect and also the piston force acting on the crossover. The acting loads during the initial state and information if the initial bends and DLS are influencing the calculations can be seen below:

```
Shut-In (Initial Conditions)
-------------------------------
Self-Weight Load Surface: 2022261.844 [N]
Buoyancy Load: -221878.457 [N]
Crossover Load: -27935.515 [N]
Surface Load: 1772447.872 [N]
Bottom Load: -221878.457 [N]
-------------------------------
The initial doglegs do not have an influence on the maximum tension.
The initial doglegs do not have an influence on the maximum compression.
-------------------------------
```

Figure 45: Loads during initial conditions.

The safety factors for tension and compression with the assessment if the design factors requirements are fulfilled:

```
Safety Factors for Tension and Compression
-------------------------------
Tension Safety Factor: 2.647 [-]
The Tension Safety Factor fulfils the requirements!
Compression Safety Factor: 14.955 [-]
The Compression Safety Factor fulfils the requirements!
```

Figure 46: Safety factors for tension and compression during initial conditions.

The realistic burst rating during initial conditions cannot be assessed because the inside and outside pressure is equivalent. Since no pressure differential is acting on the tieback's inside and outside area (in the safety factor determination for burst), it will not burst. The collapse safety factor uses the equivalent external pressure and can be calculated. The design factor requirements are automatically fulfilled. The obtained collapse mode can also be seen. Realistic burst and collapse safety factors:

```
-------------------------------
Realistic Case Safety Factors - Burst & Collapse
Pi = Max & Po = Max for Burst
Equivalent Outside Pressure for Collapse
-------------------------------
Burst Rating: 62.514 [MPa]
The Burst Safety Factor fulfils the requirements!
No Burst will occur since the inside and outside pressure are equivalent!
Collapse Mode: Plastic
Collapse Rating: 59.362 [MPa]
Collapse Safety Factor: 12.426 [-]
The Collapse Safety Factor fulfils the requirements!
```

Figure 47: Safety factors for realistic burst and collapse during initial conditions.

The tieback is not entirely under tension, but it is assumed that the overall influence of tension is more significant on the total tieback length. Therefore, the maximum axial tension has been used to calculate the realistic biaxial safety factors. The safety factors are following the expected behaviour of reduced collapse rating and increased burst rating due to applied tension on the tieback.

Realistic Case Biaxial Safety Factors

Burst Rating: 72.119 [MPa]
The Biaxial Burst Safety Factor fulfils the requirements!
No Burst will occur since the inside and outside pressure are equivalent!
Biaxial Collapse Mode: Plastic
Biaxial Collapse Rating: 41.087 [MPa]
Biaxial Collapse Safety Factor: 8.600 [-]
The Biaxial Collapse Safety Factor fulfils the requirements!

Figure 48: Safety factors for realistic biaxial burst and collapse during initial conditions.

The pressure distribution of the water during shut-in can be seen below. The pressure follows a linear, purely hydrostatic slope.

Figure 49: Pressure distribution during initial conditions.

Finally, the load distribution, including the bending loads from the two section with DLS can be found below. As discussed previously, bending loads are always to be considered positive and simultaneously negative over the length they occur. Minimum and maximum values of the axial load and the point of zero axial load are marked for convenience. A small change of axial load from the lower to the upper section can be observed even during shut-in.
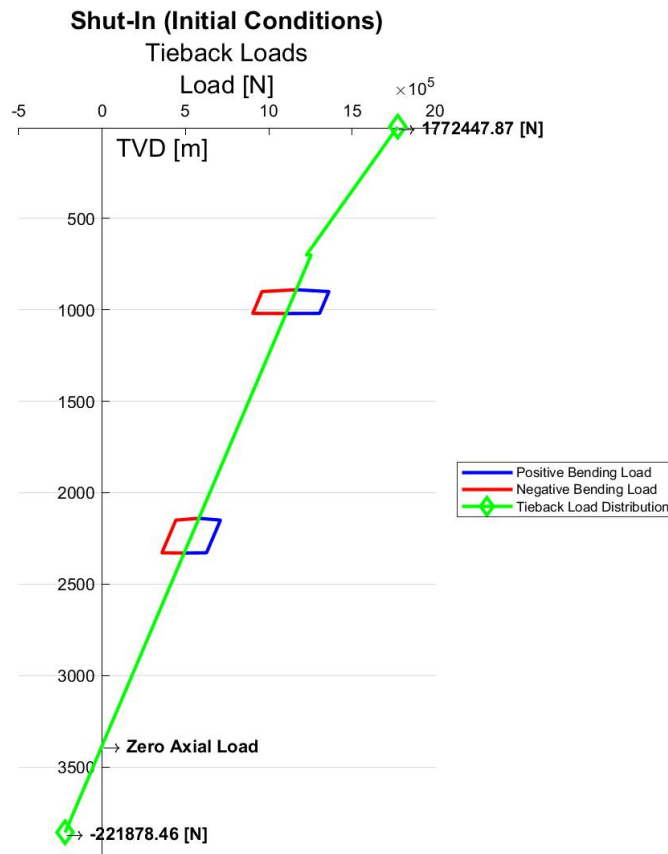
Figure 50: Load distribution during initial conditions.

7.2 Production

Two productions cases are presented. The first case features a bottomhole pressure only slightly higher than the pressure during shut-in with 450 [bar] and the second one with elevated pressures at 650 [bar]. All other influencing factors remain equal. Each case will show the influence of a rigid completion with induced forces and the compensation of these forces with a change in length. Buckling is discussed in both options.

7.2.1 Case 1

The used bottomhole pressure, mass flow rate, and elapsed time since the mode of operation has been changed from initial conditions to production and pre-calculated values for the temperature reduced density of the water, the wellhead pressure and temperature can be seen below. The dynamic viscosity and specific heat capacity has been adjusted to the temperature and pressure conditions.

Production					
Bottomhole Temperature [°C]	152.86	Bottomhole Pressure [barA]	450.00	Water Density [kg/m³]	909.58
Mass Flow Rate [kg/s]	20.00	Elapsed Time [days]	30.00	Specific Heat Capacity [J/kg°C]	3500.00
Dynamic Viscosity [cP]	0.19	Wellhead Temperature [°C]	137.01	Wellhead Pressure [barA]	53.23

Figure 51: Set and pre-calculated values during production case 1.

First, the numerical results and load diagram during a rigid completion is presented, followed by the freely moveable variation.

The load changes in respect to the initial state are dominated primary by the temperature-induced loads followed by the load caused due to the ballooning effect smaller by a power of ten. As anticipated, does the production of hot fluid cause a compressive load, and the increased internal pressure causes a tensile load. The tieback is under compression at the bottom but also on top.


```
-----------------------------
Production after Shut-In
-----------------------------
From Initial Conditions:
Self-Weight Load Surface: 2022261.844 [N]
Buoyancy Load: -221878.457 [N]
Crossover Load: -27935.515 [N]
From Load Case:
Change in Piston Force: -18760.121 [N]
Crossover Load: 55436.865 [m]
Packer Piston Load: -26745.219 [N]
Balloning Load: 135052.380 [N]
Temperature Load: -3166992.458 [N]
Fluid Drag Load: -5482.793 [N]
Total Surface Load: -96628.649 [N]
Total Bottom Load: -1425798.621 [N]
```

Figure 52: Loads during production case 1.

The buckling analysis shows that the effective axial load is below the critical onset force for helical buckling. Thus, helical buckling occurs. Interesting is that the effective axial load is greater than the total compression on the bottom, suggesting that the outside pressure's influence on the calculations of the effective axial load is more severe than the inside pressure under this operating conditions. All buckling associated values such as the helix angle, pitch, dogleg severity, point below which buckling occurs, and the calculated local bending loads can be obtained from the figure below.

```
-----------------------------
Buckling Analysis
-----------------------------
Sinusoidal Buckling tend to happen if -Fc,hel < Feff < -Fc,sin
Helical Buckling tend to happen if Feff < -Fc,hel
Effective Axial Load Feff: -1236774.201 [N]
Critical Sinusoidal Buckling Force Fc,sin: 157908.218 [N]
Critical Helical Buckling Force Fc,hel: 252653.149 [N]
Buckling Mode: Helical
Helix Angle: 0.371 [rad/m]
Pitch of helically buckled tieback: 16.928 [m]
Buckling induced Dogleg Severity: 9.774 [°/30m]
Neutral Point below which buckling occurs (from bottom): 115.199 [m]
Resulting in 6.805 helices.
Local Buckling Bending Load: +-653300.362 [N]
```

Figure 53: Buckling analysis outcome during production case 1.

The safety factors for tension and compression have been obtained once with and without the buckling loads. The top and the bottom of the tieback are under compression. Nonetheless, a tiny part of the load diagram is in the tensile area, thus the high safety factor for tension. Taking buckling into account the safety factor for compression does not fulfil the desired design factor.

```
Safety Factors for Tension and Compression (with Buckling)
-----------------------------
Tension Safety Factor: 66.715 [-]
The Tension Safety Factor fulfils the requirements!
Compression Safety Factor: 1.596 [-]
The Compression Safety Factor does NOT fulfil the requirements!
-----------------------------
Safety Factors for Tension and Compression (without Buckling)
-----------------------------
Tension Safety Factor: 66.715 [-]
The Tension Safety Factor fulfils the requirements!
Compression Safety Factor: 2.327 [-]
The Compression Safety Factor fulfils the requirements!
```

Figure 54: Safety factors for tension and compression (with and without buckling) during production case 1.

The realistic safety factors for burst and collapse under the given operating conditions are:

```
Realistic Case Safety Factors - Burst & Collapse
Pi = Max & Po = Max for Burst
Equivalent Outside Pressure for Collapse
-----------------------------
Burst Rating: 62.514 [MPa]
Burst Safety Factor: 30.072 [-]
The Burst Safety Factor fulfils the requirements!
Collapse Mode: Plastic
Collapse Rating: 59.362 [MPa]
Collapse Safety Factor: 19.134 [-]
The Collapse Safety Factor fulfils the requirements!
```

Figure 55: Safety factors for realistic burst and collapse during production case 1.

The realistic biaxial safety factors show the influence of the compression in reducing the biaxial burst rating. The influence of the additional compression due to buckling does further reduce the burst rating.

```
Realistic Case Biaxial Safety Factors (with Buckling)
--------------------------------
Biaxial Burst Rating: 32.925 [MPa]
Biaxial Burst Safety Factor: 15.838 [-]
The Biaxial Burst Safety Factor fulfils the requirements!
Biaxial Collapse Mode: Plastic
Biaxial Collapse Rating: 65.842 [MPa]
Biaxial Collapse Safety Factor: 21.223 [-]
The Biaxial Collapse Safety Factor fulfils the requirements!
```

Figure 56: Safety factors for realistic biaxial burst and collapse with buckling during production case 1.

```
Realistic Case Biaxial Safety Factors (without Buckling)
--------------------------------
Biaxial Burst Rating: 44.593 [MPa]
Biaxial Burst Safety Factor: 21.451 [-]
The Biaxial Burst Safety Factor fulfils the requirements!
Biaxial Collapse Mode: Plastic
Biaxial Collapse Rating: 65.425 [MPa]
Biaxial Collapse Safety Factor: 21.088 [-]
The Biaxial Collapse Safety Factor fulfils the requirements!
```

Figure 57: Safety factors for realistic biaxial burst and collapse without buckling during production case 1.

The load diagram of the first production case with the initial conditions added as a reference, including the positive and negative bending loads caused by buckling and the effective axial load at the bottom of the tieback, are illustrated in the following graph.
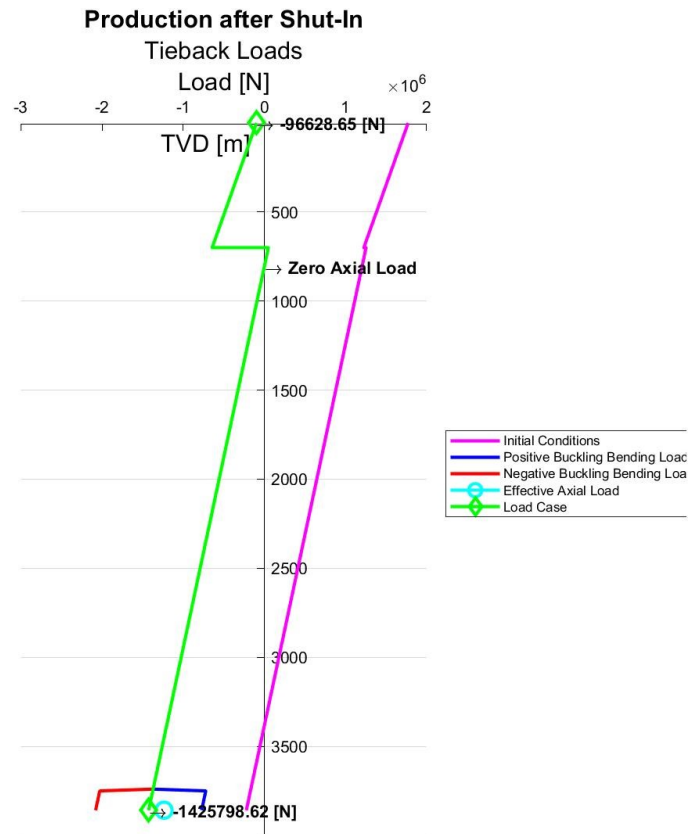
Figure 58: Load distribution during production case 1.

Now the same operating conditions are simulated with a freely moveable tieback. The resulting total loads are essentially the same as before in the initial state because a change in length has compensated all new loads. The most significant change in length is the tieback's elongation due to the increased temperature during production.

Figure 59: Loads and length changes during production case 1 (with length changes).

The buckling analysis leads to the conclusion that no buckling occurs if all loads are compensated.

```
Buckling Analysis
--------------------------------
Sinusoidal Buckling tend to happen if -Fc,hel < Feff < -Fc,sin
Helical Buckling tend to happen if Feff < -Fc,hel
Effective Axial Load Feff: -32854.037 [N]
Critical Sinusoidal Buckling Force Fc,sin: 157908.218 [N]
Critical Helical Buckling Force Fc,hel: 252653.149 [N]
No Buckling occurs!
```

Figure 60: Buckling analysis outcome during production case 1 (with length changes).

The safety factors for tension and compression are virtually the same as in the initial state.

```
Safety Factors for Tension and Compression
--------------------------------
Tension Safety Factor: 2.647 [-]
The Tension Safety Factor fulfils the requirements!
Compression Safety Factor: 14.955 [-]
The Compression Safety Factor fulfils the requirements!
```

Figure 61: Safety factors for tension and compression during production case 1 (with length changes).

The realist burst and collapse safety factors are not subject to change since the internal and external pressure remain the same.

The realistic biaxial burst and collapse safety factors show an increase of the burst rating and a decrease of the collapse rating due to the tension that is now dominant (as for the initial state).

```
Realistic Case Biaxial Safety Factors
--------------------------------
Biaxial Burst Rating: 72.119 [MPa]
Biaxial Burst Safety Factor: 34.693 [-]
The Biaxial Burst Safety Factor fulfils the requirements!
Biaxial Collapse Mode: Plastic
Biaxial Collapse Rating: 41.087 [MPa]
Biaxial Collapse Safety Factor: 13.243 [-]
The Biaxial Collapse Safety Factor fulfils the requirements!
```

Figure 62: Safety factors for realistic biaxial burst and collapse without buckling during production case 1 (with length changes).

The load diagram is reduced to the initial load profile.
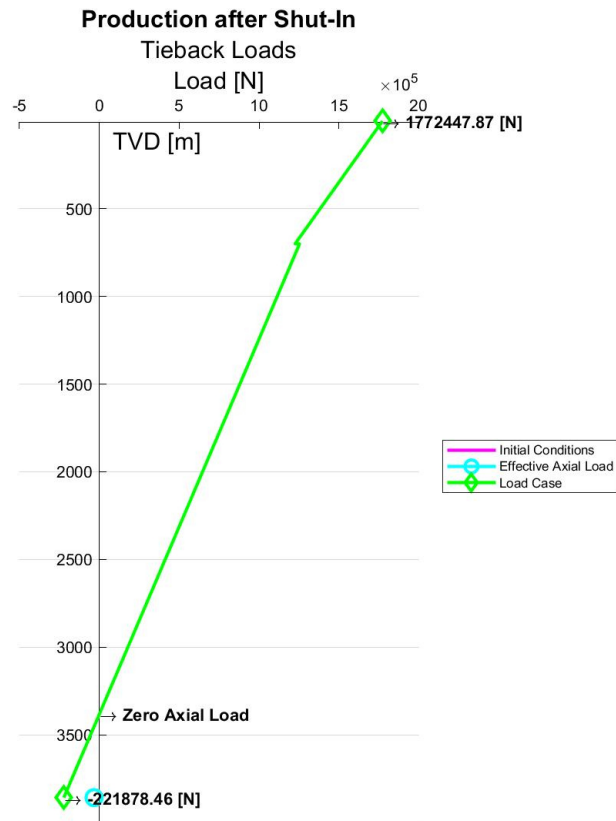
Figure 63: Load distribution during production case 1 (with length change).

7.2.2   Case 2

The second production case only differs with an increase of the bottomhole pressure to 650 [bar].

As before, the load changes in respect to the initial state are dominated primary by the temperature-induced loads followed by the load caused due to the ballooning effect. The ballooning load is more significant due to higher internal pressure but still much smaller than temperature-induced loads. Piston forces acting on the bottom of the tieback and the packer are compressive and more significant due to higher pressure, while the crossover load features higher tension due to increased internal pressure.

```
Production after Shut-In
------------------------------
From Initial Conditions:
Self-Weight Load Surface: 2022261.844 [N]
Buoyancy Load: -221878.457 [N]
Crossover Load: -27935.515 [N]
From Load Case:
Change in Piston Force: -138983.199 [N]
Crossover Load: 417321.155 [m]
Packer Piston Load: -284057.611 [N]
Balloning Load: 759219.864 [N]
Temperature Load: -3166992.458 [N]
Fluid Drag Load: -5482.793 [N]
Total Surface Load: 301131.513 [N]
Total Bottom Load: -1592577.951 [N]
```

Figure 64: Loads during production case 2.

The buckling analysis shows that the buckling effect is more severe compared to the first case, and the length where it occurs has increased. More significant local bending loads are to be observed as well. Helical buckling occurs again because the effective axial load is below the critical onset force. The effective axial load is lower than the total compression on the bottom, suggesting that the inside pressure's influence has increased.

```
------------------------------
Buckling Analysis
------------------------------
Sinusoidal Buckling tend to happen if -Fc,hel < Feff < -Fc,sin
Helical Buckling tend to happen if Feff < -Fc,hel
Effective Axial Load Feff: -1779903.782 [N]
Critical Sinusoidal Buckling Force Fc,sin: 157908.218 [N]
Critical Helical Buckling Force Fc,hel: 252653.149 [N]
Buckling Mode: Helical
Helix Angle: 0.445 [rad/m]
Pitch of helically buckled tieback: 14.111 [m]
Buckling induced Dogleg Severity: 14.066 [°/30m]
Neutral Point below which buckling occurs (from bottom): 1223.516 [m]
Resulting in 86.706 helices.
Local Buckling Bending Load: +-940197.317 [N]
```

Figure 65: Buckling analysis outcome during production case 2.

The safety factors for tension and compression with and without the buckling loads are presented below. Taking buckling into account, the safety factor for compression does not fulfil the desired design factor. It is even lower than in case one due to the additional compression of the buckling effect.

```
Safety Factors for Tension and Compression (with Buckling)
---------------------------------
Tension Safety Factor: 18.386 [-]
The Tension Safety Factor fulfils the requirements!
Compression Safety Factor: 1.310 [-]
The Compression Safety Factor does NOT fulfil the requirements!
---------------------------------
Safety Factors for Tension and Compression (without Buckling)
---------------------------------
Tension Safety Factor: 18.386 [-]
The Tension Safety Factor fulfils the requirements!
Compression Safety Factor: 2.084 [-]
The Compression Safety Factor fulfils the requirements!
```

Figure 66: Safety factors for tension and compression (with and without buckling) during production case 2.

The realistic safety factors for burst and collapse under the given operating conditions would lead to a negative safety factor for collapse due to higher internal pressure, suggesting that no collapse failure will occur.

```
Realistic Case Safety Factors - Burst & Collapse
Pi = Max & Po = Max for Burst
Equivalent Outside Pressure for Collapse
---------------------------------
Burst Rating: 62.514 [MPa]
Burst Safety Factor: 2.831 [-]
The Burst Safety Factor fulfils the requirements!
Collapse Mode: Plastic
Collapse Rating: 59.362 [MPa]
The equivalent outside pressure is negative (high internal pressure).
No collapse failure will occur!
```

Figure 67: Safety factors for realistic burst and collapse during production case 2.

The realistic biaxial safety factors show the influence of the compression in reducing the biaxial burst rating. The influence of the additional compression due to buckling does further reduce the burst rating. The reduction is more significant than in the first case.

```
---------------------------------
Realistic Case Biaxial Safety Factors (with Buckling)
---------------------------------
Biaxial Burst Rating: 23.048 [MPa]
Biaxial Burst Safety Factor: 1.044 [-]
The Biaxial Burst Safety Factor does NOT fulfil the requirements!
Biaxial Collapse Mode: Plastic
Biaxial Collapse Rating: 64.972 [MPa]
The equivalent outside pressure is negative (high internal pressure).
No collapse failure will occur!
```

Figure 68: Safety factors for realistic biaxial burst and collapse with buckling during production case 2.

Realistic Case Biaxial Safety Factors (without Buckling)

Biaxial Burst Rating: 41.856 [MPa]
Biaxial Burst Safety Factor: 1.896 [-]
The Biaxial Burst Safety Factor fulfils the requirements!
Biaxial Collapse Mode: Plastic
Biaxial Collapse Rating: 65.689 [MPa]
The equivalent outside pressure is negative (high internal pressure).
No collapse failure will occur!

Figure 69: Safety factors for realistic biaxial burst and collapse without buckling during production case 2.

In the load diagram of the second production case below, it can be seen how the length where buckling occurs has increased.
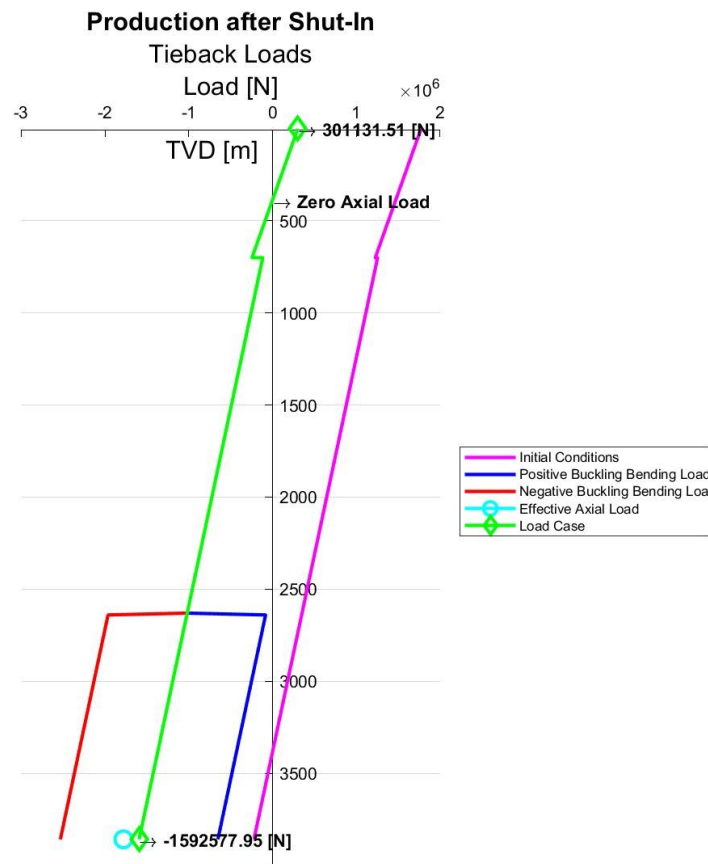
Figure 70: Load distribution during production case 2.

Now the same operating conditions are simulated with a freely moveable tieback. The resulting total loads are essentially the same as before in the initial state because a change in length has compensated all new loads. The most significant elongation is still the temperature-induced change, but due to higher internal pressures and more significant piston forces, the overall length change is reduced compared to the first case.

```
Production after Shut-In
-------------------------------
From Initial Conditions:
Self-Weight Load Surface: 2022261.844 [N]
Buoyancy Load: -221878.457 [N]
Crossover Load: -27935.515 [N]
From Load Case:
Piston Force Length Change: -0.194 [m]
Crossover Length Change: 0.068 [m]
Packer Piston Length Change: -0.396 [m]
Balloning Length Change: -0.385 [m]
Temperature Length Change: 3.568 [m]
Fluid Drag Length Change: -0.006 [m]
Total Surface Load: 1772447.872 [N]
Total Bottom Load: -221878.457 [N]
Total Length Change: 2.655 [m]
```

Figure 71: Loads and length changes during production case 2 (with length changes).

The buckling analysis concludes that buckling and a small additional contraction occurs even if all loads are compensated. Buckling will happen due to the increased internal pressure and the lowered effective axial load.

```
Buckling Analysis
-------------------------------
Sinusoidal Buckling tend to happen if -Fc,hel < Feff < -Fc,sin
Helical Buckling tend to happen if Feff < -Fc,hel
Effective Axial Load Feff: -409204.288 [N]
Critical Sinusoidal Buckling Force Fc,sin: 157908.218 [N]
Critical Helical Buckling Force Fc,hel: 252653.149 [N]
Buckling Mode: Helical
Helix Angle: 0.213 [rad/m]
Pitch of helically buckled tieback: 29.430 [m]
Buckling induced Dogleg Severity: 3.234 [°/30m]
Neutral Point below which buckling occurs (from bottom): 1223.516 [m]
Resulting in 41.574 helices.
Buckling Shortening: -0.032 [m]
Total Length Change: 2.623 [m]
Local Buckling Bending Load: +-216153.692 [N]
```

Figure 72: Buckling analysis outcome during production case 2 (with length changes).

The safety factors for tension and compression without buckling are virtually the same as in the initial state. The compression safety factor taking buckling into account is reduced due to the additional local compressive load caused by buckling.

```
-------------------------------
Safety Factors for Tension and Compression (with Buckling)
-------------------------------
Tension Safety Factor: 2.647 [-]
The Tension Safety Factor fulfils the requirements!
Compression Safety Factor: 7.575 [-]
The Compression Safety Factor fulfils the requirements!
-------------------------------
Safety Factors for Tension and Compression (without Buckling)
-------------------------------
Tension Safety Factor: 2.647 [-]
The Tension Safety Factor fulfils the requirements!
Compression Safety Factor: 14.955 [-]
The Compression Safety Factor fulfils the requirements!
```

Figure 73: Safety factors for tension and compression (with and without buckling) during production case 2 (with length changes).

The realist burst and collapse safety factors are not subject to change since the internal and external pressure remain the same.

The realistic biaxial burst and collapse safety factors show an increase of the burst rating and a decrease of the collapse rating due to the tension that is now dominant (as for the initial state). Since the tieback is dominantly under tension, only the additional tension due to buckling has been taken into account. Since the buckling effect does not change the maximum tension, the biaxial safety factors with and without buckling are equal.

```
Biaxial Burst Rating: 72.119 [MPa]
Biaxial Burst Safety Factor: 3.266 [-]
The Biaxial Burst Safety Factor fulfils the requirements!
Biaxial Collapse Mode: Plastic
Biaxial Collapse Rating: 41.087 [MPa]
The equivalent outside pressure is negative (high internal pressure).
No collapse failure will occur!
```

Figure 74: Safety factors for realistic biaxial burst and collapse (with and without buckling) during production case 2 (with length changes).

The load diagram is reduced to the initial load profile, and the local bending loads due to buckling can be observed.
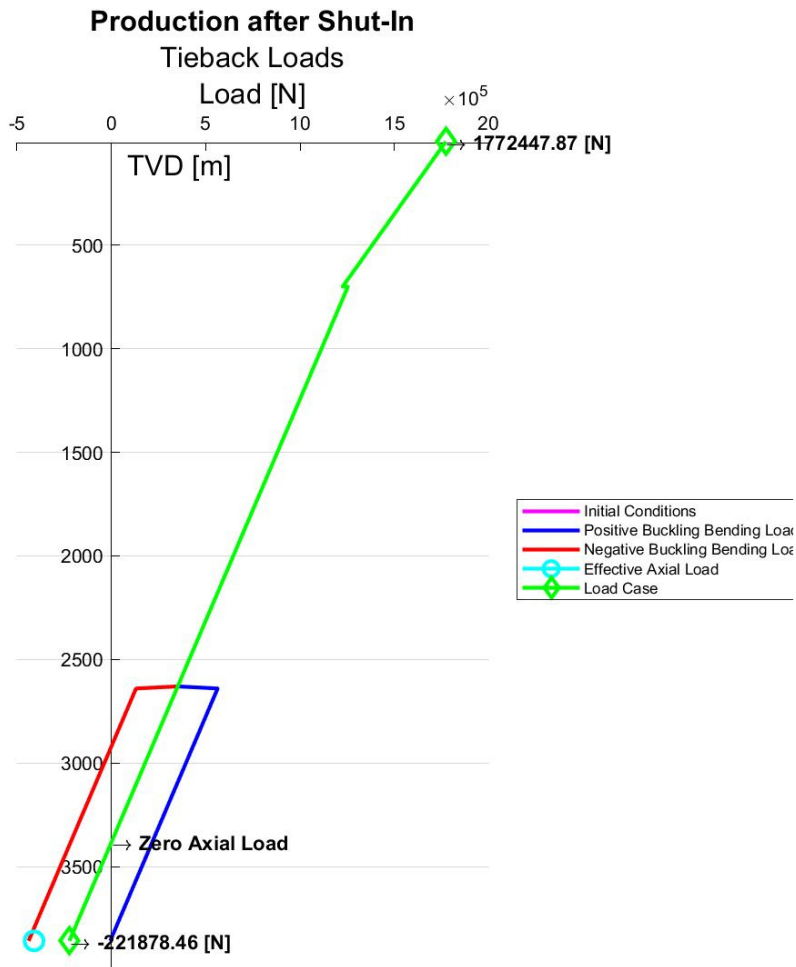
Figure 75: Load distribution during production case 2 (with length change).

7.3 Injection

Two injection cases are presented. The first case features a wellhead pressure with 300 [bar], and for the second case, the maximum injection pressure at the surface of 590 [bar] is applied. All other influencing factors remain equal. Each case will show the influence of a rigid completion with induced forces and the compensation of these forces with a change in length. Buckling is discussed in both options.

7.3.1 Case 1

The used wellhead pressure, injection water temperature, mass flow rate, and elapsed time since the mode of operation has been changed from initial conditions to injection in addition to the pre-calculated values for the bottomhole pressure and temperature can be seen below. The dynamic viscosity, specific heat capacity and injection water density are adjusted to the temperature and pressure conditions.

Injection					
Wellhead Temperature [°C]	10.00	Wellhead Pressure [barA]	300.00	Water Density [kg/m³]	1000.00
Mass Flow Rate [kg/s]	20.00	Elapsed Time [days]	30.00	Specific Heat Capacity [J/kg°C]	4150.00
Dynamic Viscosity [cP]	1.00	Bottomhole Temperature [°C]	23.53	Bottomhole Pressure [barA]	729.51

Figure 76: Set and pre-calculated values during injection case 1.

First, the numerical results and load diagram during a rigid completion is presented, followed by the freely moveable variation.

As for the production cases, the load changes in respect to the initial state are dominated primary by the temperature-induced loads followed by the load caused due to the ballooning effect. The gap in magnitude between the two loads is smaller as for the production cases since the high internal pressures cause more significant ballooning loads. The acting load on the crossover is also generating additional tension in the upper section. Piston forces acting on the bottom of the tieback and on the packer contribute with compressive loads. The injection of cold fluid causes a tensile load. The tieback is under tension at the bottom but also on top.

Injection after Shut-In

From Initial Conditions:
Self-Weight Load Surface: 2022261.844 [N]
Buoyancy Load: -221878.457 [N]
Crossover Load: -27935.515 [N]
From Load Case:
Change in Piston Force: -184389.451 [N]
Crossover Load: 512805.482 [m]
Packer Piston Load: -381240.210 [N]
Balloning Load: 929697.742 [N]
Temperature Load: 2508699.710 [N]
Fluid Drag Load: 5234.737 [N]
Total Surface Load: 3906472.555 [N]
Total Bottom Load: 469275.208 [N]

Figure 77: Loads during injection case 1.

The buckling analysis shows that no buckling will occur, and the effective axial load is reduced but remains positive even with the influence of the elevated internal pressure.

Buckling Analysis

Sinusoidal Buckling tend to happen if -Fc,hel < Feff < -Fc,sin
Helical Buckling tend to happen if Feff < -Fc,hel
Effective Axial Load Feff: 139808.164 [N]
Critical Sinusoidal Buckling Force Fc,sin: 157908.218 [N]
Critical Helical Buckling Force Fc,hel: 252653.149 [N]
No Buckling occurs!

Figure 78: Buckling analysis outcome during injection case 1.

There is no safety factor for compression because the entire tieback is under tension. The two sections' lowest tension safety factor is displayed, which concludes that these operating conditions are not aligned with the required design factors.

```
Safety Factors for Tension and Compression
-------------------------------
Tension Safety Factor: 1.417 [-]
The Tension Safety Factor does NOT fulfil the requirements!
The entire Tieback is under Tension. No Safety Factor for Compression.
```

Figure 79: Safety factors for tension and compression during injection case 1.

The equivalent outside pressure reached a negative value due to the high internal pressure, suggesting that no collapse failure occurs. The realistic safety factor for burst under the given operating conditions is:

```
Realistic Case Safety Factors - Burst & Collapse
Pi = Max & Po = Max for Burst
Equivalent Outside Pressure for Collapse
-------------------------------
Burst Rating: 62.514 [MPa]
Burst Safety Factor: 2.110 [-]
The Burst Safety Factor fulfils the requirements!
Collapse Mode: Plastic
Collapse Rating: 59.362 [MPa]
The equivalent outside pressure is negative (high internal pressure).
No collapse failure will occur!
```

Figure 80: Safety factors for realistic burst and collapse during injection case 1.

As mentioned at the beginning of this chapter, there are some limits to the biaxial safety factors' calculations. The high axial load causes complex numbers, not leading to numerical results. Tension still reduces the collapse rating and increases the burst rating. Due to the high internal pressures, the assumption can be made that the tieback is not subject to collapse even if the high axial tension reduces the collapse rating to a minimum.

```
Biaxial Safety Factors - Burst & Collapse
-------------------------------
Tension increases Burst Resistance and reduces Collapse Resistance.
Compression increases Collapse Resistance and reduces Burst Resistance.
The tieback is completely under tension.
Axial load too significant. Biaxial calculations out of range.
```

Figure 81: Safety factors for realistic biaxial burst and collapse during injection case 1.

The load diagram of the first injection case with the initial conditions added as a reference, and the effective axial load at the bottom of the tieback, are illustrated in the following graph.
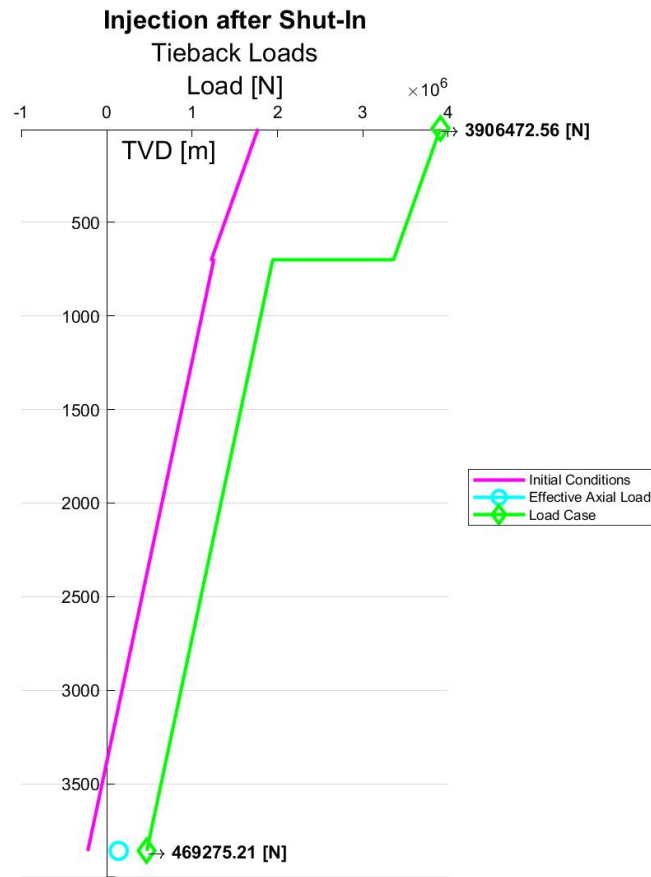
Figure 82: Load distribution during injection case 1.

Now the same operating conditions are simulated with a freely moveable tieback. The resulting total loads are essentially the same as before in the initial state because a reduction in length has compensated all new loads. The most significant change in length is a shortening of the tieback due to the cooling during the injection. Mentionable is the contraction of the tieback due to piston forces and the ballooning effect as well.


```
-----------------------------
Injection after Shut-In
-----------------------------
From Initial Conditions:
Self-Weight Load Surface: 2022261.844 [N]
Buoyancy Load: -221878.457 [N]
Crossover Load: -27935.515 [N]
From Load Case:
Piston Force Length Change: -0.257 [m]
Crossover Length Change: 0.083 [m]
Packer Piston Length Change: -0.532 [m]
Balloning Length Change: -0.485 [m]
Temperature Length Change: -2.827 [m]
Fluid Drag Length Change: 0.006 [m]
Total Surface Load: 1772447.872 [N]
Total Bottom Load: -221878.457 [N]
Total Length Change: -4.011 [m]
```

Figure 83: Loads and length changes during injection case 1 (with length changes).

The buckling analysis concludes that buckling occurs even if all loads are compensated due to the effect of the elevated internal pressure on the effective axial load during the injection.

```
Buckling Analysis
--------------------------------
Sinusoidal Buckling tend to happen if -Fc,hel < Feff < -Fc,sin
Helical Buckling tend to happen if Feff < -Fc,hel
Effective Axial Load Feff: -551345.502 [N]
Critical Sinusoidal Buckling Force Fc,sin: 157908.218 [N]
Critical Helical Buckling Force Fc,hel: 252653.149 [N]
Buckling Mode: Helical
Helix Angle: 0.248 [rad/m]
Pitch of helically buckled tieback: 25.354 [m]
Buckling induced Dogleg Severity: 4.357 [°/30m]
Neutral Point below which buckling occurs (from bottom): 1583.134 [m]
Resulting in 62.441 helices.
Buckling Shortening: -0.055 [m]
Total Length Change: -4.066 [m]
Local Buckling Bending Load: +-291236.845 [N]
```

Figure 84: Buckling analysis outcome during injection case 1 (with length changes).

The safety factors for tension and compression with and without buckling are listed below. The additional local bending load reduces the compression safety factor.

```
Safety Factors for Tension and Compression (with Buckling)
--------------------------------
Tension Safety Factor: 2.647 [-]
The Tension Safety Factor fulfils the requirements!
Compression Safety Factor: 6.467 [-]
The Compression Safety Factor fulfils the requirements!
--------------------------------
Safety Factors for Tension and Compression (without Buckling)
--------------------------------
Tension Safety Factor: 2.647 [-]
The Tension Safety Factor fulfils the requirements!
Compression Safety Factor: 14.955 [-]
The Compression Safety Factor fulfils the requirements!
```

Figure 85: Safety factors for tension and compression (with and without buckling) during injection case 1 (with length changes).

The realist burst and collapse safety factors are not subject to change since the internal and external pressure remain the same.

The realistic biaxial burst and collapse safety factors show an increase of the burst rating and a decrease of the collapse rating due to the tension that is now dominant (as for the initial state). Since the tieback is dominantly under tension, only the additional tension due to buckling has been taken into account. Since the buckling effect does not change the maximum tension, the biaxial safety factors with and without buckling are equal.

Biaxial Burst Rating: 72.119 [MPa]
Biaxial Burst Safety Factor: 2.434 [-]
The Biaxial Burst Safety Factor fulfils the requirements!
Biaxial Collapse Mode: Plastic
Biaxial Collapse Rating: 41.087 [MPa]
The equivalent outside pressure is negative (high internal pressure).
No collapse failure will occur!

Figure 86: Safety factors for realistic biaxial burst and collapse (with and without buckling) during injection case 1 (with length changes).

The load diagram with the positive and negative local buckling loads is presented below.
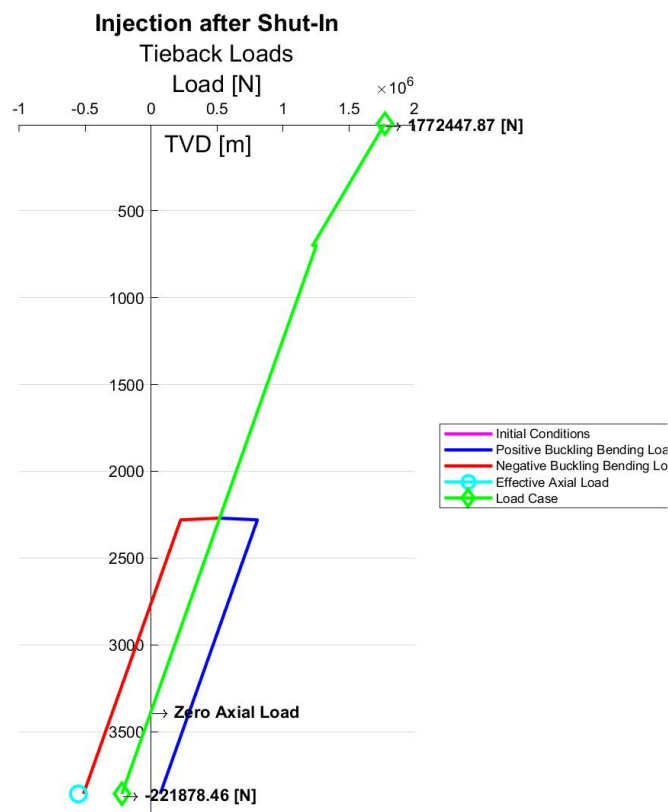
Figure 87: Load distribution during injection case 1 (with length change).

7.3.2 Case 2

The second injection case only differs with an increase of the wellhead injection pressure to 590 [bar]. This case is the most extreme regarding buckling. Buckling occurs even though the entire tieback is under much tension.

As before, the load changes in respect to the initial state are the most influenced by the temperature-induced loads, followed closely by the load caused due to the ballooning effect because of the high internal pressure. The injection of cold fluid causes a tensile load. Piston forces acting on the bottom of the tieback and the packer are compressive and more significant

due to higher pressure, while the crossover load features higher tension due to increased internal pressure. The entire tieback is under tension at the top and the bottom.

```
Injection after Shut-In
------------------------------
From Initial Conditions:
Self-Weight Load Surface: 2022261.844 [N]
Buoyancy Load: -221878.457 [N]
Crossover Load: -27935.515 [N]
From Load Case:
Change in Piston Force: -358712.915 [N]
Crossover Load: 1037537.702 [m]
Packer Piston Load: -754343.178 [N]
Balloning Load: 1834740.593 [N]
Temperature Load: 2508699.710 [N]
Fluid Drag Load: 5234.737 [N]
Total Surface Load: 4483224.790 [N]
Total Bottom Load: 227445.180 [N]
```

Figure 88: Loads during injection case 2.

Interesting is that the buckling analysis shows that buckling will occur even though the entire tieback is under a lot of tension. The effective axial load is decreased below 0 because of the high pressure applied to the wellhead during the injection. The buckling effect is not as severe as during the production cases because the total effective load at the bottom of the tieback is greater (less negative). Thus, the bending loads are also of smaller magnitude. Due to the high internal pressure, the neutral point is predicted to be more than 3100 meters above the end of the tieback. One must note that at 2310 meters MD, a change in the casing diameter is present. At this point, the radial clearance changes and values might not be representable anymore to the onset conditions at the bottom of the tieback.

```
Buckling Analysis
------------------------------
Sinusoidal Buckling tend to happen if -Fc,hel < Feff < -Fc,sin
Helical Buckling tend to happen if Feff < -Fc,hel
Effective Axial Load Feff: -647729.728 [N]
Critical Sinusoidal Buckling Force Fc,sin: 157908.218 [N]
Critical Helical Buckling Force Fc,hel: 252653.149 [N]
Buckling Mode: Helical
Helix Angle: 0.269 [rad/m]
Pitch of helically buckled tieback: 23.392 [m]
Buckling induced Dogleg Severity: 5.119 [°/30m]
Neutral Point below which buckling occurs (from bottom): 3132.477 [m]
Resulting in 133.913 helices.
Local Buckling Bending Load: +-342149.817 [N]
```

Figure 89: Buckling analysis outcome during injection case 2.

The safety factors for tension and compression with and without the buckling loads are presented below. Without buckling, the entire tieback is under tension. With buckling, a short length at the bottom is subject to compression. In either case, the safety factor for tension does not fulfil the required design factor and is even lower than in the first injection case.

```
----------------------------------
Safety Factors for Tension and Compression (with Buckling)
----------------------------------
Tension Safety Factor: 1.235 [-]
The Tension Safety Factor does NOT fulfil the requirements!
Compression Safety Factor: 28.928 [-]
The Compression Safety Factor fulfils the requirements!
----------------------------------
Safety Factors for Tension and Compression (without Buckling)
----------------------------------
Tension Safety Factor: 1.235 [-]
The Tension Safety Factor does NOT fulfil the requirements!
The entire Tieback is under Tension. No Safety Factor for Compression.
```

Figure 90: Safety factors for tension and compression (with and without buckling) during injection case 2.

The realistic safety factors for burst and collapse under the given operating conditions would lead to a negative safety factor for collapse due to higher internal pressure, suggesting that no collapse failure will occur. The safety factor for burst does not fulfil the requirements suggesting that the inside pressure is too high.

```
Realistic Case Safety Factors - Burst & Collapse
Pi = Max & Po = Max for Burst
Equivalent Outside Pressure for Collapse
----------------------------------
Burst Rating: 62.514 [MPa]
Burst Safety Factor: 1.066 [-]
The Burst Safety Factor does NOT fulfil the requirements!
Collapse Mode: Plastic
Collapse Rating: 59.362 [MPa]
The equivalent outside pressure is negative (high internal pressure).
No collapse failure will occur!
```

Figure 91: Safety factors for realistic burst and collapse during injection case 2.

As for the first injection case, no biaxial safety factors can be calculated numerically because of the extensive axial tension.

```
Biaxial Safety Factors - Burst & Collapse
----------------------------------
Tension increases Burst Resistance and reduces Collapse Resistance.
Compression increases Collapse Resistance and reduces Burst Resistance.
The tieback is completely under tension.
Axial load too significant. Biaxial calculations out of range.
```

Figure 92: Safety factors for realistic biaxial burst and collapse during injection case 2.

In the load diagram of the second injection case below, it can be seen how buckling occurs even tough the entire tieback is under tension and the significant predicted length of where buckling occurs.
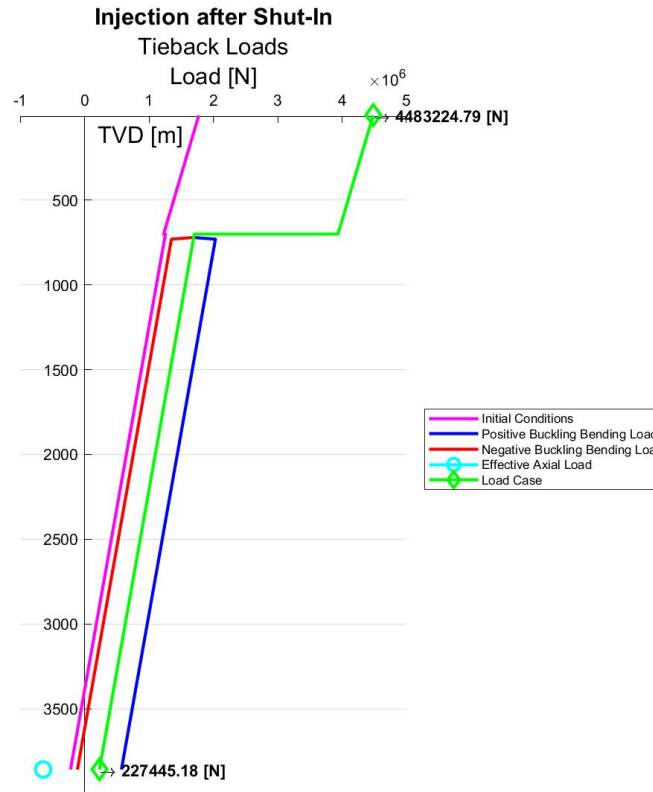
Figure 93: Load distribution during injection case 2.

Now the same operating conditions are simulated with a freely moveable tieback. The resulting total loads are essentially the same as before in the initial state because a change in length has compensated all new loads. The most significant shortening is still the temperature-induced change, and due to higher internal pressures and more significant piston forces, the overall shortening is increased (more contraction) compared to the first case.

Figure 94: Loads and length changes during injection case 2 (with length changes).

The buckling analysis concludes that buckling occurs over a great length (more than 3100 meters above the tiebacks bottom) with moderate severity and bending loads compared to the production cases.

```
------------------------------
Buckling Analysis
------------------------------
Sinusoidal Buckling tend to happen if -Fc,hel < Feff < -Fc,sin
Helical Buckling tend to happen if Feff < -Fc,hel
Effective Axial Load Feff: -1097053.366 [N]
Critical Sinusoidal Buckling Force Fc,sin: 157908.218 [N]
Critical Helical Buckling Force Fc,hel: 252653.149 [N]
Buckling Mode: Helical
Helix Angle: 0.350 [rad/m]
Pitch of helically buckled tieback: 17.974 [m]
Buckling induced Dogleg Severity: 8.670 [°/30m]
Neutral Point below which buckling occurs (from bottom): 3132.477 [m]
Resulting in 174.277 helices.
Buckling Shortening: -0.216 [m]
Total Length Change: -5.380 [m]
Local Buckling Bending Load: +-579495.724 [N]
```

Figure 95: Buckling analysis outcome during injection case 2 (with length changes).

The safety factors for tension and compression without buckling are virtually the same as in the initial state. The compression safety factor taking buckling into account is reduced due to the additional local compressive load caused by buckling.

```
Safety Factors for Tension and Compression (with Buckling)
------------------------------
Tension Safety Factor: 2.647 [-]
The Tension Safety Factor fulfils the requirements!
Compression Safety Factor: 4.141 [-]
The Compression Safety Factor fulfils the requirements!
------------------------------
Safety Factors for Tension and Compression (without Buckling)
------------------------------
Tension Safety Factor: 2.647 [-]
The Tension Safety Factor fulfils the requirements!
Compression Safety Factor: 14.955 [-]
The Compression Safety Factor fulfils the requirements!
```

Figure 96: Safety factors for tension and compression (with and without buckling) during injection case 2 (with length changes).

The realist burst and collapse safety factors are not subject to change since the internal and external pressure remain the same.

The realistic biaxial burst and collapse safety factors show a small change in the burst and collapse ratings taking buckling into account due to a slightly higher maximum tension caused by the buckling loads. Since the tieback is initially dominantly under tension, only the additional tension due to buckling has been considered.

Realistic Case Biaxial Safety Factors (with Buckling)

Biaxial Burst Rating: 72.155 [MPa]
Biaxial Burst Safety Factor: 1.231 [-]
The Biaxial Burst Safety Factor does NOT fulfil the requirements!
Biaxial Collapse Mode: Plastic
Biaxial Collapse Rating: 40.377 [MPa]
The equivalent outside pressure is negative (high internal pressure).
No collapse failure will occur!

Figure 97: Safety factors for realistic biaxial burst and collapse (with buckling) during injection case 2 (with length changes).

Biaxial Burst Rating: 72.119 [MPa]
Biaxial Burst Safety Factor: 1.230 [-]
The Biaxial Burst Safety Factor does NOT fulfil the requirements!
Biaxial Collapse Mode: Plastic
Biaxial Collapse Rating: 41.087 [MPa]
The equivalent outside pressure is negative (high internal pressure).
No collapse failure will occur!

Figure 98: Safety factors for realistic biaxial burst and collapse (without buckling) during injection case 2 (with length changes).

The load diagram is reduced to the initial load profile, and the local bending loads due to buckling can be observed as well as the great length where buckling occurs.
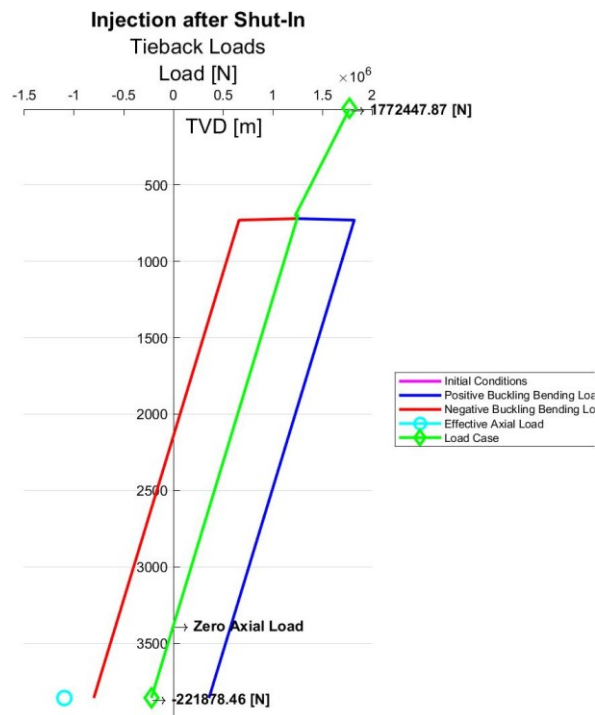
Figure 99: Load distribution during injection case 2 (with length change).

7.4 Pressure Test

A pressure test is being simulated to test the completion's integrity with anticipated operating conditions. The pressure test is being conducted with a plug at the end of the tieback completion. The temperature distribution of the water inside the tieback does not change and is equal to the temperature distribution during initial conditions because no fluid flow is present. The testing pressure at the wellhead is 200 [bar].

Pressure Test

Wellhead Pressure [barA]	200.00		Pressure at Plug [barA]	569.11
Wellhead Temperature [°C]	10.00		Temperature at Plug [°C]	134.99

Figure 100: Set and pre-calculated values during the pressure test.

First, the numerical results and load diagram during a rigid completion is presented, followed by the freely moveable variation.

Compared to the case of production and injection before no loads are introduced due to temperature changes or additional pressure acting on the bottom of the tieback and the packer. The acting load on the packer is small but tensile because the water density in the annulus is assumed to be constant 1000 [kg] compared to the temperature reduced density below the tieback. Most influential is the ballooning load due to the internal pressure followed by the load created at the pressure testing plug due to the pressure differential above and below it.

```
Pressure Test after Shut-In
-------------------------------
From Initial Conditions:
Self-Weight Load Surface: 2022261.844 [N]
Buoyancy Load: -221878.457 [N]
Crossover Load: -27935.515 [N]
From Load Case:
Change in Piston Force: 0.000 [N]
Crossover Load: 333569.911 [m]
Packer Piston Load: 13406.902 [N]
Balloning Load: 616578.671 [N]
Temperature Load: 0.000 [N]
Pressure Testing Plug Load: 376350.251 [N]
Total Surface Load: 2908961.087 [N]
Total Bottom Load: 371271.215 [N]
```

Figure 101: Loads during the pressure test.

The buckling analysis shows that no buckling will occur, and the effective axial load is reduced but remains positive even with the influence of the elevated internal pressure.

```
-----------------------------
Buckling Analysis
-----------------------------
Sinusoidal Buckling tend to happen if -Fc,hel < Feff < -Fc,sin
Helical Buckling tend to happen if Feff < -Fc,hel
Effective Axial Load Feff: 242672.678 [N]
Critical Sinusoidal Buckling Force Fc,sin: 157908.218 [N]
Critical Helical Buckling Force Fc,hel: 252653.149 [N]
No Buckling occurs!
```

Figure 102: Buckling analysis outcome during the pressure test.

There is no safety factor for compression because the entire tieback is under tension. The lowest tension safety factor of the two tieback sections complies with the design factor requirements.

```
Safety Factors for Tension and Compression
-----------------------------
Tension Safety Factor: 1.797 [-]
The Tension Safety Factor fulfils the requirements!
The entire Tieback is under Tension. No Safety Factor for Compression.
```

Figure 103: Safety factors for tension and compression during the pressure test.

The equivalent outside pressure reached a negative value due to the high internal pressure, suggesting that no collapse failure occurs. The realistic safety factor for burst under the given operating conditions complies with the design factor requirements.:

```
Realistic Case Safety Factors - Burst & Collapse
Pi = Max & Po = Max for Burst
Equivalent Outside Pressure for Collapse
-----------------------------
Burst Rating: 62.514 [MPa]
Burst Safety Factor: 3.298 [-]
The Burst Safety Factor fulfils the requirements!
Collapse Mode: Plastic
Collapse Rating: 59.362 [MPa]
The equivalent outside pressure is negative (high internal pressure).
No collapse failure will occur!
```

Figure 104: Safety factors for realistic burst and collapse during the pressure test.

The realistic biaxial safety factors show a greatly reduced collapse rating due to the present tension but like before the equivalent outside pressure is negative due to high internal pressure suggesting that no collapse failure will occur.

Realistic Case Biaxial Safety Factors

Biaxial Burst Rating: 68.088 [MPa]
Biaxial Burst Safety Factor: 3.592 [-]
The Biaxial Burst Safety Factor fulfils the requirements!
Biaxial Collapse Mode: Yield
Biaxial Collapse Rating: 14.199 [MPa]
The equivalent outside pressure is negative (high internal pressure).
No collapse failure will occur!

Figure 105: Safety factors for realistic biaxial burst and collapse during the pressure test.

The load diagram of the pressure test with the initial conditions added as a reference, and the effective axial load at the bottom of the tieback, are illustrated in the following graph.
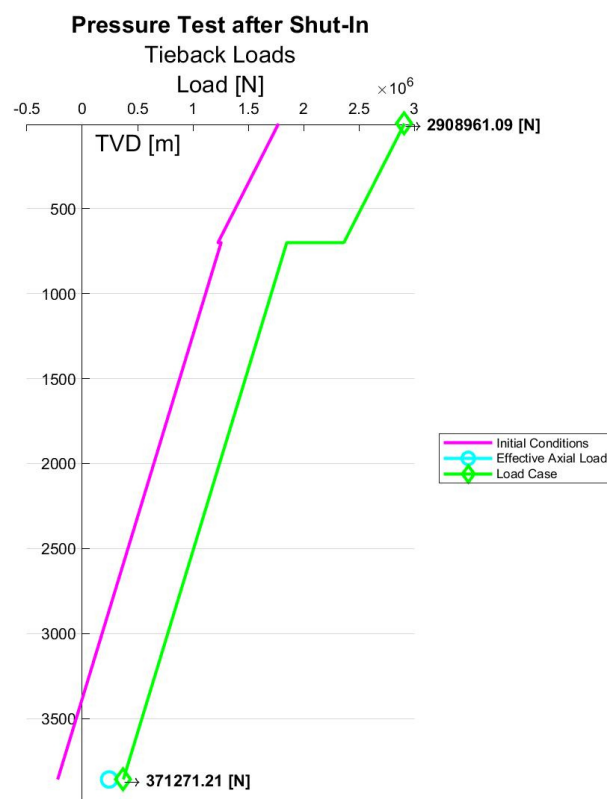
Figure 106: Load distribution during the pressure test.

Now the same operating conditions are simulated with a freely moveable tieback. The resulting total loads are essentially the same as before in the initial state because a reduction in length has compensated all new loads. Without a change in temperature the most influential elongation is due to the tension created on the pressure testing plug followed by the shortening due to the ballooning effect. The total length change is small compared to the previous cases.

```
Pressure Test after Shut-In
-------------------------------
From Initial Conditions:
Self-Weight Load Surface: 2022261.844 [N]
Buoyancy Load: -221878.457 [N]
Crossover Load: -27935.515 [N]
From Load Case:
Piston Force Length Change: 0.000 [m]
Crossover Length Change: 0.054 [m]
Packer Piston Length Change: 0.019 [m]
Balloning Length Change: -0.318 [m]
Temperature Length Change: 0.000 [m]
Pressure Testing Plug Elongation: 0.525 [m]
Total Surface Load: 1772447.872 [N]
Total Bottom Load: -221878.457 [N]
Total Length Change: 0.280 [m]
```

Figure 107: Loads and length changes during the pressure test (with length changes).

The buckling analysis concludes that less severe buckling occurs over a moderate length even if all loads are compensated due to the effect of the elevated internal pressure on the effective axial load during. The associated change in length is small.

```
-------------------------------
Buckling Analysis
-------------------------------
Sinusoidal Buckling tend to happen if -Fc,hel < Feff < -Fc,sin
Helical Buckling tend to happen if Feff < -Fc,hel
Effective Axial Load Feff: -350476.993 [N]
Critical Sinusoidal Buckling Force Fc,sin: 157908.218 [N]
Critical Helical Buckling Force Fc,hel: 252653.149 [N]
Buckling Mode: Helical
Helix Angle: 0.198 [rad/m]
Pitch of helically buckled tieback: 31.800 [m]
Buckling induced Dogleg Severity: 2.770 [°/30m]
Neutral Point below which buckling occurs (from bottom): 1012.839 [m]
Resulting in 31.850 helices.
Buckling Shortening: -0.023 [m]
Total Length Change: 0.257 [m]
Local Buckling Bending Load: +-185132.215 [N]
```

Figure 108: Buckling analysis outcome during the pressure test (with length changes).

The safety factors for tension and compression with and without buckling are listed below. The additional local bending load reduces the compression safety factor.

```
-------------------------------
Safety Factors for Tension and Compression (with Buckling)
-------------------------------
Tension Safety Factor: 2.647 [-]
The Tension Safety Factor fulfils the requirements!
Compression Safety Factor: 8.153 [-]
The Compression Safety Factor fulfils the requirements!
-------------------------------
Safety Factors for Tension and Compression (without Buckling)
-------------------------------
Tension Safety Factor: 2.647 [-]
The Tension Safety Factor fulfils the requirements!
Compression Safety Factor: 14.955 [-]
The Compression Safety Factor fulfils the requirements!
```

Figure 109: Safety factors for tension and compression (with and without buckling) during the pressure test (with length changes).

The realist burst and collapse safety factors are not subject to change since the internal and external pressure remain the same.

The realistic biaxial burst and collapse safety factors show an increase of the burst rating and a decrease of the collapse rating due to the tension that is now dominant (as for the initial state). Since the tieback is dominantly under tension, only the additional tension due to buckling has been taken into account. Since the buckling effect does not change the maximum tension, the biaxial safety factors with and without buckling are equal.

Biaxial Burst Rating: 72.119 [MPa]
Biaxial Burst Safety Factor: 3.804 [-]
The Biaxial Burst Safety Factor fulfils the requirements!
Biaxial Collapse Mode: Plastic
Biaxial Collapse Rating: 41.087 [MPa]
The equivalent outside pressure is negative (high internal pressure).
No collapse failure will occur!

Figure 110: Safety factors for realistic biaxial burst and collapse (with and without buckling) during the pressure test (with length changes).

The load diagram with the positive and negative local buckling loads is presented below.
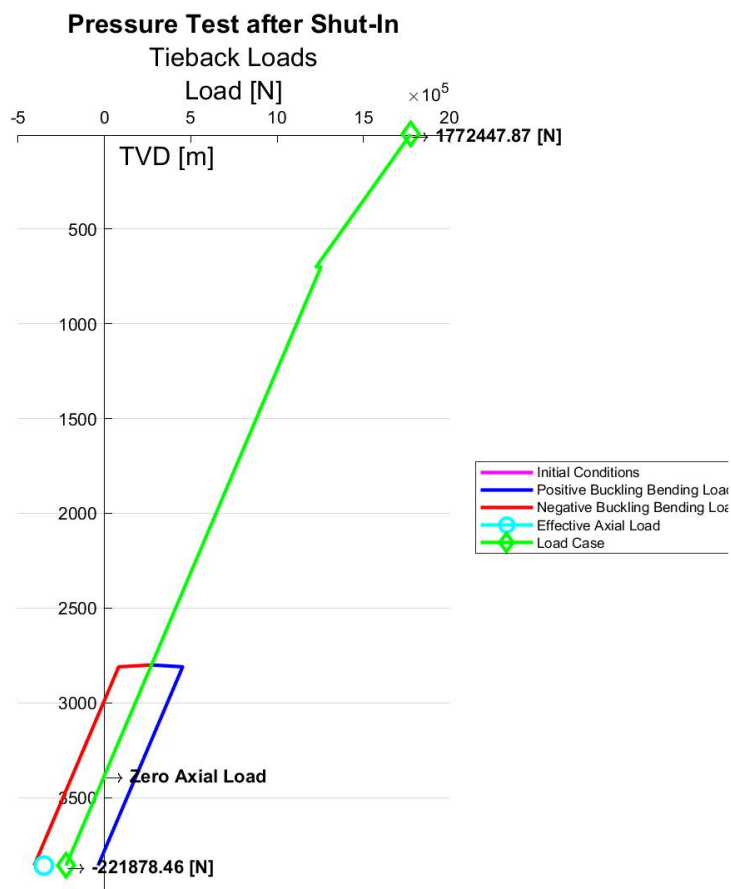
Figure 111: Load distribution during the pressure test (with length change).

8 Conclusion

Many interesting findings have been presented in the results that lead to the following conclusions in terms of the onset and severity of buckling. It has been proven that during production of hot water the use of expansion devices and therefore the compensation of high compressive axial loads is a reliable method to completely mitigate buckling or at least lessen the magnitude of the occurring dogleg severities and bending loads. Applying additional tension during the installation process can further help to no pass the threshold of the buckling onset. Additionally, compensating high axial compression may benefit to fulfil the required design factors.

During injection and also pressure test activities a driving factor causing buckling is the high internal pressure. A compensation of high axial tension due to injection of cold water or the use of a pressure testing plug does not show direct benefits in terms of the onset and severity of buckling – rather the opposite. The axial tension delays the onset of buckling and without it the driving factor of pressure still remains worsening the outcome. However, as for production scenarios a compensation of loads with a change in length may provide significant benefits to the fulfilment of required safety factors. A good combination of using the axial tension as a benefit and still reducing the maximum axial loads to remain in reasonable limits could be to only allow for a certain amount of length change, namely the compensation of the temperature-induced loads during injection.

Even tough not numerically proven special attention must be given shortly to the use of centralizers which can provide substantial benefits in terms of buckling.

Lastly, the publicly acknowledged equations and models for buckling provide a good impression of when the onset of buckling might occur and what the expected outcome may be. However, there is an inconsistency in the used factors that govern the threshold for the helical buckling onset in deviated wellbores and together with all the underlying simplifications and assumptions, certain influencing factors are often not considered in the basic calculations for buckling. The determination of the buckling onset and its outcome is therefore, a rather dynamic process that requires more than the same equations for each completion design under different operating conditions and the implementation of case specific factors to match real life results.

List of Tables

List of Figures

Abbreviations

API	American Petroleum Institute
BTC	Buttress Thread Coupling
DLS	Dogleg Severity
EGS	Enhanced Geothermal System
GUI	Graphical User Interface
HDR	Hot Dry Rock
ID	Inner Diameter
LTC	Long Round Thread Coupling
MD	Measured Depth
OD	Outer Diameter
STC	Short Round Thread Coupling
t	Wall Thickness
TOC	Top of Cement
TOL	Top of Liner
TVD	True Vertical Depth
VME	Von Mises equivalent stress

Nomenclature

$(OD/t)_P$	Maximum slenderness ratio for the plastic collapse [-]
$(OD/t)_T$	Maximum slenderness ratio for the transitional collapse [-]
$(OD/t)_{Yp}$	Maximum slenderness ratio for the yield strength collapse [-]
$\left(\dfrac{dP}{dD}\right)_{Water}$	Linear hydraulic water pressure gradient of the formation [Pa/m]
$\left(\dfrac{dT}{dD}\right)_{Formation,i}$	Geothermal temperature gradient of the formation section i [°C/m]
$\left(\dfrac{dT}{dD}\right)_{Formation}$	Linear geothermal temperature gradient of the formation [°C/m]
ΔP_{Loss}	Total amount of friction pressure losses [Pa]
$\dfrac{\Delta P}{\Delta L}$	Frictional pressure loss gradient [Pa/m]
$\Delta L_{Balloon}$	Ballooning length change due to relative pressure changes [m]
ΔL_{Buck}	Shortening due to buckling [m]
$\Delta L'_{Buck}$	Shortening due to buckling of the entire tieback [m]
$\Delta L_{Crossover}$	Length change due to a diameter change of a crossover [m]
ΔL_{Drag}	Length change due to flowing fluid [m]
ΔL_{Packer}	Length change due to a pressure differential on the packer [m]
ΔL_{Plug}	Length change due to a pressure differential on the plug [m]
ΔL_{Temp}	Length change due to temperature differentials [m]
ΔL_{Total}	Maximum length change [m]
ΔL_{Weight}	Elongation due to tieback self-weight in air [m]
ΔP_I	Internal pressure change [Pa]
ΔP_O	External pressure change [Pa]
$A_{I,1}$	Inside area of the upper tieback section of a crossover [m²]
$A_{I,2}$	Inside area of the lower tieback section of a crossover [m²]

$A_{I,Bottom}$	Inside area of the tieback's bottom [m²]
$A_{I,Casing}$	Inside area of the casing [m²]
A_I	Inside area of the tieback [m²]
$A_{O,1}$	Outside area of the upper tieback section of a crossover [m²]
$A_{O,2}$	Outside area of the lower tieback section of a crossover [m²]
$A_{O,Bottom}$	Outside area at the bottom of the tieback [m²]
A_O	Outside area of the tieback [m²]
A_P	Packer bore area [m²]
A_T	Constant for water density dependency on temperature [1/°C]
A_X	Variable to insert A_I or A_O for the triaxial stress calculations [m²]
B_T	Constant for water density dependency on temperature [1/°C²]
D_{Diff}	Diffusion depth [m]
$D_{Res,TVD}$	Reservoir TVD [m]
$D_{i,TVD}$	TVD of section i [m]
$D_{n,TVD}$	TVD at depth n [m]
$F_{Axial,Eff}$	Effective axial load [N]
$F_{Axial,Max}$	Axial strength [N]
$F_{Axial,Total}$	Total axial load [N]
$F_{Balloon}$	Ballooning force due to relative pressure changes [N]
$F_{Bending}$	Bending force due to the bending stress [N]
$F_{Buoyancy}$	Buoyancy force on the tieback's bottom [N]
$F_{C,S}$	Critical force for sinusoidal buckling [N]
$F_{Crossover}$	Force due to a diameter change of a crossover [N]
F_{Drag}	Drag force due to flowing fluid [N]

$F_{H,S}$	Critical force for helical buckling [N]
$F_{N,Dev}$	Normal force due to tieback self-weight in air in a deviated wellbore [N]
F_{Packer}	Force due to a pressure differential on the packer [N]
F_{Plug}	Force due to a pressure differential on the pressure testing plug [N]
$F_{Setting}$	Setting force of a packer [N]
F_{Temp}	Force due to temperature differentials [N]
F_{Weight}	Load due to tieback self-weight in a wellbore [N]
ID_{Casing}	Inside diameter of the casing [m]
$K_{Formation}$	Average thermal conductivity of the formation [W/m°C]
$L_{Balloon}$	Length of the tieback subject to the ballooning effect (MD) [m]
$L_{Crossover}$	Length from the surface to the crossover (MD) [m]
L_{Drag}	Flowed through length (MD) [m]
L_{Packer}	Length from the surface to the packer (MD) [m]
L_{Plug}	Length from the surface to the plug (MD) [m]
L_{Temp}	Length of the tieback subject to the temperature change (MD) [m]
$L_{Tieback}$	Length of the Tieback (MD) [m]
$P_{Above,Packer}$	Annulus pressure above the packer [Pa]
$P_{Above,Plug}$	Pressure above the pressure testing plug [Pa]
$P_{Annulus,Max}$	Maximum annulus pressure [Pa]
P_B	Burst rating [Pa]
$P_{Below,Packer}$	Pressure below the packer [Pa]
$P_{Below,Plug}$	Pressure below the pressure testing plug [Pa]
P_{Bottom}	Pressure at the bottom of the well [Pa]
$P_{C,E}$	Elastic collapse rating [Pa]

$P_{C,P}$	Plastic collapse rating [Pa]
$P_{C,T}$	Transitional collapse rating [Pa]
$P_{C,Yp}$	Yield strength collapse rating [Pa]
P_C	Collapse rating [Pa]
$P_{Dn,Annulus}$	Annulus pressure at a depth n [Pa]
$P_{Dn,Injector}$	Pressure of an injector well at a depth n [Pa]
$P_{Dn,Producer}$	Pressure of a producer well at a depth n [Pa]
$P_{Dn,Shut,Temp}$	Temperature-accounted pressure during shut-in at a depth n[Pa]
P_{Equ}	Equivalent outside pressure for the collapse rating [Pa]
$P_{I,Max}$	Maximum internal pressure [Pa]
$P_{I,Packer}$	Inside pressure of the tieback at the packer [Pa]
P_I	Internal pressure [Pa]
$P_{O,Max}$	Maximum outside pressure [Pa]
P_O	External pressure [Pa]
$P_{Res,Temp}$	Temperature-accounted pressure of an undisturbed reservoir [Pa]
$P_{Reservoir}$	Reservoir pressure [Pa]
$P_{Surface}$	Surface pressure [Pa]
$P_{Wellhead}$	Wellhead pressure [Pa]
SF_A	Axial safety factor (tension and compression) [-]
SF_B	Burst safety factor [-]
SF_C	Collapse safety factor [-]
SF_T	Triaxial safety factor [-]
$T_{Dn,Inj}$	Temperature during injection at a depth n [°C]
$T_{Dn,Pro}$	Temperature during production at a depth n [°C]

$T_{Injection}$	Injection water temperature at the wellhead [°C]
$T_{Reservoir}$	Reservoir Temperature [°C]
$T_{Surface}$	Surface Temperature [°C]
$T_{Wh,P/S}$	Expected wellhead temperature during production or while shut-in [°C]
Y_P	Yield strength of the tieback [Pa]
Y_{Pa}	Effective yield strength of the tieback [Pa]
c_W	Specific heat capacity of water [J/kg°C]
$\dot{m}$	Mass flow rate [kg/s]
r_C	Radial clearance [m]
$r_{Tieback,O}$	Outer radius of a representable tieback section [m]
w_B	Buoyed weight of the tieback [N/m]
w_I	Linear weight of the fluid inside the tieback [N/m]
w_O	Linear weight of the fluid in the annulus [N/m]
w_T	Linear weight of the tieback [N/m]
$\dfrac{w}{l}$	Mass per unit length of the tieback [kg/m]
$\theta_{Helix,Max}$	Maximum helix angle for sinusoidal buckling [rad/m]
θ_{Helix}	Helix angle for helical buckling [rad/m]
$\kappa_{Formation}$	Average thermal diffusivity of the formation [m²/s]
ρ_{Brine}	Water density of the brine inside the reservoir [kg/m³]
$\rho_{Water,Annulus}$	Water density in the annulus [kg/m³]
$\rho_{Water,Reservoir}$	Water density at reservoir conditions [kg/m³]
$\rho_{Water,Surface}$	Water density at surface conditions [kg/m³]
$\rho_{Water,Temp,Dn}$	Temperature-accounted water density at depth n [kg/m³]
$\sigma_{Axial,Total}$	Total axial stress [Pa]

σ_{Axial}	Axial stress [Pa]
$\sigma_{Bending}$	Bending stress due to doglegs [Pa]
σ_{Radial}	Radial stress [Pa]
σ_{Tan}	Tangential stress [Pa]
σ_{VME}	Von Mises equivalent stress for triaxial design [Pa]
σ_{VME}	Von Mises equivalent stress [Pa]
σ_a	Amplitude of cyclic stress [Pa]
σ_m	Mean stress due to cyclic stresses [Pa]
σ_{max}	Maximum cyclic stress [Pa]
σ_{min}	Minimum cyclic stress [Pa]
h	Height between two points of interest where pressure loss occurs [m]
ΔT	Average change in temperature over the effected length [°C]
A	Dimensionless factor for the collapse resistance calculation [-]
B	Dimensionless factor for the collapse resistance calculation [-]
C	Dimensionless factor for the collapse resistance calculation [-]
DLS	Dogleg severity in [°/30m]
E	Modulus of elasticity (Young's Modulus) of the tieback [Pa]
F	Dimensionless factor for the collapse resistance calculation [-]
G	Dimensionless factor for the collapse resistance calculation [-]
I	Moment of inertia of the tieback [m^4]
ID	Inner diameter of the tieback [m]
OD	Outer diameter of the tieback [m]
$Pitch$	Distance from one maximum of the bend to the next [m]
Q	Flow rate [m³/s]

Re	Dimensionless Reynold's number [-]
W	Weight force of the tieback due to self-weight [N]
$f(t)$	Time-dependent heat conduction function of the formation [-]
g	Gravitational acceleration [m/s²]
n	Neutral point below which buckling occurs [m]
t	Wall thickness of the tieback [m]
$time$	Elapsed time since the well has been switched from its last state [s]
v	Flowing velocity of the fluid [m/s]
α	Coefficient of thermal expansion of the tieback [1/°C]
β	Variable to calculate the buckling-induced torque [m^{-1}]
ε	Roughness of the tieback [m]
θ	Inclination at the bottom section of the well [°]
λ	Dimensionless friction factor [-]
μ	Dynamic viscosity of the flowing fluid causing pressures losses [N*s/m²]
ν	Dimensionless Poisson's Ratio of the tieback [-]
ρ	Density of the flowing fluid causing pressure losses [kg/m³]
τ	Buckling-induced torque [Nm]

Appendices

Appendix A

Outer Diameter [in]	Nominal Linear Mass [lb/ft]	Wall Thickness [in]	Inner Diameter [in]
4 1/2	9,500	0,205	4,090
4 1/2	10,500	0,224	4,052
4 1/2	11,600	0,250	4,000
4 1/2	13,500	0,290	3,920
4 1/2	15,100	0,337	3,826
5	11,500	0,220	4,560
5	13,000	0,253	4,494
5	15,000	0,296	4,408
5	18,000	0,362	4,276
5	21,400	0,437	4,126
5	23,200	0,478	4,044
5	24,100	0,500	4,000
5 1/2	14,000	0,244	5,012
5 1/2	15,500	0,275	4,950
5 1/2	17,000	0,304	4,892
5 1/2	20,000	0,361	4,778
5 1/2	23,000	0,415	4,670
5 1/2	26,800	0,500	4,500
5 1/2	29,700	0,562	4,376
5 1/2	32,600	0,625	4,250
5 1/2	35,300	0,687	4,126
5 1/2	38,000	0,750	4,000
5 1/2	40,500	0,812	3,876
5 1/2	43,100	0,875	3,750
6 5/8	20,000	0,288	6,049
6 5/8	24,000	0,352	5,921
6 5/8	28,000	0,417	5,791
6 5/8	32,000	0,475	5,675
7	17,000	0,231	6,538
7	20,000	0,272	6,456
7	23,000	0,317	6,366
7	26,000	0,362	6,276
7	29,000	0,408	6,184
7	32,000	0,453	6,094
7	35,000	0,498	6,004
7	38,000	0,540	5,920
7	42,700	0,625	5,750
7	46,400	0,687	5,626
7	50,100	0,750	5,500
7	53,600	0,812	5,376
7	57,100	0,875	5,250
7 5/8	24,000	0,300	7,025

7 5/8	26,400	0,328	6,969
7 5/8	29,700	0,375	6,875
7 5/8	33,700	0,430	6,765
7 5/8	39,000	0,500	6,625
7 5/8	42,800	0,562	6,501
7 5/8	45,300	0,595	6,435
7 5/8	47,100	0,625	6,375
7 5/8	51,200	0,687	6,251
7 5/8	55,300	0,750	6,125
7 3/4	46,100	0,595	6,560
8 5/8	24,000	0,264	8,097
8 5/8	28,000	0,304	8,017
8 5/8	32,000	0,352	7,921
8 5/8	36,000	0,400	7,825
8 5/8	40,000	0,450	7,725
8 5/8	44,000	0,500	7,625
8 5/8	49,000	0,557	7,511
9 5/8	32,300	0,312	9,001
9 5/8	36,000	0,352	8,921
9 5/8	40,000	0,395	8,835
9 5/8	43,500	0,435	8,755
9 5/8	47,000	0,472	8,681
9 5/8	53,500	0,545	8,535
9 5/8	58,400	0,595	8,435
9 5/8	59,400	0,609	8,407
9 5/8	64,900	0,672	8,281
9 5/8	70,300	0,734	8,157
9 5/8	75,600	0,797	8,031
10 3/4	32,750	0,279	10,192
10 3/4	40,500	0,350	10,050
10 3/4	45,500	0,400	9,950
10 3/4	51,000	0,450	9,850
10 3/4	55,500	0,495	9,760
10 3/4	60,700	0,545	9,660
10 3/4	65,700	0,595	9,560
10 3/4	73,200	0,672	9,406
10 3/4	79,200	0,734	9,282
10 3/4	85,300	0,797	9,156
11 3/4	42,000	0,333	11,084
11 3/4	47,000	0,375	11,000
11 3/4	54,000	0,435	10,880
11 3/4	60,000	0,489	10,772
11 3/4	65,000	0,534	10,682
11 3/4	71,000	0,582	10,586
13 3/8	48,000	0,330	12,715
13 3/8	54,400	0,380	12,615
13 3/8	61,000	0,430	12,515

13 3/8	68,000	0,480	12,415
13 3/8	72,000	0,514	12,347
16	65,000	0,375	15,250
16	75,000	0,438	15,124
16	84,000	0,495	15,010
16	109,000	0,656	14,688
18 5/8	87,500	0,435	17,755
20	94,000	0,438	19,124
20	106,500	0,500	19,000
20	133,000	0,635	18,730

Table 17: Casing & Tieback sizes, masses, wall thickness and inner diameter (Modified from: *Specification for Casing and Tubing - API Specification 5CT - ISO 11960:2004*, Eighth Edition 2005. American Petroleum Institute and ISO, 184–186)

Appendix B

Group	Name in the Application	Component Type	Tooltip & Function
	Left Panel		
Mode of Operation	Choose Mode of Operation	Drop-down list	Choose an operation mode from the drop-down list.
Preliminary Data	Temperature Gradient	Button	Upload file with temperature gradient data.
	Borehole Path	Button	Upload file with borehole depths, inclinations and dogleg severities.
	Tieback Dimensions	Button	Upload file with tieback dimensions, steel grades and setting depths.
	Casing Dimensions	Button	Upload file with casing dimensions and setting depths.
	Surface Temperature [°C]	Number box	Surface temperature in [°C].
	Surface Pressure [barA]	Number box	Surface pressure in [barA]. Adjust value if necessary.
Geological & Reservoir Parameters	Reservoir Temperature [°C]	Number box	Reservoir temperature is calculated automatically from the preliminary temperature gradient data in [°C].
	Thermal Conductivity [W/m*C]	Number box	Insert an average formation thermal conductivity in [W/m°C] which is representable for all formation sections.
	Thermal Diffusivity [E-06m²/s]	Number box	Insert an average formation thermal diffusivity in [E-06m²/s] which is representable for all formation sections.
Shut-In	Bottomhole Temperature [°C]	Number box	The expected bottomhole temperature during shut-in in [°C] is equal to the reservoir temperature.

	Bottomhole Pressure [barA]	Number box	The expected bottomhole pressure in [barA] after 30 days of shut-in shall be in equilibrium with the hydrostatic pressure at reservoir depth.
	Wellhead Temperature [°C]	Number box	The expected wellhead temperature after 30 days of shut-in in [°C].
	Wellhead Pressure [barA]	Number box	The hydrostatic water column inside the tieback is expected to be in equilibrium with the reservoir. There is no excess pressure on the wellhead after 30 days of a shut-in.
Injection	Wellhead Temperature [°C]	Number box	Insert the injection water's temperature at the wellhead in [°C].
	Wellhead Pressure [barA]	Number box	Insert applied absolute wellhead pressure in [barA].
	Water Density [kg/m³]	Number box	The injection water density in [kg/m³] is a function of the geothermal temperature gradient(s). Adjust value if necessary.
	Mass Flow Rate [kg/s]	Number box	Insert the injection water's mass flow rate in [kg/s].
	Elapsed Time [days]	Number box	Elapsed time in [days] since the well has been switched from steady-state shut-in to injection. Values below 1 day are more inaccurate and not valid. Adjust value if necessary. The elapsed time is set to 30 [days] if the injector only plays a passive role.
	Specific Heat Capacity [J/kg°C]	Number box	Insert the injection water's specific heat capacity in [J/kg°C]. The value is assumed to be constant, along with the completion depth. 4150 [J/kg°C] is the value under surface temperature.

	Dynamic Viscosity [cP]	Number box	Insert the injection water's dynamic viscosity in [cP]. The value is assumed to be constant, along with the completion depth. 1,0005 [cP] is the value under surface temperature.
	Bottomhole Temperature [°C]	Number box	The expected bottomhole temperature in [°C] during injection. Value can be adjusted through the reservoir parameters, the injection water's mass flow rate and specific heat capacity and the elapsed time.
	Bottomhole Pressure [barA]	Number box	Expected absolute bottomhole pressure in [barA] during injection. Value can be adjusted through the injection water's the mass flow rate, density and dynamic viscosity and the pipe roughness.
Production	Bottomhole Temperature [°C]	Number box	The expected bottomhole temperature during production in [°C] is equal to the reservoir temperature.
	Bottomhole Pressure [barA]	Number box	The expected bottomhole pressure in [barA] during production is equal to the injection well's bottomhole pressure. Adjust value if necessary.
	Water Density [kg/m³]	Number box	The production water density at the bottom of the well in [kg/m³] is equal to the injection well's density. The density is a function of the geothermal temperature gradient(s). Adjust value if necessary.
	Mass Flow Rate [kg/s]	Number box	Insert the production water's mass flow rate in [kg/s].
	Elapsed Time [days]	Number box	Elapsed time in [days] since the well has been switched from steady-state shut-in to production. Values below 1 day are more inaccurate and not valid. Adjust value if necessary.

	Specific Heat Capacity [J/kg°C]	Number box	Insert the production water's specific heat capacity in [J/kg°C]. The value is assumed to be constant, along with the completion depth. 4150 [J/kg°C] is the value under surface temperature. Please adjust to reservoir temperature conditions.
	Dynamic Viscosity [cP]	Number box	Insert the production water's dynamic viscosity in [cP]. The value is assumed to be constant, along with the completion depth. 1,0005 [cP] is the value under surface temperature. Please adjust to reservoir temperature conditions.
	Wellhead Temperature [°C]	Number box	Expected wellhead temperature in [°C] during production. Value can be adjusted through the reservoir parameters, the production water's mass flow rate and specific heat capacity and the elapsed time.
	Wellhead Pressure [barA]	Number box	Expected absolute wellhead pressure in [barA] during production. Value can be adjusted through the production water's the mass flow rate, density and dynamic viscosity and the pipe roughness.
Pressure Test	Wellhead Pressure [barA]	Number box	Insert the applied wellhead pressure during a pressure test in [barA].
	Pressure at Plug [barA]	Number box	The pressure at the plug is the pressure during shut-in at the bottom of the tieback plus any additional applied wellhead pressure in [barA].
	Wellhead Temperature [°C]	Number box	The temperature at the wellhead is the shut-in wellhead temperature in [°C].

	Temperature at Plug [°C]	Number box	The temperature at the plug is the temperature during shut-in at the bottom of the tieback in [°C].
Steel Grades	Choose Steel Grade	Drop-down list	Choose a steel grade from the drop-down list.
	Min. Yield Strength [MPa]	Number box	Minimum yield strength of the selected steel grade in [MPa]. The value is assumed to be constant, along with the completion depth. If necessary, adjust value to temperature conditions.
	Min. Tensile Strength [MPa]	Number box	Minimum tensile strength of the selected steel grade in [MPa]. The value is assumed to be constant, along with the completion depth. If necessary, adjust value to temperature conditions.
	Modulus of Elasticity [GPa]	Number box	Modulus of elasticity of the selected steel grade in [GPa]. The value is assumed to be constant, along with the completion depth. If necessary, adjust value to temperature conditions.
	Poisson's Ratio [-]	Number box	Poisson's ratio of steel [-]. The value is assumed to be constant, along with the completion depth. If necessary, adjust value to temperature conditions.
	Expansion Coefficient [E-06/°C]	Number box	Coefficient of thermal expansion of the selected steel grade in [E-06/°C]. The value is assumed to be constant, along with the completion depth. If necessary, adjust value to temperature conditions.
	Coating / Pipe Roughness [mm]	Number box	Insert a pipe or coating roughness for the selected steel grade in [mm]. The value is assumed to be constant, along with the completion depth.

Annulus Fluid between Casing and Tieback	Annulus fluid Density [kg/m³]	Number box	Insert the annulus fluid's density in [kg/m³].
Design Factors	Tension	Number box	Insert the desired design factor for tension failure. Typical values range from 1.3-1.6.
	Compression	Number box	Insert the desired design factor for compression failure. Typical values range from 1.3-1.6.
	Burst	Number box	Insert the desired design factor for burst failure. Typical values range from 1.1-1.25.
	Collapse	Number box	Insert the desired design factor for collapse failure. Typical values range from 1.0-1.1.
Additional Information & Settings	Measuring Interval [m]	Number box	Measuring interval for calculated data points per meter for all applicable calculations. Define an interval between 1-10 [m]. Adjust value if necessary.
	Free Tieback String	Checkbox	Check to select a tieback string which is allowed to move freely in the vertical direction. The none-checked option automatically means that the tieback string is restrained from vertical movement.
	Setting Force [N]	Number box	Insert any additional force applied during the setting process (tension or compression). Any value other than zero will be applied automatically to the load calculations.
	Helical Buckling Onset in a deviated Well	Number box	Enter the factor governing the onset of helical buckling in a deviated wellbore. Values range from 1.41 to 1.83.

	Run	Button	Run the program.
Execute	Reset	Button	Reset all calculated values. Enable input elements again and disable the plots.
Right Panel			
Input Summary		Tab	This tab shows a summary of all pre-defined and custom user input data.
Numerical Results		Tab	This tab shows all calculated numerical values and results. Full information is only available after the program has been run.
Plots		Tab	This tab shows a variety of different plots. Full information is only available after the program has been run.
Plots	Choose Plot	Drop-down list	Choose a plot from the drop-down list. Some selections do not show plots depending on the chosen mode of operation. All applicable plots are only available after the program has been run.

Table 18: MATLAB GUI - Input panel description

Appendix C

Figure 112 shows the dependency of input parameters on the mathematical functions governing the calculations of the water column's hydrostatic pressure distribution at any given depth.
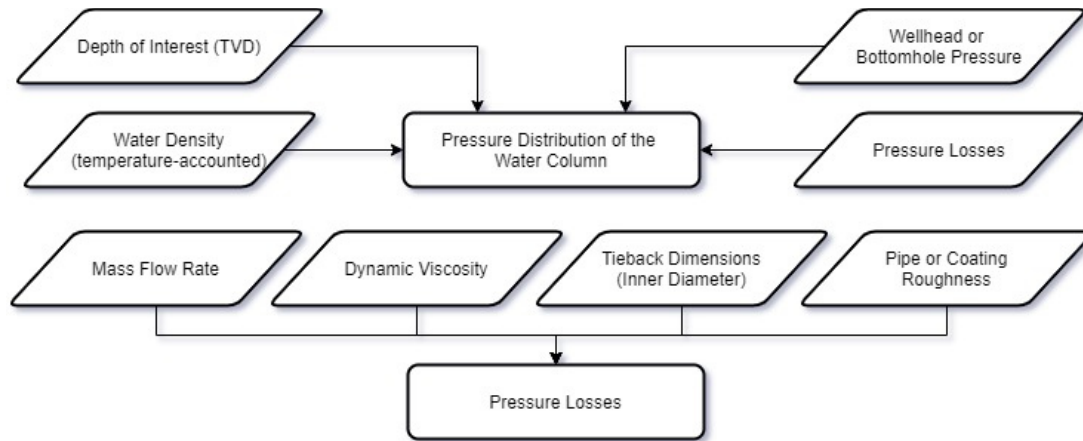

Figure 112: Input Parameters to calculate the hydrostatic pressure at any depth

Figure 113 shows the dependency of input parameters on the mathematical functions governing the calculations of the water column's temperature distribution at any given depth.

The inflowing water temperature at the surface is only necessary for the temperature distribution during injection activities. Thus, these factors are in brackets.
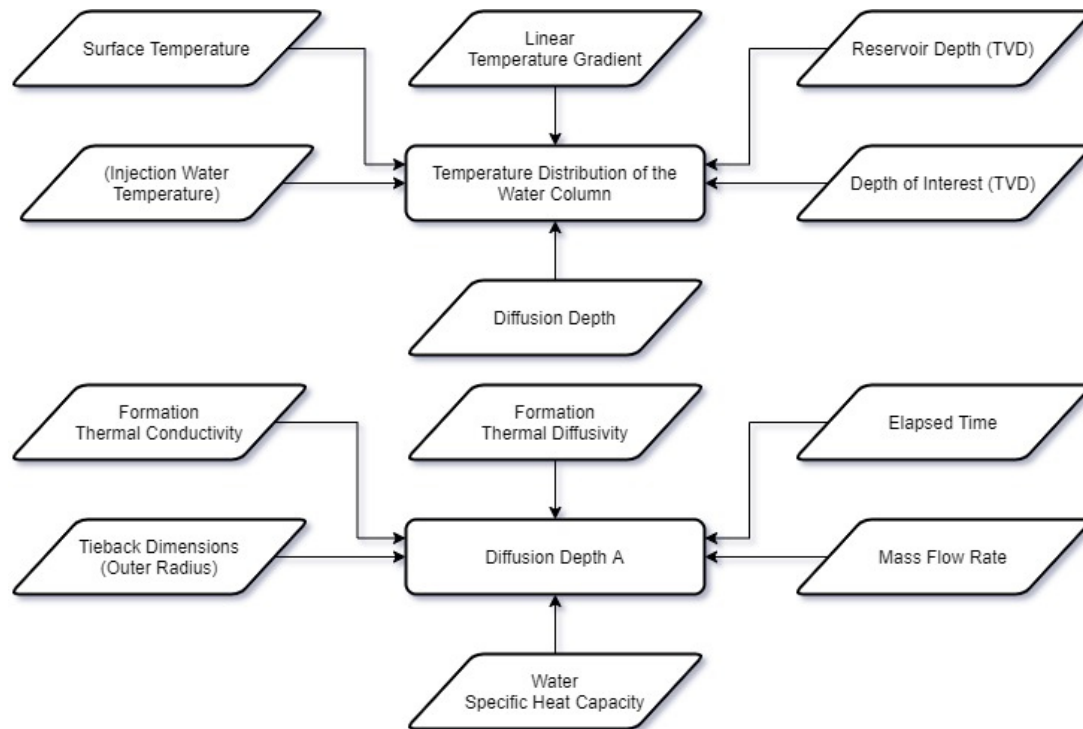
Figure 113: Input Parameters to calculate the water temperature distribution at any depth

Figure 114 shows the dependency of input parameters on the mathematical functions governing the calculations of the tieback's axial loads.

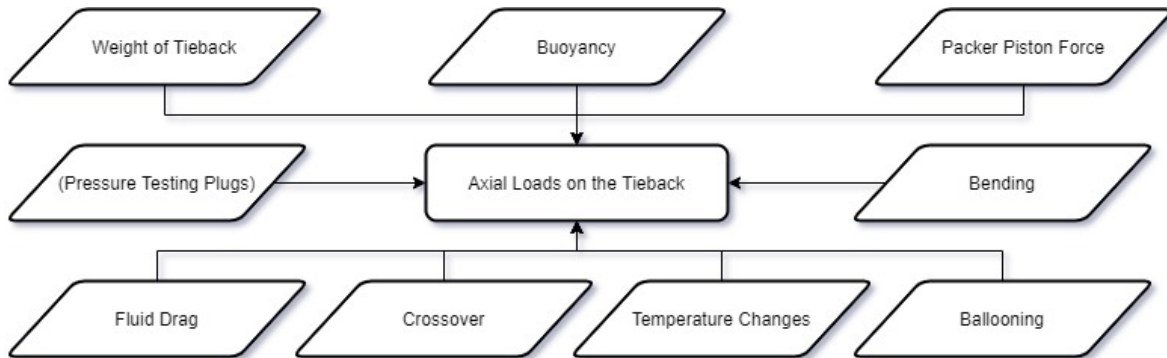The pressure test plug is only applicable during pressure testing activities.

Figure 114: Input parameters to calculate the axial loads on the tieback

Figure 115 shows the dependency of input parameters on the mathematical functions governing the buckling assessment of the tieback. Additionally, it is shown how buckling influences certain output parameters.

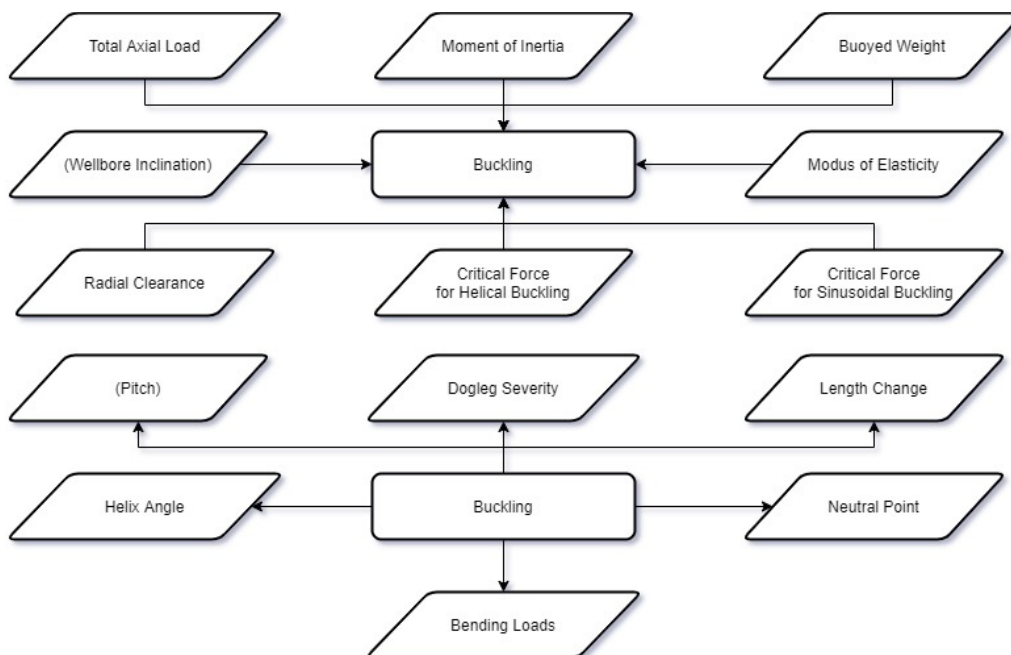The wellbore inclination is only applicable in deviated wellbores. The pitch is only for helically buckled pipes.

Figure 115: Input & output parameters of the buckling calculations

9 References

Bauer, M., Freeden, W., Jacobi, H. et al. 2014. *Handbuch Tiefe Geothermie: Prospektion, Exploration, Realisierung, Nutzung*. Berlin, Heidelberg: Springer Berlin Heidelberg. https://doi.org/10.1007/978-3-642-54511-5.

Bellarby, J. 2009. *Well Completion Design*. Amsterdam, London: Elsevier.

Boden, D. R. 2016. *Geologic Fundamentals of Geothermal Energy*. Boca Raton: CRC Press.

Bschorer, S. 2018. *Technische Strömungslehre: Lehr- und Übungsbuch / Sabine Bschorer*, Eleventh edition. Wiesbaden: Springer Fachmedien Wiesbaden. https://doi.org/10.1007/978-3-658-20037-4.

Bulletin on Formulas and Calculations for Casing, Tubing, Drill Pipe, and Line Pipe Properties - API BULLETIN 5C3, Sixth Edition. 1994. American Petroleum Institute.

Byrom, T. G. 2015. *Casing and liners for drilling and completion: Design and application*, Second edition. Waltham, MA: Gulf Professional Publishing is an imprint of Elsevier.

Campbell, F. C. 2008. *Elements of Metallurgy and Engineering Alloys*. Materials Park, Ohio: ASM International.

Code of practice for deep geothermal wells. 2015. New Zealand Standard.

Cunha, J. C. 2004. Buckling of Tubulars Inside Wellbores: A Review on Recent Theoretical and Experimental Works. *SPE Drilling & Completion* **19** (01): 13–19. https://doi.org/10.2118/87895-PA.

Dake, L. P. 1978. *Fundamentals of Reservoir Engineering*. Amsterdam: Elsevier.

DiPippo, R. 2016. *Geothermal Power Generation: Developments and Innovation*. Duxford, UK: Woodhead Publishing is an imprint of Elsevier.

Durrant, A. J. and Thambynayagam, R. 1986. Wellbore Heat Transmission and Pressure Drop for Steam/Water Injection and Geothermal Production: A Simple Solution Technique. *SPE Reservoir Engineering* **1** (02): 148–162. https://doi.org/10.2118/12939-PA.

Erdwerk GmbH. Erdwerk GmbH.

Forsberg, C. H. 2021. *Heat Transfer: Principles and Applications*, first edition. London, San Diego, CA: Academic Press. https://doi.org/10.1016/B978-0-12-802296-2.01001-5.

Grant, M. A. and Bixley, P. F. 2011. *Geothermal Reservoir Engineering*, secondnd ed. / Malcolm A. Grant, Paul F. Bixley. Burlington, MA: Academic Press.

Gunnlaugsson, E., Ármannsson, H., Thorhallsson, S. et al. Problems in Geothermal Operation - Scaling and Corrosion.

Hagoort, J. 2004. Ramey's Wellbore Heat Transmission Revisited. *SPE Journal* **9** (04): 465–474. https://doi.org/10.2118/87305-PA.

Hahn, B. D. and Valentine, D. T. 2019. *Essential Matlab for Engineers and Scientists*. [Place of publication not identified]: ELSEVIER ACADEMIC Press.

Hibbeler, R. C. and Yap, K. B. 2017. *Fluid mechanics in SI units*, Global edition. Boston: Pearson.

Huenges, E. 2010. *Geothermal Energy Systems: Exploration, Development, and Utilization*. Weinheim: Wiley-VCH.

Jaculli, M. A. and Mendes, J. R. P. 2018. *Dynamic Buckling of Columns Inside Oil Wells*. Cham: Springer International Publishing. https://doi.org/10.1007/978-3-319-91208-0.

Kang, Y., Samuel, R., Gonzales, A. et al. 2020. Force Calculation with Oil Well Packer: A Revisit. Paper presented at the International Petroleum Technology Conference, Dhahran, Kingdom of Saudi Arabia, 2020-01-13. https://doi.org/10.2523/IPTC-20324-MS.

Kaya, T. and HOŞHAN, P. Corrosion and Material Selection for Geothermal Systems. In *Proceedings World Geothermal Congress 2005*.

Kretzschmar, H.-J. and Wagner, W. 2019. *International Steam Tables: Properties of Water and Steam based on the Industrial Formulation IAPWS-IF97 Tables · Algorithms · Diagrams*. Berlin, Heidelberg: Springer Berlin Heidelberg. https://doi.org/10.1007/978-3-662-53219-5.

Krupp, U. 2007. *Fatigue Crack Propagation in Metals and Alloys: Microstructural Aspects and Modelling Concepts*, first., Auflage. Weinheim: Wiley-VCH.

Leitfaden Futterrohrberechnung. 2006. Wirtschaftsverband Erdöl- und Erdgasgewinnung e.V.

Lemaitre, J. and Desmorat, R. 2005. *Engineering Damage Mechanics: Ductile, creep, fatique and brittle failures*. Berlin/Heidelberg: Springer-Verlag. https://doi.org/10.1007/b138882.

Liu, Y., Wang, G., Yue, G. et al. 2019. Comparison of enhanced geothermal system with water and CO 2 as working fluid: A case study in Zhacanggou, Northeastern Tibet, China. *Energy Exploration & Exploitation* **37** (2): 736–755. https://doi.org/10.1177/0144598718795492.

Longo, S., Tanda, M. G., and Chiapponi, L. 2021. *Problems in Hydraulics and Fluid Mechanics*. Cham: Springer International Publishing. https://doi.org/10.1007/978-3-030-51387-0.

Lyons, W. C., Plisga, G. J., and Lorenz, M. 2015. *Standard Handbook of Petroleum and Natural Gas Engineering*, Third edition. Amsterdam: Gulf Professional Publishing.

MathWorks. 2020. MathWorks, https://www.mathworks.com (accessed 2020).

MATLAB R2020b. MATLAB R2020b.

Mitchell, R. F. 2005. Tubing Buckling-The Rest of the Story. Paper presented at the SPE Annual Technical Conference and Exhibition, Dallas, Texas, 2005-10-09. https://doi.org/10.2118/96131-MS.

Mitchell, R. F. 2006. Tubing Buckling - The State of the Art. Paper presented at the SPE Annual Technical Conference and Exhibition, San Antonio, Texas, USA, 2006-09-24. https://doi.org/10.2118/104267-MS.

Mitchell, R. F. 2007. Tubing Buckling Analysis with Expansion Joints. Paper presented at the SPE/IADC Drilling Conference, Amsterdam, The Netherlands, 2007-02-20. https://doi.org/10.2118/105067-MS.

Mitchell, R. F. and Miska, S. Z. 2006. Helical Buckling of Pipe With Connectors and Torque. *SPE Drilling & Completion* **21** (02): 108–115. https://doi.org/10.2118/87205-PA.

Naterer, G. F. 2018. *Advanced Heat Transfer*, Second edition. Boca Raton: CRC Press Taylor & Francis Group.

Noack, V., Scheck-Wenderoth, M., and Cacace, M. 2012. Sensitivity of 3D thermal models to the choice of boundary conditions and thermal properties: a case study for the area of Brandenburg (NE German Basin). *Environ Earth Sci* **67** (6): 1695–1711. https://doi.org/10.1007/s12665-012-1614-2.

Nogara, J. and Zarrouk, S. J. 2018. Corrosion in Geothermal Environment: Part 1: Fluids and their impact. *Renewable and Sustainable Energy Reviews* **82:** 1333–1346. https://doi.org/10.1016/j.rser.2017.06.098.

Okotie, S. and Ikporo, B. 2019. *Reservoir Engineering: Fundamentals and Applications*. Cham, Switzerland: Springer.

Onay, M. E. 2020. Analytical Solutions for Predicting Fracture Outlet Temperature of Produced Fluid from Enhanced Geothermal Systems with Different Well-Completion Configurations. Paper presented at the SPE Annual Technical Conference and Exhibition. https://doi.org/10.2118/204274-STU.

Pang, X.-F. 2014. *Water: Molecular Structure and Properties*. New Jersey: World Scientific.

Parkeh, R. 2020. *Fundamentals of Graphics using MATLAB*. Boca Raton: CRC Press.

Ramey, H. J. 1962. Wellbore Heat Transmission. *Journal of Petroleum Technology* **14** (04): 427–435. https://doi.org/10.2118/96-PA.

Sanchez, R. A., Brown, C. F., and Adams, W. 2012. Casing Centralization in Horizontal and Extended Reach Wells. Paper presented at the SPE/EAGE European Unconventional Resources Conference and Exhibition, Vienna, Austria, 2012-03-20. https://doi.org/10.2118/150317-MS.

Sizemore, J. and Mueller, J. 2014. *MATLAB for Dummies*. Hoboken, NJ: John Wiley & Sons Inc.

Specification for Casing and Tubing - API Specification 5CT - ISO 11960:2004, Eighth Edition. 2005. American Petroleum Institute and ISO.

Stephan, P., Kabelac, S., Kind, M. et al. 2019. *VDI-Wärmeatlas: Fachlicher Träger VDI-Gesellschaft Verfahrenstechnik und Chemieingenieurwesen / Peter Stephan, Stephan Kabelac, Matthias Kind, Dieter Mewes, Karlheinz Schaber, Thomas Wetzel, Hrsg*, twelfth. Auflage. Berlin, Heidelberg: Springer Berlin Heidelberg. https://doi.org/10.1007/978-3-662-52989-8.

Stober, I. and Bucher, K. 2013. *Geothermal Energy: From Theoretical Models to Exploration and Development*, firstst ed. twentieththirteenth. Berlin, Heidelberg: Springer Berlin Heidelberg. https://doi.org/10.1007/978-3-642-13352-7.

Tao, G., Matthews, C., and Adams, A. 2020. Special Considerations for Well Tubular Design at Elevated Temperatures. Paper presented at the IADC/SPE International Drilling Conference and Exhibition. https://doi.org/10.2118/199570-MS.

Teodoriu, C. and Falcone, G. 2009. Comparing completion design in hydrocarbon and geothermal wells: The need to evaluate the integrity of casing connections subject to thermal stresses. *Geothermics* **38** (2): 238–246. https://doi.org/10.1016/j.geothermics.2008.11.006.

Tóth, A. and Bobok, E. 2016. *Flow and Heat Transfer in Geothermal Systems: Basic Equations for Describing and Modeling Geothermal Phenomena and Technologies*. Amsterdam: Elsevier.

Vallejo Vitaller, A., Angst, U., and Elsener, B. 2019. Corrosion Behaviour of L80 Steel Grade in Geothermal Power Plants in Switzerland. *Metals* **9** (3): 331. https://doi.org/10.3390/met9030331.

Watson, A. 2013. *Geothermal Engineering: Fundamentals and applications*. New York, NY: Springer New York. https://doi.org/10.1007/978-1-4614-8569-8.

Wood Group Intetech Ltd. 2017. *Corrosion Review and Materials Selection for Geothermal Wells*.